Summer 8-1-2019

Drought impacts assessment in Brazil - a remote sensing approach

Denis Mariano
University of Nebraska - Lincoln, mariano@huskers.unl.edu

DROUGHT IMPACTS ASSESSMENT IN BRAZIL – A REMOTE SENSING APPROACH

by

Denis Araujo Mariano

A DISSERTATION

Presented to the Faculty of

The School of Natural Resources at the University of Nebraska

In Partial Fulfillment of Requirements

For the Doctor of Philosophy

Major: Natural Resources Sciences

(Climate Impacts & Assessment)

Under the Supervision of Professor Brian D. Wardlow

Lincoln, Nebraska

August, 2019

DROUGHT IMPACTS ASSESSMENT IN BRAZIL – A REMOTE SENSING APPROACH

Denis Araujo Mariano, Ph.D.

University of Nebraska, 2019

Advisor: Brian D. Wardlow

Climate extremes are becoming more frequent in Brazil; studies project an increase in drought occurrences in many regions of the country. In the south, drought events lead to crop yield losses affecting the value chain and, therefore, the local economy. In the northeast, extended periods of drought lead to potential land degradation, affecting the livelihood and hindering local development. In the southern Amazon, an area that experienced intense land use change (LUC) in the last, the impacts are even more complex, ranging from crop yield loss and forest resilience loss, affecting ecosystem health and putting a threat on the native population traditional way of living. In the studies here we analyzed the drought impacts in these regions during the 2000s, which vary in nature and outcomes. We addressed some of the key problems in each of the three regions: i) for the southern agriculture, we tackled the problem of predicting soybean yield based on within-season remote sensing (RS) data, ii) in the northeast we mapped areas presenting trends of land degradation in the wake of an extended drought and, iii) in southern Amazon, we characterized a complex degradation cycle encompassing LUC, fire occurrence, forest resilience loss, carbon balance, and the interconnectedness of these factors impacting the local climate. The studies integrated RS data of evapotranspiration, temperature, precipitation, soil moisture, albedo, and biomass-related indicators. Official

data for population and agricultural statistics were also utilized to better connect climate extremes to human factors. Our results indicate that crop yield in southern Brazil can be predicted using RS data and therefore, provide valuable information for decision-makers in the agriculture value chain. In the northeast, extended drought associated with anthropogenic pressure for resources represent a threat to the ecosystem health by affecting soil and water quality, micrometeorological conditions and, thus, people's livelihood. Finally, in southern Amazon, the LUC led to a regional LD which has positive feedback on the climate, causing even more damage as the degradation cycle advances, putting a threat on the local agriculture economic sustainability.

ACKNOWLEDGEMENTS

First and foremost, thanks to the Coordination for the Improvement of Higher Education Personnel (CAPES) for providing the funding for my education abroad. I acknowledge the difficulties surfaced in the wake of budgetary constraints for the funding agency and, the effort taken by them on maintaining students financial support. That being said, I am grateful to Brian Wardlow, my advisor, who gave me all the support and freedom to carry on this research. Thanks also to my graduation committee, which is composed by Tsegaye Tadesse, Mark Svoboda, John Gamon and, Christopher Neale, a great team on drought studies, providing support and insights. Thanks to all the School of Natural Resources staff for always providing help promptly.

I am also pleased to have worked with Carlos A.C. dos Santos (and family) (Federal University of Campina Grande, Brazil) for partnering on this research and many others to come. Carlos was determinant on broaden my understanding of the problems we're studying. Also, people that contributed to our work: Martha Anderson (USDA), Christopher Hain (NASA), Fábio Marin (ESALQ/USP), Javier Tomasella (Cemaden - Brazil), and Joana Nogueira (INPE - Brazil). Not to mention the anonymous reviewers from Remote Sensing of Environment and Global Change Biology; I believe dealing with success and failure is an essential part of learning to be a scientist, especially the failure part.

I'm thankful to the institutions that are part of my superior education: the University of São Paulo at Piracicaba (USP/ESALQ) and the National Institute for Space Research (INPE). In times where science and education are being discredited, these institutions form the barricades against setbacks.

The graduate school abroad comes with an intangible cost: distance from my family. For the period here, my friends became my family and made these four years more bearable. Thanks to Felipe Alves, Anna Dempsey, Ivo Zution, John Dorn, Lindsey Day, Benjamin Langley, Michael Neale (and family), Juan Ortuzar, Michelle Lute, Isidro Campos, Carolina Camargo, Debora Montezano, Karen Silva, Pedro Queiroz, and Allie Schiltmeyer (and family).

I also want to praise the old (and some contemporary) masters, who have influenced my understanding about the meaning of science, so I recommend you to read George Orwell, Carl Sagan, Thomas Kuhn, C.P. Snow, Ralph Waldo Emerson, Henry David Thoreau, Nassim Nicholas Thaleb, Michael Sandel, Angela Davis, Octavia Butler, Claudio Angelo, Marcelo Gleiser, and many other gifted minds that are nowadays very influential to my understanding of the nature, world, people and ideas.

Special thanks to Joana, Valder, Karina, Ícaro, Madalena and Ivã for their unconditional support and comprehension. Finally, I'm thankful to Rosey Ybarra, who now is also part of the family. Grunt!

Funding Acknowledgements

The research discussed in Chapter 2 was funded by the Brazilian National Council for Scientific and Technological Development (CNPq) grant (205932/2014-2), and is partially based on Denis A. Mariano PhD dissertation carried out at the School of Natural Resources, University of Nebraska-Lincoln. We would like to thank the Holland Computing Center at the University of Nebraska-Lincoln (hcc.unl.edu) for providing the platform to perform high demanding computational tasks. The second author is thankful to the Coordination for the Improvement of Higher Education Personnel - Brazil (CAPES) - Finance Code 001 (Research project Pró-Alertas - Grant N. 88887.091737/2014-01) and, Visiting Professor Fellowship – Grant N. 88881.172029/2018-01). The second author also thanks the CNPq for the Research Productivity Grant (Grant N. 301348/2015-4). We also acknowledge Fábio R. Marin (University of São Paulo - ESALQ) for the valuable suggestions.

We are thankful to the three anonymous reviewers for their extremely valuable suggestions, which contributed to improve the manuscript used in Chapter 3. The research discussed in Chapter 3 was funded by the Brazilian National Council for Scientific and Technological Development (CNPq) (grant 205932/2014-2), and is partially based on Denis Mariano Ph.D. dissertation carried out at the School of Natural Resources, University of Nebraska - Lincoln. The authors are grateful to the CNPq for funding the Research Project 446172/2015-4 and the Research Productivity Grant, as well as the CAPES for funding the Research Project 88887.091737/2014-01. We would like to thank the Holland Computing Center at the University of Nebraska-Lincoln (hcc.unl.edu) for providing the platform to perform high demanding computational tasks.

We would like to thank the Brazilian National Institute for Semiarid (www.insa.gov.br) for the rich material about the NEB. For our research and time expenses, many effusive regards.

TABLE OF CONTENTS

LIST OF TABLES

LIST OF FIGURES

PREFACE

Chapter 2 (Early detection of agricultural drought in Southern Brazil) is being prepared for submission.

Chapter 3 is published: Mariano, D. A., Santos, C. A. C. dos, Wardlow, B. D., Anderson, M. C., Schiltmeyer, A. V., Tadesse, T., & Svoboda, M. D. (2018). Use of remote sensing indicators to assess effects of drought and human-induced land degradation on ecosystem health in Northeastern Brazil. *Remote Sensing of Environment*, 213(April), 129–143.

Chapter 4 (Drought impacts on crop yields, wildfire occurrence, and the carbon budget in the Southeastern Amazon) is being prepared for submission.

CHAPTER 1.

INTRODUCTION

Brazil is the 5th largest country on the planet (8.5 million square kilometers), with five biomes and climates ranging from equatorial to temperate. The country, whose development is largely based on the use of natural resources, experienced a period of substantial economic growth in the 2000s, promoting the development and, therefore reshaping social structure (Lavinas, 2017). Increased class mobility redirected the population toward more consumerism, with access to credit and the eagerness for development.

For developing countries such as the BRICS (Brazil, Russia, India, China, and South Africa), growth is highly correlated with energy consumption through fossil fuels, water (hydropower) and biofuels (agriculture) (Sasana & Ghozali, 2017). Moreover, in the case of Brazil, the focus of our studies, the economic growth was also leveraged by a boom in agricultural commodities prices, which is a recurrent feature of the 2000s that pushed land use changes (conversion into agricultural enterprises) forward (Hargrave & Kis-Katos, 2013; Yao, Hertel, & Taheripour, 2018). With the BRICS getting "late in the game", increased pressure for resources is thus expected and, as a result, CO_2 (and other greenhouse gases) emissions also increase, promoting changes in the climate and amplifying effects of the altered radiation balance (Sellers et al., 1996). The increase in climate extremes is a problem of global concern. In 2015, during the COP21 in Paris, an agreement was signed by 174 countries and the European Union, with the long-term commitment of keeping the increase in global average temperature under 2 ^{o}C above pre-

industrial levels (we have already increased the temperature by 0.85 ºC) - in general terms, the Paris agreement is considered a remarkable global initial effort on keeping the Earth a planet that we can still live in (Kinley, 2017). 2015 was also the year of one of the most severe droughts ever recorded in Amazon and, the fourth year of an extended drought in northeastern Brazil, two regions covered in our studies. It is well known that many of the Paris agreement signatories countries are concerned, among other things, with extreme weather events. In the case of Brazil: a country with high dependence on rainfed agriculture and exploration of its vegetal resources, one of the most feared natural hazards is drought. This can sound contradictory to the old Brazilian cultural belief that water resources are infinite - this belief is changing (PBMC, 2016).

Drought is traditionally defined as a period of below-average precipitation levels, leading to an insufficient water supply to human needs, plant health, and ecosystem stability (Wilhite, 2000). A global study by Dai et al., (2013) indicates a trend of increasing drought incidence under a scenario of global warming, with dire predictions for South America. In the fifth Assessment Report (AR5) of the International Panel for Climate Change (IPCC), models indicate with medium confidence prediction, a temperature increase ranging from 1.6 to 6.7 ºC in South America by 2100 (Magrin et al., 2014). This global warming scenario is not far off of the forthcoming reality, as reported by the WorldBank (2012) when considering "business as usual" strategies to cope with CO_2 emissions, with expected global warming of 4 ºC. Lately, scientists are proposing a broader definition for drought in a way to include humans as a cause - the drought in the Anthropocene (Van Loon et al., 2016), where the occurrence is also tied to positive feedback incurred from human actions.

In Brazil, future climate scenarios are dire and droughts are expected to increase in frequency and intensity. In the south, a traditional agricultural commodities production region (soybeans and corn), changes in the precipitation regime are altering crop growing season patterns, as drier conditions are expected early in the growing season (from September to November) (Pereira, Blain, de Avila, Pires, & Pinto, 2018). Moreover, higher temperatures and shorter, but more intense rainfall are likely to reduce corn yields in the region (Resende, Miranda, Cooke, Chu, & Chou, 2019). Farmers are having to rely on shorter-cycle (and less productive) breeds of corn and soybeans to diminish exposure to drought. In the northeast, which comprehends the most populated dryland in the planet (Denis A. Mariano et al., 2018), the prognostics are of pure desolation; studies performed by Marengo et al., (2016) and Oliveira et al., (2017) indicate longer dry spells, less precipitation, and higher temperatures, in short, leading to aridization. This scenario associated with increasing local human pressure for natural resources is, therefore, a pathway toward land degradation. In the Amazon biome, a region containing the largest forest on the planet, the trends are toward more intense droughts and longer dry seasons (Espinoza, Ronchail, Marengo, & Segura, 2019; Fu et al., 2013), especially in the southern parts of the area as a result of combined anthropogenic activities and climatological teleconnections (Lopes, Chiang, Thompson, & Dracup, 2016).

Drought is, therefore, a subject of primary concern for Brazilian policymakers. Despite the long history and experience in dealing with related issues, there are still many gaps in providing tools to support decision making and overcome political shortsightedness. Gutiérrez et al., (2014) identified some of these gaps in the Brazilian drought framework, suggesting the development/improvement of studies related to

impacts assessment, monitoring, prediction, and adequate mitigatory responses. That being said, we designed a series of studies addressing part of these needs and, therefore, providing new insights to Brazilian development in face of an unwelcoming climate scenario. The background for the studies is set: i) an increasing variability of the climate; *ii)* the unpreparedness of the decision makers for dealing with the fact that the climate variability increases at a pace faster than strategies and science address them (in Brazil); *iii)* climate change also becomes a matter of political debate, and policies to deal with the risks posed are bound to biased interests rather than scientific evidence; in Brazil, often times bribes and other forms of corruption allow for land clearances and illegal logging (Povitkina, 2018).

1.1 Literature review

1.1.1 Extrinsic drought drivers

Several global and oceanic indices are key for local precipitation anomalies explanation; therefore, those indicators are usual inputs in global climate models (GCM). One of the main factors promoting precipitation anomalies in Brazil is the teleconnection of climate variability related to the El Niño Southern Oscillation (ENSO), partially explaining droughts in the south, increasing agricultural drought risk (W. Anderson, Seager, Baethgen, & Cane, 2018; Cirino, Féres, Braga, & Reis, 2015; Gelcer et al., 2013; Gusso, 2013). In the northeast, precipitation anomalies are promoted by changes in climate forcings such as the ENSO, Intertropical Convergence Zone (ITCZ), cold fronts coming from the south and upper air cyclonic vortex (Pezzi & Cavalcanti, 2001; Vieira et al., 2015). In the Amazon, ENSO is one of the factors promoting precipitation anomalies, however, the association of ENSO with Madden-Julian Oscillation (MJO) further

amplifies hydrological extremes (Shimizu, Ambrizzi, & Liebmann, 2017). ENSO, ITCZ, MJO and other forcings are, therefore, useful indicators for precipitation prediction as they partially explain variability (Awange, Mpelasoka, & Goncalves, 2016).

1.1.2 Drought impacts

Drought is characterized by a series of environmental conditions that influence vegetation. Evaporation and plant transpiration draws moisture from the soil in what is called evapotranspiration (ET); in a drought, with soil moisture (SM) depleting and plant potentially getting drier, the radiation will find less water to spend energy in evaporation - the latent heat (LE). The energy, instead, will be put into increasing local temperature (T) - the sensible heat (H). The consequence of this simple mechanism has direct impacts on vegetation, as shown by (da Rocha et al., 2009) in a comprehensive study addressing water and heat fluxes patterns in cerrado and tropical forests in Brazil.

1.1.2.1 Crop yields

Crops affected by drought have their yield reduced. In a RS approach, crop yields are traditionally associated with biomass, which in turn can be estimated based on vegetation indices (VI) (Esquerdo et al., 2011; Liu and Kogan, 2002), that allows for assessing the damage caused by drought. Plants like soybeans and corn have their probability of emergence reduced if drought happens early in the season. During the growth phase, the biomass gain rate decreases and, in the reproductive/grain-filling phase have their seeds (grains) development compromised or, when severe, aborted. RS-based data for T and ET are used to assess drought impacts in soybeans and corn for southern Brazil (Battisti et al., 2017; Carmello and Neto, 2016; Gusso, 2013; Gusso et al., 2014; Mariano, 2015) and in the whole country (Anderson et al., 2015, 2016). Measuring pre- and within- stage VI

data is an approach to forecasting soybean yields (Johnson, 2014), but not yet tested in Brazil. Yield estimation based on water and energy variables has the advantage of anticipating the effects on biomass (assessed by VIs), as SM, T and ET anomalies impact biomass accumulation and therefore, plant development (Bolton and Friedl, 2013). Thus, tracking precipitation, T and ET anomalies (instead of just VIs) have the potential for estimating final yield before plants reach maturity and accounting for the drought-induced effects. Such information is expected to be of interest for stakeholders in the agriculture value chain and, assessing the impacts of drought within season is an underexplored topic in Brazil.

1.1.2.2 Fire occurrence

In Amazon, fires are mostly associated with land management practices (commercial or traditional); however, the occurrence is also related to environmental conditions (Cochrane and Laurance, 2008; Uhl, 1990; Uhl et al., 1988). Drought leads to moisture reduction and, potentially to higher T and, when associated with deforestation border effects increase forest flammability, thus, making land management more challenging because of the difficulty to control the fire (Davidson et al., 2012). LUC also promotes forest fragmentation, increasing border effects and further accelerating degradation through tree mortality, understory fires and species diversity loss (Anderegg et al., 2018; Laurance et al., 2011). In regional studies, decoupling natural and human causes for fire occurrence is not trivial, since the human factors are less tangible and subject to enforcement, legislation and economy. The National Institute for Space Research (INPE, Brazil) has monitored fire occurrence since 1988 through RS data, with frequent improvements in methodology and data sources for the BDQueimadas (Fire Database),

allowing for accurate tracking of fire occurrence in the country (Setzer, Pereira, & Pereira, 1994). Using this database, several studies analyzed drought-fire relations in Amazon (Aragão et al., 2018; Brando et al., 2014, 2019; Rappaport et al., 2018). Assessing occurrences through time allows for tracking forest resilience loss by associating fire with increased flammability, a sign of land degradation (LD).

1.1.2.3 Land degradation

LD is commonly defined as the reduction or loss of biological or economic productivity. Although the term is associated with fires in tropical forests, the LD subject is also extensively studied in drylands, as an intermediate step to desertification. In the Northeast of Brazil (NEB), the most populated dryland in the planet, the problem of LD is well documented. Signals of LD in drylands include soil erosion, soil compaction and, loss of vegetation coverage (Tomasella et al., 2018). Drought is usually harmful for the vegetation; however, when these events are repeated (or extended), the consequences for vegetation go beyond the interannual variation by leading to the cumulative effects on deteriorating environmental conditions for plant development. In RS, a popular approach to detect LD is by analyzing trends of biomass-related VI or albedo (to associate with soil exposure) (Eckert et al., 2015; Pan and Li, 2013; Samain et al., 2008; Vicente-Serrano, 2007). Anthropization, like land use changes, overgrazing and population increase, is also a factor that can amplify or catalyze LD, exerting furthering the pressure for resources (Hein and de Ridder, 2006; Salazar et al., 2015; Tomasella et al., 2018).

1.1.2.4 Drought and carbon balance

LUC drives changes in water and energy balance, also altering carbon budget. Post-drought analysis of net carbon balance in the Amazon tropical forest indicates a

decrease in above ground biomass carbon density due to three factors: deforestation and associated fires, fire occurrences increase due to micrometeorological conditions and disturbances impacting mature forests (Yang et al., 2018). Even considering the decrease in deforestation rates in Amazon, which would reduce carbon loss, repeated drought events led to more fire occurrences counteracting the decline in carbon emissions (Aragão et al., 2018). For the other regions covered in our research (south and northeast), there are no studies linking carbon balance and drought, which we attribute to the small contribution of these regions for global assessments (Nemani, 2003).

1.1.2.5 Drought-related impacts and human factors feedback on climate change

Another contributor to drought causation is the potential positive feedback promoted by the impacts. Feedback mechanisms are usually assessed at large geographical scale studies, therefore, most of the references are related to large systems, such as the Amazon. A GCM simulation presented by Shukla et al., (1990) assesses the effects on climate promoted by LUC (forest to pasture) in Amazon, suggesting an increase in surface T and decrease in ET and precipitation. At the local scale, gases released by forest fires may alter the wet season onset timing due to a decrease in ET, which is an important source of water for local precipitation formation (Wright et al., 2017). At the large scale, Avissar and Werth (2005) suggest that tropical deforestation (like those in Amazon) contribute to alter precipitation regimes at mid and high latitudes through hydrometeorological teleconnections; for example, the extreme drought of 2014 in the southeast and part of the south of Brazil is partially explained by alterations in the Amazon basin water balance (Nobre et al., 2016). The land-atmosphere water flux changes also contributes to alter the climate, as demonstrated by Fisher et al. (2009), as

ET is one of the main contributors to precipitation formation in the tropical areas. Therefore, ET reduction is likely to decrease precipitation formation, thus contributing to drought occurrence (Fisher et al., 2017).

The effects of these positive feedbacks promoting drought associated with anthropogenic factors acting on the land surface can turn into what we could consider a tipping point in the case of Amazon. Although the carbon balance of tropical forests remains uncertain, studies indicate that parts of Amazon can act as a modest carbon source (Baccini et al., 2019). However, Davidson et al., (2012) found signs that impacts of drought may surpass the magnitude of natural variations, indicating that in some portions of southern and eastern Amazon, the ecosystem acts neutral or a source of carbon, instead of the expected sink, suggesting a potential permanent shift on local carbon dynamics.

1.2 Objectives

The overall objective of this study is to assess the impacts of drought in Brazil by applying several RS dataset and analysis techniques. The focus is on vegetation and related impacts of crop yield loss, fire occurrence, forest resilience loss, and LD, as well as how they affect human society and economic activities. The scope and objective of each research chapter are further detailed in Section 1.3.

1.3 Dissertation structure

The core data source is RS observations, which includes precipitation, soil moisture, temperature, evapotranspiration, vegetation indices, gross primary productivity, and albedo. The data used in these studies range from medium spatial resolution at 250 m to coarse at 25 km pixel size. Most of the datasets used in these studies are provided at a

temporal resolution of eight or fewer days, thus establishing dense time-series enabling the traceability of events. The temporal and spatial scales of the data allowed us to pursue large scale studies, addressing short-term, highly dynamic impacts as well as long-term cumulative effects assessments. This dissertation was initially imagined to address the drought problem affecting soybeans production in the south of Brazil. However, opportunities and increasing interest in applying drought impacts assessment in other regions and situations broaden the scope of this research. Figure 1.1 shows a map showing study areas per Chapter and the main features of each study.

In Chapter 2 (early detection of agricultural drought in southern Brazil) we addressed the need for better tools to anticipate drought impacts on soybean crops in this area (our initial purpose of the dissertation). During the last 16 years, at least three drought occurrences severely impacted soybean production and, therefore, the local economy. The agroindustrial soybean chain is composed of various stakeholders, including farmers, banks, insurance companies, logistics agents (storage and transport), and suppliers. These players are affected by anomalies in climatological conditions through the unpredictability of crop yields. In this study, we addressed the short-term drought effects on soybean crops. We designed a study proposing a methodology to estimate final soybean yields within the growing season. The method makes use of RS data of soil moisture, evapotranspiration, precipitation and leaf area index (LAI) as inputs to a mathematical model that explains how each of these variables is capable of predicting the final soybean yield. In short, this study aims at evaluating how RS data can be incorporated in an agricultural drought monitoring system for southern Brazil, as well as assessing data capabilities (or limitations) in accurately providing in-season rather than

post hoc assessments of crop condition and projected yield in the wake of anomalous climate events.

In Chapter 3 (use of remote sensing indicators to assess effects of drought and human-induced land degradation on ecosystem health in Northeastern Brazil), published in the journal *Remote Sensing of Environment* (RSE), we addressed the land degradation problem in the wake of an extended drought event. During the Water for Food Global Conference of 2017, held in Lincoln, Nebraska, I had the opportunity to become more familiar with (at that time) the ongoing drought situation in the northeast of Brazil, which was not my study focus. The region registered a drought starting in 2011/2012 and, at the end of the study (2018) the situation remained the same. We aimed to map the areas showing consistent trends of LAI reduction under the effect of drought. We also investigated the human factors impacting areas that we mapped as "potential land degradation" (we cannot confirm land degradation without post-drought data, so we softened it as "potential"). The study also implemented an innovative mathematical approach to assess the timing of cause-effect of pairs of variables. In this way, we could understand how land degradation (better represented by negative trends of LAI), albedo and precipitation are affecting evapotranspiration (ET), as the latter is a crucial water source for precipitation formation in the region. By understanding these relationships, we aimed at assessing the potential of land degradation having positive feedback on the local climate and, unfortunately (unsurprisingly) it has occurred. This paper expanded our scope of research for this dissertation, moving from the south to the northeast, from agriculture to land degradation, from subtropical to tropical climate, from short time scales (weeks) to more extended trend detection (16 years). As a critical difference

regarding drought, in this study, we addressed the cumulative impacts of a prolonged drought rather than a specific short-term event.

Chapter 4 (drought impacts on crop yields, wildfire occurrence, and the carbon budget in the southeastern Amazon) is what I consider the most comprehensive and complex part of the dissertation. The study investigates the Xingú Indigenous Park (PIX) and its surrounding area, whose extensive land use changes - the conversion of natural vegetation into pastures and agriculture - are affecting the local climate, ecosystem, population and potentially the economy. In this study, we addressed land use changes, crop yield loss due to drought, fire occurrences, forest resilience loss and effects on the carbon budget. One additional layer of complexity addresses the indigenous population growth during part of the study period. To tie all these elements together, we had to further understand how they are connected, therefore establishing the PIX degradation cycle. The reader will notice that this chapter contains aspects of the two previous studies, such as crop yield anomalies and land degradation as a result of both specific and repeated drought events in the southern Amazon region. It is in this study where we addressed more emphatically the concept of drought in the Anthropocene - at what human activities have positive feedback on drought causation.

Finally, Chapter 5 addresses final remarks and outlooks. It is the opportunity to point out issues and identify future possibilities of research based on what was presented in the previous research chapters and the findings.

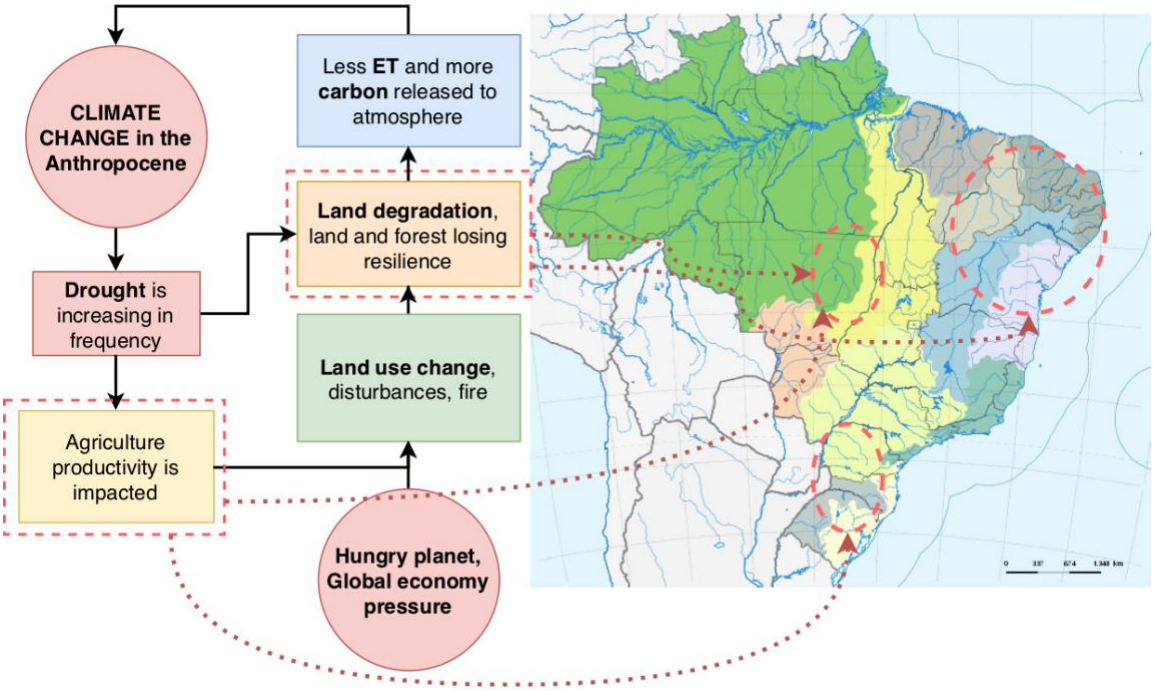

Figure 1.1: Studied regions and main subjects covered in a briefly presented climate change cycle.

CHAPTER 2.

EARLY DETECTION OF AGRICULTURAL DROUGHT IN SOUTHERN BRAZIL

Abstract:

Drought is the most common natural hazard impacting crops in tropical and subtropical regions. In southern Brazil, this negative precipitation anomaly can potentially lead to below-average plant development and therefore, yield loss. Tracking drought is possible by relying on remote sensing-based indicators; however, early detection of the potential effects is critical for drought mitigation and better decision making. We detected meteorological drought occurrences in the south region of Brazil (SB) for the summer season from 2004 to 2016 and, how they transitioned into agricultural drought impacting soybean (*Glycine max*), the dominant crop in this season. To track these events, we analyzed: *i)* two versions of the Evaporative Stress Index product (ESI), one provided by the United States Department of Agriculture (USDA-ESI, one week temporal resolution at 5 km spatial resolution) and the other derived from Moderate Resolution Imaging Spectro-radiometer ET data (MODIS-ESI, 8-day, 500 m), *ii)* soil moisture (SM) [through the Soil Water Deficit Index (SWDI, daily, 25 km)] datasets as drought indicators and, MODIS Leaf Area Index (LAI, 8-day, 500 m) as the reference for biomass. We delimited the intra-annual growing season through phenology analysis and used these periods to focus our analysis and, to use the peak of season (POS) as reference for lagging drought indicators. Therefore, considering only the growing season, a severe drought was detected in 2006, extreme drought in 2005 and 2012 and, an extremely wet year in 2016.

An Impulse Response Analysis (IRA) method was used to determine the lead time of drought indicators (considering all the years) and both ESI products were found to track agricultural drought with a 3 to 5 weeks lead time of ESI effects on maximum LAI. Similar time ranges were achieved by SWDI in the best cases, however, with lower magnitudes, highlighting this dataset inability on capturing the temporal behavior of the crops due to spatial resolution limitations. Regionally, USDA-ESI provided a longer lead time than MODIS-ESI for a few regions, however, from a spatial resolution standpoint, MODIS-ESI has proven to be more efficient on resolving the landscape heterogeneity and, therefore, providing more reliable spatial insights on agricultural drought early detection. Overall, even considering the spatial limitations, USDA-ESI and SWDI were able to detect early-stage drought for few regions under extreme drought occurrences (2005 and 2012), when the effects were more widespread and conditions more severe. MODIS-ESI, on the other hand, was effective for most regions and drought years, but the same was not observed for the wet year. We concluded that MODIS-ESI proved valuable for early detection of agricultural drought with up to 5 weeks lead time at a municipality level, whereas SWDI and USDA-ESI are not appropriate for regional monitoring because of lower spatial resolution for the study area.

2.1 Introduction

Drought is one of the most dangerous hydroclimatic hazards for societies with substantial dependence on agriculture for subsistence or market purposes. In Brazil, a country in which a large part of the Gross Domestic Product derives from the agriculture, drought is a phenomenon that often negatively impacts the economy (Mariano, 2015). In developing countries, drought is a threat for livelihoods, food security and hence,

economic sovereignty, as these nations are heavily dependent on crops for subsistence or *commodities* trading (Wilhelmi and Wilhite, 2002). Agricultural drought is a result of an extended meteorological drought (lack of precipitation over a determined period), leading to a deficit in soil moisture (SM) causing plant stress (Behrangi et al., 2016) and, yield loss (Battisti et al., 2017).

To date, drought is assessed globally using remote sensing data translated into various indices, which relate to environmental variables as potential indicators of this phenomenon. For agriculture, many tools were developed to detect drought occurrence, starting from a meteorological point of view concerning precipitation anomalies measurement - being the Standardized Precipitation Index [SPI, Mckee et al., (1993)] the most popular (Rouault and Richard, 2004). According to Awange et al. (2016), southern Brazil (SB) has a probability of undergoing an extreme drought once every 10 years, with the areas at risk increasing at a rate of 3.4% per year; which is often an effect of an intense La Niña event that leads to a decrease in precipitation and increase in temperature (Berlato et al., 2005; Cirino et al., 2015). However, below-average precipitation does not always impact crop yields, as drought is one of the causes of yield variability whereas adaptation and management decrease crop sensitivity to climate extremes (Hlavinka et al., 2009; Lobell et al., 2014; Samanta et al., 2010). To assess drought effects on agriculture, several indicators were designed based on characteristics more closely related to the soil-plant-atmosphere continuum.

With a focus on plants, reflectance-based vegetation indices (VIs) and LAI are commonly used to assess agricultural drought over large areas, achieving remarkable results in terms of measuring geographical extent and associating deviations in the

indicators with yield variation, as they correlate well with biomass (Anderson et al., 2015; Esquerdo et al., 2011; Fang et al., 2011; Guindin-Garcia et al., 2012; Mishra et al., 2014; Nguy-Robertson et al., 2012; Tagliapietra et al., 2018; Yagci et al., 2015). Going one step further, some studies combine SPI with traditional VIs for a variety of vegetation types, in which the authors relate anomalies in SPI to changes in VIs in a lag-based manner to assess how drought impacts vegetation (Caccamo et al., 2011; Ji and Peters, 2003; Van Hoek et al., 2016). Another improvement in the modeling techniques to associate VIs with yield is the consideration of phenological features that characterize a specific crop. Bolton and Friedl (2013) found that correlation between soybean yield and VIs are ~10% higher when phenology metrics are included in the model, yet, it cannot be used as an early drought indicator, but rather for *post hoc* crop condition assessment.

Below-average precipitation is likely to imply increasing SM deficit, partially as a result of higher water demand for plant transpiration (Otkin et al., 2017). Some early indicators of plant stress and ecosystem health, which potentially can affect biomass and therefore yield, are based on canopy and soil thermal responses as a result of both energy-balance and plant water demand (Hobbins et al., 2016). Hence, below-normal ET can be an early indicator of water stress in plants and be used to estimate potential drought effects in crops. Such effects on agriculture and other types of vegetation can be assessed by an indicator such as the Evaporative Stress Index [ESI (Anderson et al., 2007a, b)], a thermal infrared-based ET anomalies indicator. Useful results were found for Brazil when analyzing ESI patterns under drought regimes (Anderson et al., 2007a, b). Many methods of ET estimation rely on land surface temperature (LST) dynamics for sensible heat and

water fluxes, highlighting changes in SM, in turn, a crucial preceding driver for ET (Kalma et al., 2008).

SM is a fundamental component of the hydrological cycle, more particularly as a source of water for atmosphere via latent heat flow through ET from soil and vegetation, playing a central role in drought monitoring (AghaKouchak et al., 2015; Seneviratne et al., 2010). With the increasing availability of active remote sensing-derived SM data, drought assessment over large areas studies (due to spatial resolution limitations) have been carried out associating SM with VIs, especially in the 2010s. These studies range from development of new indices having SM as an input like the SWDI (Martínez-Fernández et al., 2015), flash drought detection (Yuan et al., 2015), intercomparison between drought indicators (Adegoke and Carleton, 2002; Anderson et al., 2013; Mishra et al., 2014; Nicolai-Shaw et al., 2017) and comparison including timing between indicators (Bolten and Crow, 2012; Mladenova et al., 2017; Zhang et al., 2017). Authors reported the capability of assessing drought with SM or SM-derived indices and their correlation with VIs/ET (Anderson et al., 2013) and crop yield (Martínez-Fernández et al., 2016). As reported by Bolten and Crow (2012), SM is potentially a good indicator for regional scale early drought detection if assessed in a weekly basis rather than monthly, therefore, capturing agriculture temporal dynamics. However, data frequency was a limitation back when the paper was published, on top of the well-known spatial resolution issue (Kerr, 2007).

A comprehensive study was performed for Brazil to analyze yield correlation to its driving factors like precipitation, ET and LAI (Anderson et al., 2015). The current study incorporates various elements of what was done in the 2010s, but targets the

agriculture in SB making use of precipitation, SWDI and ESI as drought indicators by comparing their impacts on the maximum LAI of the crop. LAI is, therefore, the variable for phenology analysis and *post hoc* vegetation condition indicator. As intrinsic limitations, we can highlight the spatial difference between datasets, the inability to resolve the spatial heterogeneity of the study area and the degree that these issues affect our ability to detect agricultural drought. This study is part of a major effort to design an agricultural drought monitor for Brazil, a fundamental tool for increasing preparedness and adaptive capacity (Gutiérrez et al., 2014). The primary objective of the study is to track agricultural drought, understanding the capacity to anticipate drought occurrence, by analyzing a multitude of indicators. LAI is used as a proxy for biomass and thermal-based (ESI) and SM (SWDI) were used as drought indicators. The specific objectives are: *i)* map drought occurrence in the region from 2004-2016 based on precipitation analysis, *ii)* analyze how drought indicators relate to LAI in a time-lagged manner to assess their potential on early drought detection and, *iii)* assess the capability of early drought detection for these datasets spatial resolution standpoint.

2.2 Spatio-temporal domain

The study area represents a major soybeans production region of the SB, with most the agricultural areas located in the states of Paraná (PR) and Rio Grande do Sul (RS), as shown in Figure 2.1. The region is characterized by double cropping, in which the majority of the summer crop (1st) is soybeans, with a small fraction of corn. The second crop is usually corn with a small fraction dedicated to either winter crop (*e.g.* wheat) or cover crops (*e.g.* oat, rye and triticale), but rarely soybeans (Albrecht et al., 2018). SB is a traditional region for grains in Brazil, with high levels of farming

technology and investment, the crops have high productivity even considering that most of the farming is rainfed.

The regional climate is predominantly subtropical in PR and temperate in RS, with Köppen classification of Subtropical Humid (Cfa) and Marine-Mild Winter (Cfb), respectively (Carmello and Neto, 2016; Grzegozewski et al., 2016). Annual precipitation ranges from 1500 to 1700 mm and 19 ^{o}C for average temperature (Liu and Kogan, 2002). For all the region, Summer is the rainy season and therefore, the period of maximum intensity for agriculture. The local climate determines the agricultural calendar based on soybean water needs. There are two periods when water availability is critical for soybean development: emergence/germination and flowering/grain filling. For the first, lack or excess water might compromise canopy uniformity by the inability of the seeds to germinate under anomalous conditions. For the latter, lack of water leads to flower abortion or premature fall, pod malformation, insufficient grain-filling and consequently, yield loss (Carmello and Neto, 2016). Although these phases are critical for soybean yield, water availability is essential throughout the entire plant cycle; excessive water is a problem not only for physiology but also for management due to mechanization issues on wet soils. In PR, soybeans are sowed mostly in October and November and harvest takes place in February and March; the peak of biomass is usually in January, marking the end of the vegetative phase (Esquerdo et al., 2011; Grzegozewski et al., 2016). In RS, the agricultural calendar for soybeans is usually one month late as compared to PR (Gusso et al., 2014; Tagliapietra et al., 2018). From now on, we refer to a year as the end of the season, which means, the harvest year (*e.g.* year 2016 is the season that started in 2015 and finished in 2016).

2.3 Data

2.3.1 Crop mask

From the MapBiomas project (www.mapbiomas.org), we downloaded yearly land cover maps based on automatic Landsat imagery classification. These datasets were used to mask remote sensing data by restraining them to crops. Although MapBiomas provides yearly data, a quick analysis showed that the classification fluctuates among the chosen classes due to the methodology applied (partially based on NDVI thresholds), which forced us to derive an overall mask that comprises the entire studied period, rather than yearly masks. The crop mask (30 m spatial resolution) comprehends soybeans and corn; however, the summer crop (1st season) is dominated by soybeans, therefore, focusing only on this crop, as we present in Section 2.2. The crop map is shown in Figure 2.1.

2.3.2 Yield data

Yearly crop yield and percentage covered area data at municipality level were acquired from the Brazilian Institute of Geography and Statistics (IBGE, 2018a). The data for soybeans are summarized in Figure 2.1, which shows median yield and area percentage for the studied period and, yearly yield *z*-score. As shown, we grouped municipalities in five regions keeping contiguous borders within them and similar level of productivity, say: cn-PR, cw-PR, ce-PR, sw-PR and nw-RS, where cn - center-north, cw - center-west, ce is center-east, ss - southwest and nw - northwest for the PR and RS states. We preferred to keep municipalities with a reasonable percentage of crop area to, at a certain degree, avoid pixel contamination from other classes.

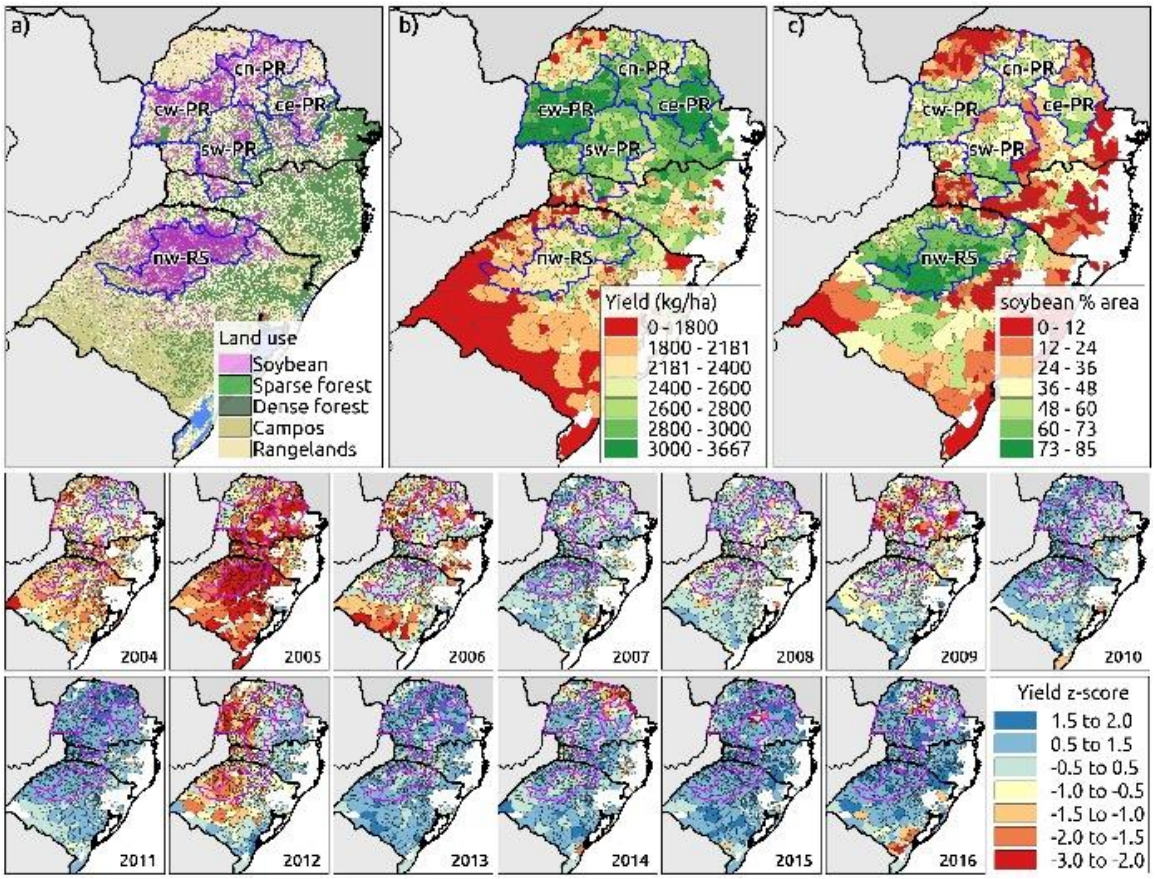

Figure 2.1: a) simplified land cover map from MapBiomas as of 2017. All the following maps are based on (IBGE, 2018a) yearly data from 2003 to 2017: b) median soybean yield, c) median percentage area and, the small maps show the annual yield variation expressed in *z*-scores.

2.3.3 Soils and agricultural aptitude maps

To support our analysis and discussion, we used soil and agricultural suitability maps of Brazil (Filho and Pereira, 1999). The agricultural suitability classes range from 1 to 8, 1 being the best. The suitability is closely associated with soil classes and topography. We summarized the main occurrences in the studied region with a short description of the predominant classes. Regarding soils, we have LV - Red latosol, LB -

tan latosol, NV - red nitosol and, CX - haplic cambisol. Nitosols are deep with good water storage/availability for plants, they are considered the best soils in the studied regions and are closely associated with the best (1) agricultural suitability. Latosols are usually associated to good to regular suitability classes for agriculture, with enough depth for roots and high capacity to store water; haplic cambisols can have good fertility, however they are not as deep as nitosols/latosols and, might not provide de ideal suitability regarding water storage/availability for crops and the topography might be hilly, they are usually associated to regular suitability. The soybean crops within each region are distributed as follows: cn-PR - mostly NV and a little LV, mostly in 1-Good, a little in 5-Regular/limited; cw-PR - mostly LV and a little less NV, about half in 1-Good, the other half divided into 4-Regular and 5-Limited; ce-PR - mostly LV and a tiny bit CX, mostly in 4-Regular and a little in 6-Limited; sw-PR - mostly LB and a little of CX, mostly in 4-Regular, a little in 6-Limited and 8-Not-recommended; nw-RS - mostly LV and a little of LB, the vast majority in 4-Regular, a little in 6-Limited and an even smaller amount in 5-Regular/Limited.

2.3.4 Precipitation

We acquired 10-day precipitation standardized anomalies (*z*-score) data from the Climate Hazards Group InfraRed Precipitation with Station [(CHIRPS-v.2) (Funk et al., 2015) delivered at 0.05 ^{o} resolution. A global validation study was performed by (Beck et al., 2017) and, for our region, the reported accuracy was about 0.7, which might not seem ideal; however, for PR, Castelhano et al. (2017) reported a correlation with ground data of 0.86 for the monthly data. The issues regarding inaccuracy are minimized by using *z*-scores rather than absolute values for comparative analysis between variables.

2.3.5 MODIS LAI

The time series of LAI data were established from MODIS sensors onboard the Terra and Aqua satellites, which have been in operation since 1999 and 2002, respectively. The MCD15A2Hv6 (Myneni et al., 2002) dataset is delivered at 500 m spatial and 8-day temporal resolutions and, are derived from Terra and Aqua combined data. The MODIS LAI dataset is used for phenology analysis (Section 2.4.2) and as a proxy for biomass to be later associated with yield data.

2.3.6 Evaporative Stress Index (ESI)

ESI represents anomalies in actual/potential ET. The lower the ET, the smaller the fraction ET/PET is, therefore, giving an idea of dryness. ESI, as a stress index, has positive values associated to drought, as shown in Equation 2.1.

$$ESI = 1 - \frac{ET}{PET} \tag{2.1}$$

where PET is the potential ET. The original product is based on a surface energy balance model, the Atmosphere-Land Exchange Inverse model (ALEXI) and LAI (Anderson et al., 2007a). ESI is calculated based on a weekly moving window and composited over periods of 1, 2, 3, 4 or 12 months at 0.05º spatial resolution for the global product (0.04 º for the United States). The data is, therefore, provided in the weekly *z*-scores form. We choose the 4-month composite as it is neither too noisy, nor too smooth, therefore being adequate for tracking crop cycle seasonality. Anderson et al.

(2016) assessed agricultural drought using ESI in Brazil, with ESI higher correlations with soybean yields 25 days earlier in comparison to LAI. To date, ESI is currently the state-of-art drought monitoring remote sensing-based tool, and it is being constantly improved by incorporating active remote sensing-based temperature retrieval for better gap-filling, once the energy balance model relies on clear-sky measurements (Holmes et al., 2015). For now on we refer to this dataset as USDA-ESI, to avoid confusion with MODIS-ESI.

We also calculated a MODIS-ESI product based on the ET datasets (MOD16A2 and MYD16A2). MODIS ET is based on the Penman-Monteith equation by combining Monteith and Priestley-Taylor methods for PET estimation, with albedo and LAI (canopy conductance and light interception) as input parameters for the surface energy balance partition algorithm, thus retrieving the actual ET (Mu et al., 2011, 2013). Ruhoff et al. (2013) validated the ET product for a basin in Brazil achieving good results when compared to eddy flux towers. The MODIS-ET version 6 (released in 2017) has an improvement in spatial resolution from 1000 m to 500 m, delivered at 8-day composites, therefore, the resolutions of our calculated MODIS-ESI dataset. As part of this study preprocessing, we held MYD16A2 (Aqua) as the main product and gap-filled it with MOD16A2 (Terra) data whenever available for a given pixel-date.

2.3.7 SWDI

SM-based indicators have a crucial advantage over precipitation-based indicators - a precipitation event during a drought period might not change the situation, but can statistically break the drought, missing the point of detecting its occurrence. SM, however, tends to have a longer memory, thus being less sensitive to small precipitation

events. The SWDI was designed to better represent the soil water availability conditions and, therefore, track agricultural drought (Martínez-Fernández et al., 2015). We calculated the SWDI based on the root-zone soil moisture product of the Global Land Evaporation Amsterdam Model [GLEAM v3.2b, (Martens et al., 2017)]. The GLEAM product is provided daily at 25 km spatial resolution. The modeling approach is based on the surface SM and land cover classes, assuming three depths (0-10, 10-100 and 100-250 cm), at which crops fall into the 10-100 cm layer. In fact, according to Franchini et al. (2017), the typical maximum depth for soybeans root-zone is 100 cm for PR. First, we averaged weekly SM and proceeded with the calculation of SWDI as follows:

$$SWDI = \theta - \theta_{FC} * \theta_{AWC} \quad (2.2)$$

where θ is the root-zone SM, θ_{FC} is the field capacity and θ_{AWC} is the available water content. According to Martínez-Fernández et al. (2016), the parameters θ_{FC} and θ_{AWC} is calculated statistically based on θ percentiles within the growing season as follows: θ_{FC} is the 95th and Wilting Point (WP) is the 5th percentile, finally, $\theta_{AWC} = \theta_{FC} - \theta_{WP}$. Figure 2.2 shows for each region the time-series of SWDI and all the other remote sensing-based variables used in this study.

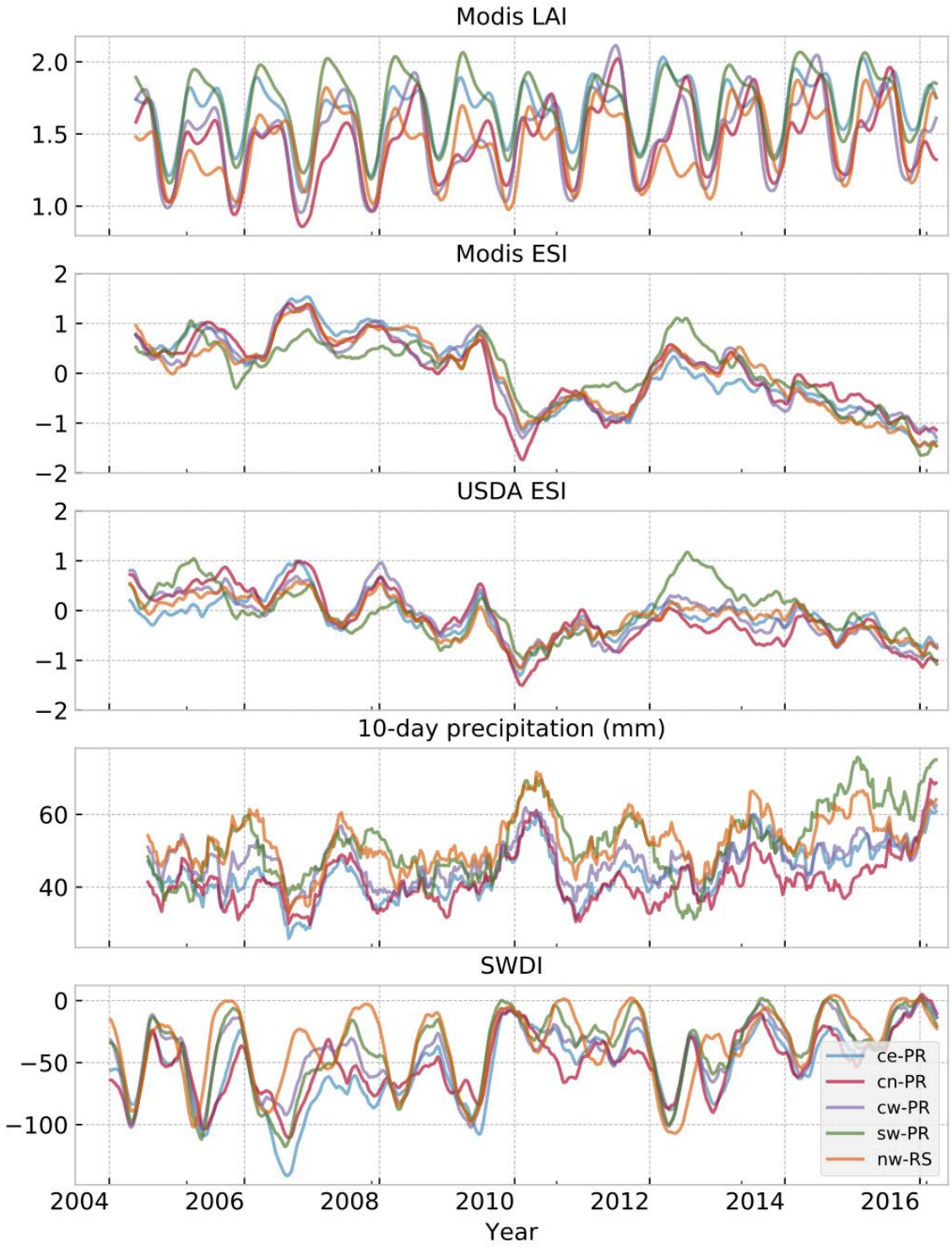

Figure 2.2: Time-series of MODIS-ESI, MODIS-LAI, USDA-ESI, precipitation and SWDI for each region. For display purposes, the resampled weekly (or 8-day) data are averaged by a 30-week rolling window.

2.4 Methodology

2.4.1 Datasets preparation

All the MODIS images were submitted to a time-series filtering process to remove/reduce data gaps and unexpected peaks producing smoother time-series. The procedure is necessary to avoid observation gaps and outliers mostly due to cloud-coverage, which is usually intense during the summer in the region (Eberhardt et al., 2016). We chose a 5-period moving average (two before and two after) as this was proven to maintain the seasonal shape of the series without altering the main features. This step is also critical for the phenology analysis described in Section 2.4.2 (Sakamoto et al., 2010; Shao et al., 2016; Verger et al., 2016).

For the comparative analysis, we prepared time-series of *z*-scores at a pixel *i, j* for a period *w* (weekly or 8-days, depending on the product). *Z*-scores have the advantage over raw or anomalies data for being inter-comparable between variables and, the property of having less seasonal effects, which is important for multivariate time-series analysis. Traditionally, *z*-scores are calculated based on deviations from the mean; however, we chose the median for being less sensitive to extremes and proceeded with the calculation as:

$$z(w,y,i,j)' = \frac{\langle v(w,y,i,j)\rangle - M\langle v(w,y,i,j)\rangle}{\hat{\sigma}(w,i,j)} \tag{2.3}$$

where the first term in the numerator is the current value *v*, the second is the historical median (M) for the period *w* considering all the years *y* and, the denominator is the median absolute deviation. For all the MODIS data, we calculated *z*-scores based on 40-

day accumulation throughout the time-series for each 8-day period, meaning the average of two observations before and two after the reference 8-day period (16 + 8 + 16) and, closely match the methodology used to calculate USDA-ESI (Anderson et al., 2007a), which uses weekly data (14 + 7 + 14). Thus, a given *z*-score data point is computed based on the historical median and standard deviation from the current date and their four immediate neighbor periods (two periods before and two after) as a way to smooth the time-series to reduce the impact of outliers (due to observational issues such as clouds). For SWDI and precipitation, we calculated weekly *z*-scores based on a 35-day period. Finally, to extract data from the images, we averaged pixels within the regions for each date. The MODIS-ESI, MODIS-LAI and USDA-ESI data were masked for soybeans, which is feasible for the MODIS spatial resolution (500 m) and marginally for USDA-ESI (5 km). For precipitation and SWDI, the extractions were performed over all the pixels within the regions based on their administrative boundaries regardless land use, as the spatial resolution is too coarse to resolve the local spatial heterogeneity.

2.4.2 Phenology analysis

In our study, phenological metrics are necessary to define the period of analysis and understand the timing effects of drought on crops. The essential phenological metrics for this study are related to the period when drought can severely impact crops leading to potential yield loss. For this, we detected start of the season (SOS), which determines the onset of the green-up phase. For soybeans, it is related to the cotyledon stage and, for a hypothetical LAI temporal curve, the SOS is the point in time when LAI starts to increase marking the vegetative stage onset. We also detected the peak of the season (POS), which is equivalent to the maximum LAI along the curve and, which is related to the soybean's

pod development phase, which occurs during the reproductive stage. After the POS, there is still water demand from the plant during the grain filling phase, which lasts typically two to three weeks and the end coincides with the beginning of LAI decreasing section of the curve, characterizing senescence. A similar approach was taken by Sakamoto et al. (2010), relying on variation of NDVI to detect phenology features for corn and soybeans in Nebraska, United States. In our study, the POS dates are used as the reference to correlate LAI with drought indicators as described in Section 2.4.5, as maximum values of VIs are often used to correlate with crop yields (Bajgain et al., 2015).

2.4.3 Meteorological drought detection

Once the phenological metrics were retrieved, we delimited the period of analysis for precipitation, which usually varies from region to region. To quantify precipitation, we considered the period that includes the month prior of SOS to the month of POS, which based on our exploratory analysis totals four months. For this, we summed the monthly precipitation *z*-scores within the season in a pixel basis for each year/season. Values of *z*-scores rarely fall outside of the range of [-1.6,1.6]. Therefore, we considered totals below -3 ($\mu = -0.75$) as severe drought and close to -4 as extreme ($\mu = -1.0$). For wet years, the same strategy applies by inverting the signals. To verify the relationship between precipitation *z*-scores and crop yield, we also calculated the Pearson correlation (*r*) for each region (Oya et al., 2004). The proposed procedure simplifies the detection of dry and wet years so that we can focus the subsequent analysis on the most extreme occurrences.

2.4.4 Impulse-response analysis

To assess how drought indicators can anticipate the response of our *post hoc* assessment variable, the LAI, we rely on the Impulse Response Analysis [IRA, (Lütkepohl, 2005)]. This is a novel approach for natural sciences (Mariano et al., 2018), although the technique is widely used in econometrics to, in a multivariate time-series system, assess how a shock in one variable impacts another in subsequent periods, independently from the other variables in the system. The lagged analysis allows us, for instance, to verify when the impact is maximum for a pair of variables and therefore, helps on detecting the timing of the highest correlation. The procedure is an extension of the Vector Autoregressive models (VAR) method for multivariate time series, where each variable is a linear function of past lags on itself and the other variables (Lütkepohl, 2005). The VAR approach for this study has Ordinary Least Squares (OLS) linear regression method under the hood; however, applied by lagging variables in relation to each other (Mangiarotti et al., 2012).

Once the VAR model over *z*-scores (less autocorrelation and seasonality, easing time-series analysis) of variables for a given region is set, we proceeded with the IRA. Further, the magnitude of the effects is orthogonalized (uncorrelated), enabling us to assess the effect of each variable on LAI independently from other variables. Although it is known that USDA-ESI and MODIS-ESI have inherently some correlation with LAI, which is at least indirectly part of their design, as LAI is an input for USDA-ESI and MODIS ET calculation (Anderson et al., 2007a; Mu et al., 2011), the IRA analysis still captures other sources of correlation. In short, IRA will elucidate how shocks in precipitation, SWDI and ESIs impact LAI.

2.4.5 Pixel-based lag correlation

A pixel-wise correlation analysis allows us to assess how the variables relate to each other taking into account the spatial resolution limitation since we aimed at verifying the capability of tracking drought. It also allows to assess the patterns on spatial variation, which determines the degree to what the datasets can spatially capture the drought spatial extension. The MODIS datasets have the highest resolution in this study (500 m), whereas USDA-ESI is 5 km and SWDI is 25 km, the lowest. We resampled USDA-ESI and SWDI to the same resolution of the MODIS images using the *cubic spline* method just to allow us to perform pixel-wise comparisons without truly creating new data (Toutin, 2004).

We used the weighted Kendall Tau correlation as a measure of similarity since it takes into account observations with low or high ranking in the data distribution, penalizing those with high rankings (Shieh, 1998). The correlations are calculated between variables having LAI at the POS date as reference and lagging the drought indicators backward in time at the point of maximum impulse-response according to the results of the IRA. Thus, we are correlating datasets from different periods in order to assess how an early drought indicator (at the point of maximum IR) can explain LAI at the POS date, which is a reasonable proxy for crop yield (Tagliapietra et al., 2018).

2.5 Results

2.5.1 Phenology analysis

Figure 2.3 shows the SOS and POS for each region at some specific years and the median LAI for all the period (2002-2016). We choose five years to represent a wide variation in the drought/wet conditions and, therefore, capture the extremes to verify whether phenology metrics shift annually due to precipitation anomalies. As expected,

the lower the latitude, the earlier the SOS. The average SOS date ranged from mid-October (northern regions of PR) to late-November (nw-RS), whereas the POS ranged from late-February (nw-RS) to mid-January (cw-PR). Finally, the time between SOS and POS was around 100 days for the regions in PR and 86 days for RS. The inter-annual changes in regional phenological metric timings are minimal, as the length of the period (SOS to POS) presented has low variation. The average SOS dates found for each region are in accordance to the literature (Esquerdo et al., 2011; Grzegozewski et al., 2016; Gusso et al., 2014; Tagliapietra et al., 2018), regardless of the drought level of a given year. Further, the SOS to POS period is not related to the number of days to maturity, which takes into account the grain filling and later phases in the crop development (Alliprandini et al., 2009) - the POS-SOS period is just a metric for biomass accumulation throughout the plant cycle. Although metrics dates remained consistent, the magnitude of them (LAI values at POS) showed inter-annual variation with smaller amplitude for the regions ce-PR, cn-PR and sw-PR (2.3-2.6, 2.4-3.0 and 2.4-3.1), and higher for cw-PR and nw-RS (2.5-3.5 and 2.7-3.6). The observed LAI amplitudes at the POS dates indicate each regions' sensitivity to hydroclimatic conditions in a given year when farming management practices are not considered.

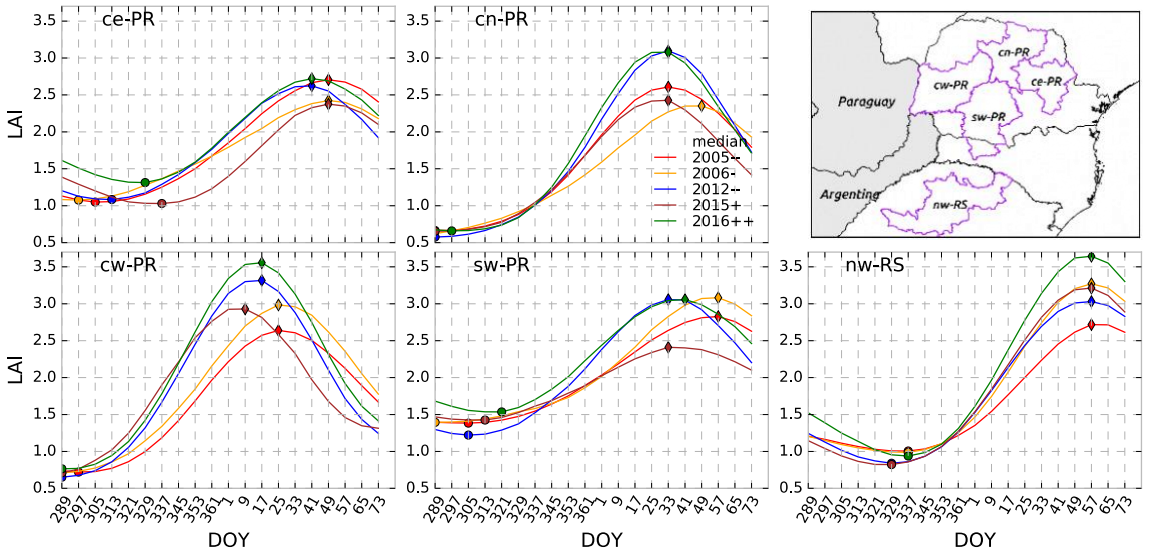

Figure 2.3: Phenology metrics for the five regions. The points on the left side of the curves are the SOS whereas POS are on the right. The median (gray line) refers to all the years (2002-2016). To ease visualization and comparison we smoothed the time-series using a 6-week moving average, standardized the y-axis and chose some representative events to be plotted (Section 2.5.2). In the legend, the signals - and -- indicate severely and extremely dry, whereas + and ++ indicate wet and extremely wet years, respectively.

With the SOS and POS date from each region/year, we finally delimited our study period within the so-called summer growing season, so we proceeded with the meteorological drought mapping for these periods. The POS dates are also later used as the reference for lagging other variables considered in this study. The analysis also gave us an overview of how the LAI curves are shaped for each region allowing us to associate drought-related events to phenology stages.

2.5.2 Drought mapping

The sum of precipitation *z*-scores from October to January for the regions in PR and November to February for RS are presented in Figure 2.4. As noteworthy events, we identified the seasons of extreme drought (2005 and 2012) and severe drought in 2006, whereas the only extremely wet year detected was 2016. On the drought side, negative

anomalies in precipitation have, at least visually, matched the yield losses presented in Figure 2.1, where the soybean yields for the seasons of 2005 and 2012 presented highly negative anomalies. The effects of precipitation on yield seem to be region-specific, as the calculated correlation (*r*) between precipitation *z*-scores and yield for each region implies: cePR = 0.72, cnPR = 0.50, cwPR = 0.79, swPR = 0.89 and nwRS = 0.85. The range of correlations (0.50 to 0.89) highlights two realizations for our study, which are in accordance with Hlavinka et al. (2009) and Lobell et al. (2014) when it comes to crops sensitivity to drought. First, lack of precipitation does not necessarily lead to yield loss; therefore, soil-plant regional characteristics might drive most of the precipitation-yield relationship. Second, the occurrence of more dry than wet years within the period can potentially bias the results towards the adverse effects of drought on yield and the relationship between negative and positive effects are asymmetrical, meaning that crops might not benefit from above-normal precipitation at the same magnitude as drought can damage them. These findings are in accordance with to (Johnson, 2014), which reports that crop yield (for soybeans and corn in the United States) is also related to precipitation distribution over the season rather than just total amounts. Our research did not fully explore the distribution of precipitation to the point of detecting dry spells, instead, we justify our approach considering that precipitation distribution is therefore encompassed in SM-related variables, which has a longer memory than precipitation itself.

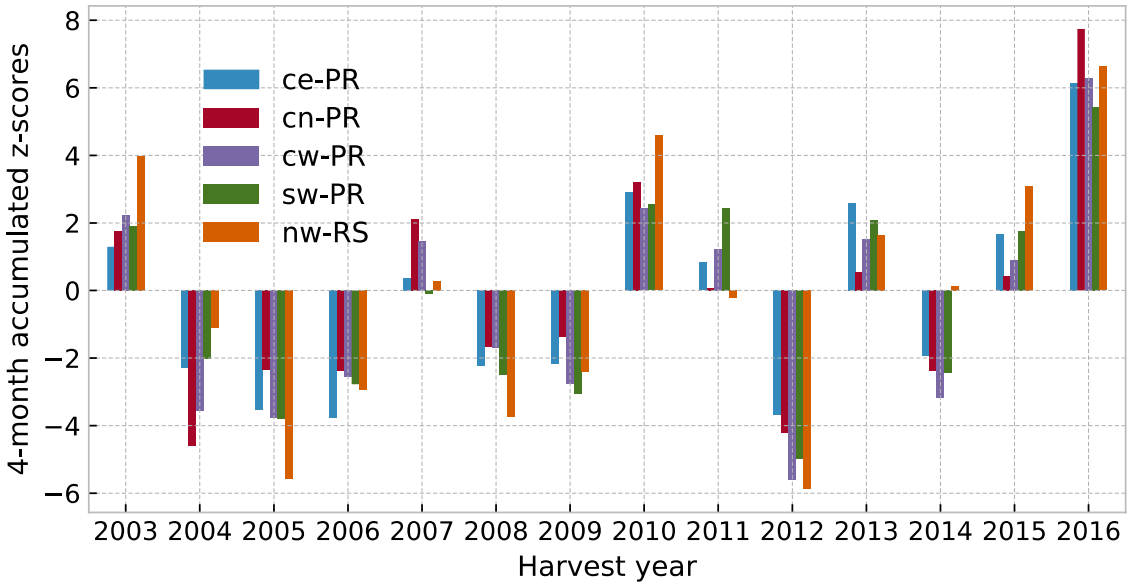

Figure 2.4: Four-month accumulated precipitation *z*-scores by region. The accumulation periods are from October to January for PR and November to February for RS. Negative values are drier years, positive values are wetter years.

2.5.3 Impulse response analysis

Figure 2.5 shows the results of the IR analysis for independent variables impulses on LAI throughout ten weeks of the growing season, as we noted that this period captures most of the interactions between variables and it is enough time for the shock's impacts to dissipate. The *y*-axis is expressed in standard deviation (σ), meaning that one unit of σ impulse on *variable A* causes *y* σ response on *variable B* at the *x*-weeks lag. USDA and MODIS ESI presented the higher values for responses on LAI, with peaks observed in region cw-PR at five and four weeks for USDA-ESI and MODIS-ESI, respectively. USDA-ESI reached peaks of IR at longer lags than for MODIS-ESI and, in the case of ce-PR and sw-PR these effects were not clear (low magnitude and therefore, long lagged response, which highlights the inability of the analysis to capture the phenomenon). Thus,

we can summarize the ESI analysis as having regional effects, such as the ability to anticipate impacts on peak LAI at a four- to five-week lead period for the regions cw-PR, cn-PR and nw-RS. In our methodology, both ESI products were masked for crops and, this is potentially a factor pointing out the limitations of the datasets on capturing the spatial heterogeneity of the regions sw-PR and ce-PR. In Figure 2.1, these regions have the crops that are more sparsely distributed. As reported by Anderson et al. (2016), the highest USDA-ESI/LAI correlations were observed on a state scale, which led us to suspect that spatial resolution might play a role in our analysis (at sub-municipality level).

For SWDI the responses magnitude was smaller than for ESI. The sw-PR and cw-PR regions showed the highest peaks of SWDI at five and three weeks respectively, whereas the responses for the other regions was weak and unclear, indicating that the SWDI dataset failed at detecting drought. The analysis of SWDI poses an unusual result for the lead time of SM anomalies impact on vegetation, which were expected to have about six weeks lead time (Adegoke and Carleton, 2002). For the nw-RS, the impulse seems to be dissipated over a long period, or the technique failed to capture the relationship, as it happened on regions ce-PR and cn-PR. These latter regions are composed mostly of high-quality soils (refer to Section 2.3.3), which tend to attenuate the effects of drought due to higher availability of soil water storage in the soybean root-zone. Further, the high heterogeneity of crop spatial distribution makes it difficult for the SWDI to capture the SM dynamics for crops, whereas the same was not observed on cw-PR, which is also a region with high-quality soils, but with lower spatial heterogeneity.

Precipitation has a shorter memory than SWDI and ESI, the other drought indicators considered in this study, with peaks occurring from 1 to 4 weeks. Regarding magnitude, the levels are low due to spatial resolution discrepancies and also for the intrinsic inability of precipitation on correlating with biomass (Hlavinka et al., 2009; Lobell et al., 2014; Samanta et al., 2010). Another factor that plays a role in this relationship is the precipitation distribution, such as the occurrence of dry-spells (not covered in our study), which can have significant consequences depending on the phenological phase where it happens (Hunt et al., 2009). Therefore, the short memory issues for precipitation are not impactful in SWDI or ESI, which is why precipitation-based drought indicators might not effectively explain variability in biomass or yield. It is worthy to observe that the region nw-RS presented comparatively high response to precipitation, which can be explained by the lower quality of the local soils (mostly regular to limited, as shown in Section 2.3.3), with a lower water storage capacity and therefore, relying more upon timely precipitation distribution.

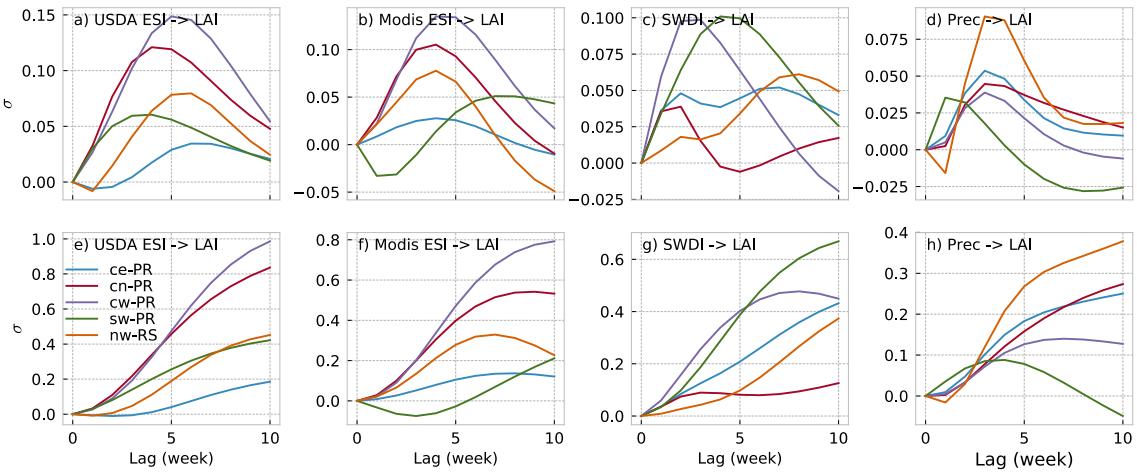

Figure 2.5: Impulse response analysis for variables impacting LAI for each region. The y-axis is presented in standard deviation (σ): the IRA shows how long a shock of 1 σ in one variable takes to dissipate in the response variable. The upper row plots [(a), (b), (c) and

(d)] represent the impulse response function and the peaks indicate the period of maximum response. The bottom row plots [(e), (f), (g) and (h)] show the responses cumulative effects.

Finally, by analyzing the cumulative effects of IR (bottom plots in Figure 2.5), we observed that the most influential variables are the USDA-ESI and MODIS-ESI, then, SWDI and finally, precipitation. In the soil-plant-atmosphere continuum, ET (and therefore ESI) is closely related to the plant response to water and energy availability, thus, exerting more impact than those observed by SWDI and precipitation, although the latter two are the source of water for the whole system. The lack of shock-response observed in SWDI and precipitation may be partially due to spatial limitation of these datasets, which is further assessed in Section 2.5.4.

2.5.4 Pixel-wise correlations

Figure 2.6 shows weighted Kendall's tau correlations between the reference LAI at the POS dates versus the resampled drought indicators at lag-max (period of maximum impulse-response). To account for the range in hydrological conditions, we chose to analyze and present four years (three for drought and one for wet), as found in Section 2.5.2 (2005 and 2012 were extremely dry, 2006 severely dry and, 2016 was extremely wet). This is a three-fold analysis encompassing indicators (ESI, SWDI, and MODIS-ET), degrees of drought (the four chosen years) and geographic regions.

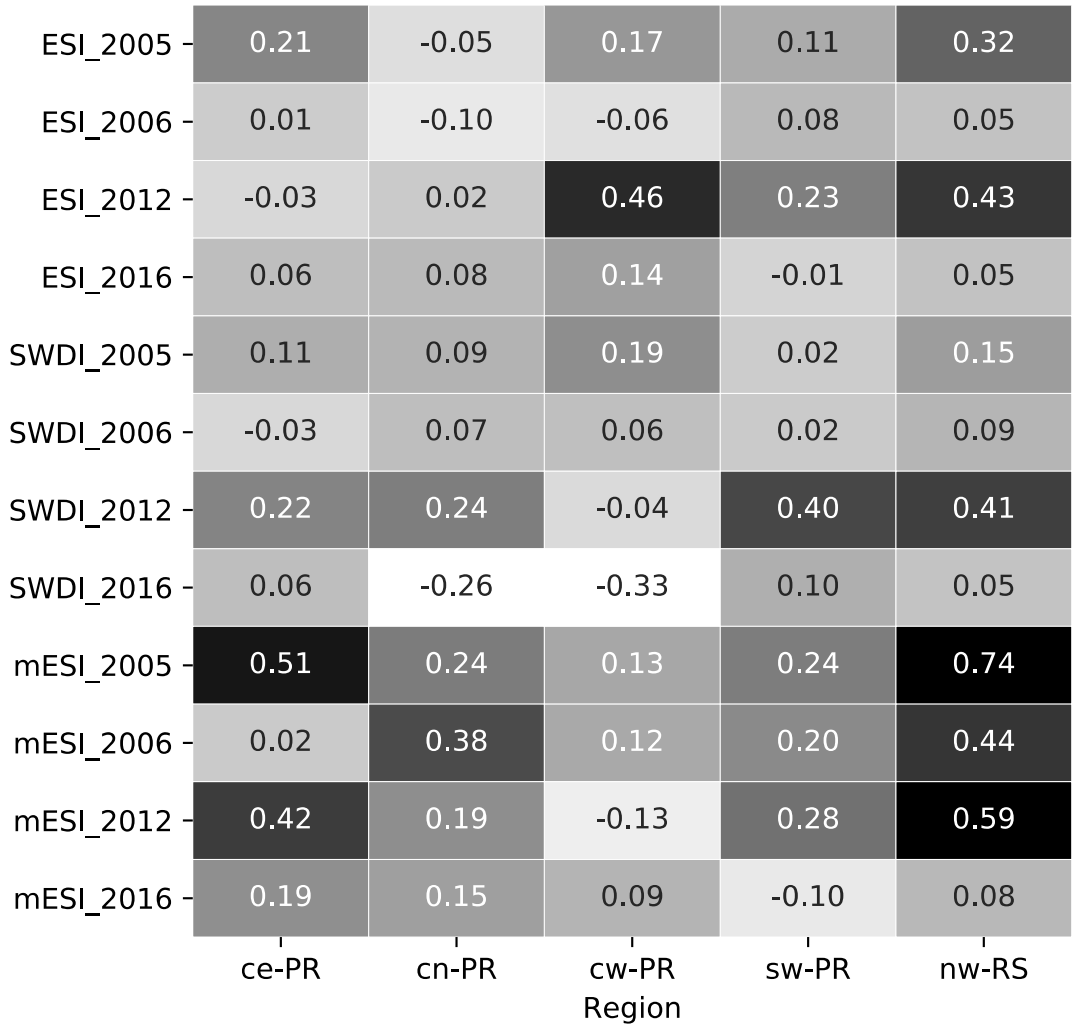

Figure 2.6: Weighted Kendall's Tau correlation at lag-max for ESI, SWDI and MODIS-ESI (*mESI*). As a reminder, 2005 and 2012 were years of extreme drought, 2006 was a severe drought and, 2016 an extremely wet year.

As presented in Figure 2.6, MODIS-ESI showed the highest correlations, followed by USDA-ESI and SWDI. The cases where USDA-ESI (for cw-PR and nw-RS) and SWDI (sw-PR and nw-RS) presented moderate correlations (0.40 to 0.45) occurred in the most extreme drought year for the study period (2012). For MODIS-ESI, most of the cases showed moderate to high correlations (0.36 to 0.75), except for the extremely wet year (2016), which corroborates with the fact that soybean yields are

asymmetrically subject to both dry or wet conditions (Anderson et al., 2016). The ability of the datasets to correlate with LAI is, apparently, closely related to their spatial resolution. Therefore, SWDI and USDA-ESI failed to detect agricultural drought in most regions. The few successful cases (correlations above 0.4) occurred in the extreme drought of 2012, as the effects are geographically widespread and more evident, and the coarse resolution datasets were able to capture the broad and pronounced phenomenon.

Regarding regions, nw-RS presented the highest correlations for both ESI indicators during the drought years. As observed in Figure 2.1, the region is densely covered by crops, which enables the datasets to spatially resolve the targets, as the landscape is more homogeneous than the other regions and, has also lower quality soils, which leads the vegetation to respond more closely to hydrological anomalies. According to Gusso et al. (2014), high temperatures are the primary driver for yield loss in the region, where heat waves eventually occur intensifying drought effects. Therefore, SM plays a smaller role in the local yield as compared to land surface energy balance (ET based indicators), partially explaining the inability of SWDI to detect drought in the region. For the other regions, where spatial heterogeneity is more evident, USDA-ESI and SWDI were less capable of capturing drought effects on LAI, implying that the use of these datasets should be restricted to regional rather than local assessments.

In short, SWDI and USDA-ESI were unable to early detect agricultural drought in most cases, except for a few occurrences in the most extreme events. On the other hand, MODIS-ESI was more highly correlated with lag-max in most of the drought cases (Figure 2.6). That suggests that only MODIS-ESI can be used for early agricultural drought detection at sub-municipality level, with a lead time ranging from 4 to 5 weeks.

To date, at the given spatial resolutions, SWDI and USDA-ESI should have their use restricted to regional drought assessment. In the case of USDA-ESI, recent studies addressed large regions with little discrimination for crop heterogeneity, where the datasets were proven to be effective for drought assessment (Anderson et al., 2015, 2016). To allow local-scale studies, progress is being made towards designing products with higher spatial scales for ET (Semmens et al., 2016; Senay et al., 2016), which we encourage to further assess their capacity for early detection of agricultural drought. The limitations of coarse resolution SM-based products are widely discussed (Loew et al., 2013; Piles et al., 2011) and the authors recommend the use of such data mostly for regional modeling purposes. To overcome these limitations, considerable efforts have been to achieve finer scales for SM products (Crow et al., 2012; Das et al., 2011; Draper et al., 2013; Kim and Hogue, 2012), thus, their usability has to be re-assessed as their quality and spatial resolution increase.

2.6 Discussion

This research study aimed at verifying methods and datasets for early detection of agricultural drought in the southern Brazil, as well as assessing several methods and data limitations. Southern Brazil is often stricken by hydroclimatic hazardous events such as drought, impacting crop yields and, therefore, the local economy. Early detection of agricultural drought has the potential of providing insights for decision makers regarding *commodities* offer, price formation, logistics and insurance planning. We relied on remote sensing datasets that capture anomalies in root-zone SM, ET and LAI, the latter as a *post hoc* vegetation condition assessment. We analyzed the summer seasons from 2004 to 2016, from which we delimited the growing season through LAI time-series phenology

analysis. We proceeded with lagged correlation investigation to assess how drought indicators can early detect events based on the IRA approach. Finally, we assessed the datasets limitations on detecting drought due to their spatial resolution, which is a severe hurdle for their usability at local scales.

The phenology analysis showed that SOS and POS dates are not related to drought occurrence, which led us to conclude that management practices (sowing dates) tend to regulate the average SOS date and therefore, the POS dates are predetermined by the soybean variety maturity group (Alliprandini et al., 2009). We mapped drought occurrence based solely on precipitation *z*-scores for the period ranging from the months of SOS and POS, totalizing four months for all the regions. We identified a severe drought in 2006 and, extreme droughts in 2005 and 2012 for all the regions. This tells us that drought effects in the SB are widespread, however, with different regional impacts for vegetation. In some cases, like for the regions cw-PR and nw-RS on 2012 drought, however, the LAI levels at the POS date dropped significantly as a result of the slower rate of biomass accumulation. Such effect is usually expected to turn into yield loss (Anderson et al., 2018; Cirino et al., 2015; Gelcer et al., 2013) - La Niña years tend to lead to drought in the SB, potentially affecting crop yields. What is alarming is that in addition to the three severe/extreme drought events, we detected four other moderate drought occurrences, adding up to seven drought years in a 14-year period, which were all not related to La Niña events. As a result, the correlation between soybean yield and precipitation anomalies varies by region, ranging from 0.50 to 0.89, with an apparent pattern of correlations increasing southwards, where lower quality soils characterize the area. Although climate change scenarios studies predict an increase in precipitation totals

for the SB in the next 40 years (Ribeiro Neto et al., 2016), the high frequency of droughts observed in our study period (7 out of 14 years) led us to be less optimistic about the projections for this region. Still, if models indicate an increase in annual precipitation at the same as the frequency of droughts also increases, implying that precipitation intensity would increase, making the distribution more narrowly distributed. Therefore, we would likely have problems of drought and inadequate distribution of precipitation in wet years, which can also have a negative impact on crops in SB.

The core of the current research was to identify how drought indicators can anticipate the effects on soybean yield. As expected, both USDA-ESI and MODIS-ESI achieved higher IR with LAI for three to five weeks lead time (Anderson et al., 2015, 2016). ESI relies on the surface capacity of meeting the potential ET given that adequate nutrient/water/radiation is supplied to the plant, therefore, a low ET/PET ratio indicates that the surface (and the plant) has failed at transferring water to the atmosphere; in the case of drought occurrence, this ratio tend to be low due to the tension at which water is retained in the soil, making it difficult for the plant root to extract it.

SWDI, which was expected to have longer lead time due to its nature in the soil-plant-atmosphere continuum, failed at describing the relation due to spatial resolution limitations on resolving the local heterogeneity, which varied among the regions. The range of IR peaks considering all the drought indicators goes from 3 up to 5 weeks prior the POS date; in the local soybean phenology cycle these periods can be equivalent to most of the early reproductive stages (R1 to R6), which are highly dependent on water availability (Farias et al., 2001). The peak IR for the datasets occurs at crucial stages for the crop concerning water needs.

To date, given the spatial resolution of the globally available datasets, we would recommend the use of USDA-ESI and SWDI to be restricted to regional monitoring, whereas MODIS-ESI use is encouraged at the local scale. In a drought monitoring system design, the spatial resolution would dictate the extent to what each of the chosen datasets can address the targets. In our ideal system, SWDI would address drought at a regional level with a long leading period, but with low reliability. Then, USDA-ESI at a municipality level, as it proved be an earlier indicator (as compared to MODIS-ESI) for some regions. Finally, MODIS-ESI would be related directly to crops rather than landscape, being closer related to the municipality level yields. This is a way of respecting each dataset limitation but taking into account their capabilities. Agricultural drought should use a holistic approach to deliver regional and local level information for decision makers in a timely manner.

2.7 Conclusions

Monitoring agricultural drought in tropical/sub-tropical regions is a challenging task because frequent cloud coverage hampers the usability of freely available higher resolution images (*e.g.* Landsat, Sentinel, China–Brazil Earth Resources Satellite (CBERS)) and, such temporally-limited data hardly capture crop dynamics. We addressed the drought problem with datasets usability in mind, recognizing their limitations but also extolling their capabilities. We analyzed datasets ranging from 500 m to 25 km spatial resolution and up to an 8-day temporal resolution. We concluded that ET, the variable that encompasses most elements related to crop development in the soil-plant-atmosphere continuum, is most capable of the variables assessed for early detecting agricultural drought more efficiently (represented by ESI, an ET stress indicator). The use

of MODIS-ESI is strongly recommended for such a task, as it has a long record of validation and application across a variety of biomes and, it has the potential of continuity through the NASA/NOAA - Suomi NPP Visible Infrared Imaging Radiometer Suite (NPP-VIIRS) (Hulley et al., 2018). Although a longer lead time can be potentially achieved with SM related products, its value is dependent on developing finer spatial resolution products; therefore, SWDI failed at delivering useful insights on agricultural drought. SM is most appropriate for regional scale analysis, but downscaling efforts could improve its applicability at more local scales. USDA-ESI and MODIS-ESI provided up to 5-week lead time for agricultural drought signals and this information is of great relevance for decision making. We encourage the development of MODIS-ESI based products tailored for a variety of stakeholders in the agricultural chain to enable data-supported decisions. We also expect improvement of USDA-ESI spatial resolution by incorporating new datasets (such as active sensors), and the re-assessment of this product capabilities.

Developing strategies for detecting/mapping and even predicting agricultural drought is of great relevance for a variety of stakeholders in the agricultural chain. Grain traders might take advantage of such information by potentially predicting the soybean offer in the local market (although the grains might already be negotiated/sold), which might affect prices and impact logistics (transportation and storage). At the government level, since credit is often provided and regulated by the government, timely information is therefore helpful on understanding the possible financial outcomes of the drought for the farmers and expecting potential defaults. Insurance companies might take advantage of early drought indicators by preventing moral hazard (the unwillingness of the farmer

to comply with the insurance contract once it is signed), making the contracts more transparent, preventing defaults and therefore, allowing the companies to lower the premium and popularize the adoption of agricultural insurance.

CHAPTER 3.

USE OF REMOTE SENSING INDICATORS TO ASSESS EFFECTS OF DROUGHT AND HUMAN-INDUCED LAND DEGRADATION ON ECOSYSTEM HEALTH IN NORTHEASTERN BRAZIL

Abstract:

Land degradation (LD) is one of the most catastrophic outcomes of long-lasting drought events and anthropogenic activities. Assessing climate and human-induced impacts on land can provide information for decision makers to mitigate the effects of these phenomena. The Northeastern region of Brazil (NEB) is the most populous dryland on the planet, making it a highly vulnerable ecosystem especially when considering the lingering drought that started in 2012. The present work consisted of detecting trends in biomass [leaf area index (LAI)] anomalies as indicators of LD in NEB. We also assessed how the loss of vegetation impacts the LD cycle, by measuring trends in albedo and evapotranspiration (ET). LAI, albedo and ET data were derived from MODIS sensors at 8-day temporal and 500 m spatial resolutions. For precipitation anomalies, we relied on CHIRPS-v2 10-day temporal at 5 km spatial resolution data. For detecting trends, we applied the Theil-Sen slope analysis on time series of MODIS LAI, albedo and ET images. Trend analysis was performed for the periods ranging from 2002-2012 (no severe droughts) and 2002-2016 (including the last drought). LAI trends were more pronounced and had a stronger signal than ET and albedo, therefore, LAI was our choice for mapping LD. The first analysis highlighted the human-induced LD prone areas whereas the last detected drought-induced LD prone areas. Considering only the trending areas, which

was about 23.4% of the total, 4.5% of this area has undergone human-induced degradation whereas drought was responsible for 73%, although, not mutually exclusive. As reported in the literature and official data, grazing intensification might be a factor driving human-induced degradation. We noticed that the range of variation of LAI is narrow and even narrower for albedo, which demonstrates that land surface response is more influenced by soil reflectivity rather than the characteristic sparse vegetation coverage (LAI ranging from 0.04 to 0.4 in the Caatinga biome), which can barely alter albedo. Finally, the effects of LD on ET anomalies were assessed by Granger causality and impulse-response analyses as means to link land surface feature changes to the hydrological cycle. Albedo had a slightly weaker impulse than LAI on ET whereas precipitation played a major role. These relations are site-specific and, land surface features (biomass and albedo) had a more substantial influence on ET in severely degraded areas. We concluded that drought led to trends indicating LD prone areas in NEB and the degradation cycle has positive feedback derived from ET reduction resulting in an increased net moisture deficit, although the latter statement has yet to be further investigated. The study warns of the desertification risk that NEB is facing and the need for the authorities to take action to mitigate degradation and drought effects on both traditionally surveyed (desertification nuclei) and newfound LD prone areas. We also highlight the limitation of confirming LD, as to date there is no post-drought data available and, lessons learned from the Sahel case make us cautious about claiming that an area is in fact degraded.

3.1 Introduction

Desertification is defined by the United Nations Convention to Combat Desertification as *"land degradation in arid, semiarid, and dry subhumid areas resulting from various factors, including climatic variations and human activities"*, within this context, land degradation (LD) is therefore defined as *"the reduction or loss of biological or economic productivity"* (UN, 1994). This interdisciplinarity definition leads the scientific community to take more integrative approaches to address the problem, considering both climate change and sustainable development, as discussed in a review by Reynolds et al. (2007), drawing special attention to drylands, which typically have low fertility and sparse vegetation coverage characterizing a fragile ecosystem. In a comprehensive work of simulations, Huang et al. (2015) argue that enhanced warming, population growth, and higher aridity will likely increase the risk of LD and, to an extreme extent, desertification. Further, the drylands in developing countries are more sensitive to climate change due to anthropogenic pressure and dependence on local natural resources – poverty is likely to increase, therefore feedbacking pressure on drylands leading to soil erosion, and eventually, desertification (Jiang and Hardee, 2011; Reynolds et al., 2011).

All the factors mentioned above are present in the Northeastern region of Brazil (NEB), the most populous dryland region in the world, with more than 53 million inhabitants and a population density of about 34 inhabitants per km^2 (Marengo et al., 2017). It is highly vulnerable to both environmental and anthropogenic LD, as observed (Oyama and Nobre, 2004). More than 10% of the area experienced intense environmental degradation processes, showing the vulnerability of the Caatinga - the local predominant

xeromorphic biome - to climate hazards, and more specifically to drought. During the period of 2011-2016, a severe, long-lasting drought has taken place in NEB, drawing the scenario for high degrees of LD (Gutiérrez et al., 2014; Marengo and Bernasconi, 2015). Simulations for climate change scenarios of global warming show that the future of the NEB may be compromised, which draws attention to the LD problem and its apparent irrevocability (Huang et al., 2017; Marengo et al., 2016).

Privette et al. (2002) and Fensholt et al. (2004) validated MODIS Leaf Area Index (LAI) with *in situ* measurements in semiarid regions of Southern Africa Kalahari and the Sahelian zone of Senegal finding strong linear relation with Normalized Difference Vegetation Index (NDVI) and characterizing phenological variability; considering the regions where the studies were carried out, LAI is potentially a good indicator for biomass loss and, therefore, LD assessment. Surface albedo as an indicator of soil exposure is often used to assess LD on arid regions. The study carried out by Oyama and Nobre (2004) relied on integrating albedo and vegetation cover fraction trends to simulate LD effects leading to precipitation reduction. A comprehensive and prominent approach was taken by Pan and Li (2013) on desertification detection by coupling NDVI and albedo information based on Landsat data, in which they could assess degradation and its intensity levels. Samain et al. (2008) thoroughly investigated albedo variability to associate it with degrees of desertification in Sahel, supporting the fact that increased albedo may affect drought occurrence and leverage LD.

Assessing LD over large areas is an issue commonly addressed by trend analysis of long-term biomass-related and environmental remote sensing based data. Vicente-Serrano (2007) analyzed 13 years of high-frequency coarse resolution imagery along with

precipitation anomalies to assess drought impacts on vegetation in the Mediterranean semiarid region. They concluded that drought occurrence is the primary driver of interannual vegetation variability based on the aridity of the region. Dubovyk et al. (2013) analyzed time-series of NDVI data to detect negative trends as an indicator of degradation in Uzbekistani irrigated croplands. Eckert et al. (2015) mapped not only LD but grass regeneration, urban expansion, and other land use changes in Mongolia using trend analysis of MODIS NDVI and precipitation. They were able to detect changes even in small-scale areas, which is an important feature to address in smallholder agriculture that characterizes some of the regions covered in this study. One concern about RS-based time-series analysis to detect LD is the strength that the signal has to have to produce significant negative slope and map these trends; moreover, decoupling vegetation persistent changes from interannual variations due to anomalies in precipitation and anthropogenic activities may require ancillary data (Wessels et al., 2012).

Once biomass changes are decoupled from environmental anomalies (mostly precipitation), human-induced LD can be assessed; nevertheless, it is not easily approachable (Evans and Geerken, 2004). Although no long-term remote sensed data exist to depict human-induced land changes, trend analysis based methods have the potential to provide a general idea of such occurrences. For both cases of drought and human-induced LD, no post-drought data are existent for NEB, considering the year of 2017, which makes the LD confirmation unfeasible, as like in the case of Sahel, which still drawing controversy related to LD and desertification processes, as reported by Prince et al. (2007). There are recent studies showing a re-greening behavior in parts of Sahel due to both anthropogenic and climatic reasons, which may weaken the claims of

desertification (popularly thought as an irreversible phenomenon) (Brandt et al., 2014; Dardel et al., 2014; Herrmann et al., 2005; Tong et al., 2017). This illustrates a limitation to the extent one can assess LD; however, LD prone areas based on trends of albedo, biomass and ecosystem health indicators are still identifiable.

Finally, albedo and LAI also play a significant role in the surface energy balance which in turn, is a key driver of evapotranspiration (ET) on partitioning sensible and latent heat fluxes. Charney et al. (1977) simulated albedo changes over semiarid areas to investigate its effect on ET and precipitation; the authors support a link between albedo, vegetation, ET and precipitation as a partial cause for recurrent drought in semiarid regions, which intensifies the effects of degradation. Li et al. (2016) studied the changing global net primary production (NPP) effects on ET, showing a complementary relationship between NPP and ET in arid regions rather than a proportional relationship in humid areas. A review on desertification described two cycles of degradation with losses of vegetation as their starting point (D'Odorico et al., 2013). The first cycle follows increases in albedo and ET; this depends on the regional characteristics of ET contributions to large fractions of total precipitation. The second cycle is simply described by an increase in soil erosion and a reduction in its fertility. In both cases, there are positive feedbacks aggravating vegetation condition, a key trigger for desertification. Nicholson et al. (1998), however, reported that the albedo increase may not be as pronounced as observed by Charney (1977) for the Sahel, because the albedo dynamic is driven by vegetation and precipitation, meaning that loss of biomass not necessarily will lead to higher albedo due to precipitation effects on the surface brightness.

The overarching objective of this study is to develop a solid basis for understanding LD trends in the NEB region for the period spanning from 2002 to 2016. The specific objectives are: (1) to analyze precipitation variation through the study period and highlight drought occurrences, (2) to detect the hotspots of LD prone areas, (3) to detect areas of human-induced degradation, and (4) analyze how LD impacts ET. This study enables us not just to locate hotspots of LD prone areas, but also determine whether human activities are catalyzing these trends and how degradation can potentially contribute to the drought feedback.

3.2 Spatio-temporal domain

The study area is the NEB, which consists of the states of Maranhão (MA), Piauí (PI), Ceará (CE), Rio Grande do Norte (RN), Paraíba (PB), Pernambuco (PE), Sergipe (SE), Alagoas (AL), and Bahia (BA). The NEB comprises the most populous semiarid region in the world (Marengo et al., 2016). The predominant biome (52.5% of the NEB) is the Caatinga [from *tupi* language: *ka'a* (forest) + *tinga* (white)], which is characterized by xeromorphic vegetation, mostly small semi-deciduous trees, shrubs, and low profile grass. The vegetation is highly responsive to climate variations and adapted to various degrees of aridity. The remaining biomes are savanna (Cerrado - 29.4%), Atlantic Forest (10.7%), and Amazon (7.4%) (P. F. da Silva et al., 2017). Our study focuses on Caatinga and Cerrado biomes. Agriculture in the region is mostly for subsistence consisting mainly of beans, cassava, potatoes and pasture (natural vegetation), with low levels of technology and input.

In the NEB, some areas historically have shown remarkable signals of desertification, such as the absence of vegetation and high degrees of erosion. These

areas were then delimited, and classified as groups of municipalities called desertification nuclei (Figure 3.1), so governmental institutions could draw particular attention to them (Perez-marin et al., 2012). The current study was not restricted to these nuclei; nevertheless, we often used them as references.

Regarding climatology, the precipitation regime varies across the region due to a diversity of climate forcings, highlighting the Intertropical Convergence Zone, cold fronts coming from the south and upper air cyclonic vortex. The wet season is usually from November to July, with high regional variability during this period. Excluding the coastal and Amazonian areas, the region is considered semiarid, with evaporative demand greater than precipitation. Normal annual precipitation ranges from 400 mm to 1800 mm from semiarid to coast, whereas potential evapotranspiration rates can surpass 500 mm, leading to a net moisture deficit (Vieira et al., 2015).

The study comprised the period spanning from 2002 to 2016, which allowed us to capture a high interannual precipitation variability and a considerable time-span of data to calculate trends. The study period was constrained by the chosen remote sensing data availability, especially for MODIS/Aqua.

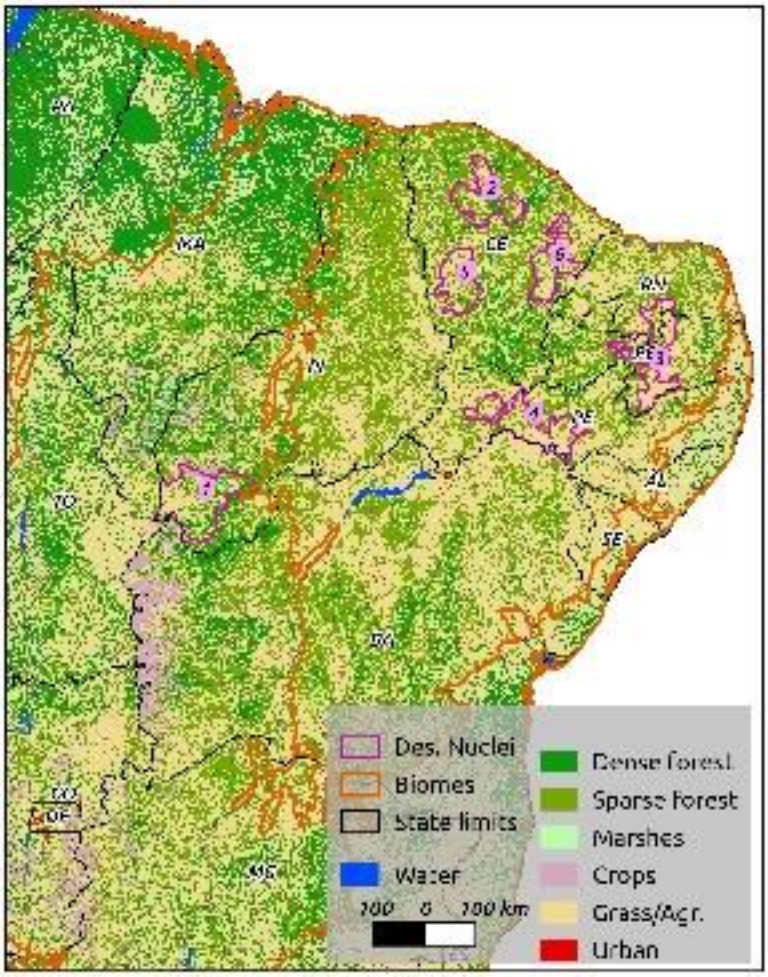

Figure 3.1: Land cover for NEB (source: www.mapbiomas.org)}. The biomes are, from northwest to southeast, Amazon, Cerrado, Caatinga and Atlantic Forest (coast). The Desertification Nucleus are: 1) Gilbués, 2) Irauçuba, 3) Seridó, 4) Cabrobró, 5) Inhamuns and 6) Jaguaríbe.

3.3 Data

3.3.1 Land use

From the MapBiomas project website (www.mapbiomas.org), we downloaded yearly land cover maps based on automatic Landsat imagery classification; the project was launched in 2015 and is recently getting more attention and supporting Brazil-based

studies (Crouzeilles et al., 2017; Noojipady et al., 2017; Tyukavina et al., 2017). These datasets were used to mask remote sensing data by restraining them to natural vegetation (forests and marshes), mixed (grasslands/pasture and subsistence agriculture), and crops (large-scale farming) (Figure 3.1). Although MapBiomas provides yearly data, a quick analysis showed that the classification fluctuates among the chosen classes due to the methodology applied (partially based on NDVI thresholds), which forced us to derive an overall mask that comprises the entire studied period, rather than yearly masks. The mask resolution is finer (30 m) than all the remote sensing data used in this study, eliminating large non-vegetated areas such as urban, dunes and beaches, and water catchments. As reported by Dias et al. (2016) and visually confirmed in the MapBiomas platform, land use changes in the Caatinga were minimal during the 2000-2016 period. Within the NEB region, the most noticeable land change was the agricultural expansion in western Bahia, and to a lesser degree, in western Piauí, both regions are located in the Cerrado biome (Noojipady et al., 2017).

3.3.2 Cattle herd

To support the analysis results and given that traditionally, in most of the considered region, ranching is one of the most important factors that lead to human-induced LD, we considered the yearly cattle herd (bovine, caprine, and ovine) by municipality in the NEB. The data is provided by the Brazilian Institute of Geography and Statistics (IBGE, 2017), which regularly collects information from various sources, such as self-reporting, slaughterhouse and vaccines count data (IBGE, 2002), supporting studies in different fields of knowledge (Millen et al., 2011; Parente et al., 2017; Ruviaro et al., 2014). For our study, we collected herd data from 1991 to 2016; to ease

interpretation, we considered the summation of all the kinds of cattle for each municipality as a rough indicator of density.

3.3.3 Precipitation

We acquired monthly precipitation absolute values and *z*-score data from the Climate Hazards Group InfraRed Precipitation with Station [(CHIRPS-v.2) (Funk et al., 2015)], delivered at 0.05º resolution. Dinku et al. (2018) validated the CHIRPS products for the Greater Horn of Africa, showing the good applicability of these datasets on semiarid regions and the advantages over traditional weather stations. Paredes-Trejo et al. (2017) validated the CHIRPS product for the NEB, showing some accuracy issues such as precipitation detection and, on dealing with extremes by overestimating lower monthly precipitation and, underestimating higher values. They recommended the CHIRPS product due to the poor meteorological station density in the region and the good possibilities of application in drought studies. In our study, the issues related to extreme occurrences were minimized due to the use z-scores for comparative analysis, rather than absolute precipitation values, although we still relying on the latter for discussion purposes.

3.3.4 MODIS data

LAI and albedo: The time series of remote sensing optical data were established from MODIS sensors onboard of the Terra and Aqua satellites, which have been in operation since 1999 and 2002, respectively. The LAI [MCD15A2H, (Myneni et al., 2002)] and albedo [MCD43A3 (Aqua+Terra), (Schaaf et al., 2002)] datasets are delivered at 500 m spatial and 8-day temporal resolutions from the collection 6 (available at

www.reverb.echo.nasa.gov), and are derived from Terra and Aqua combined data. Figure 3.2 shows the statistical distribution of LAI and albedo of the wet period for each region in NEB, based on 15 years time series data.

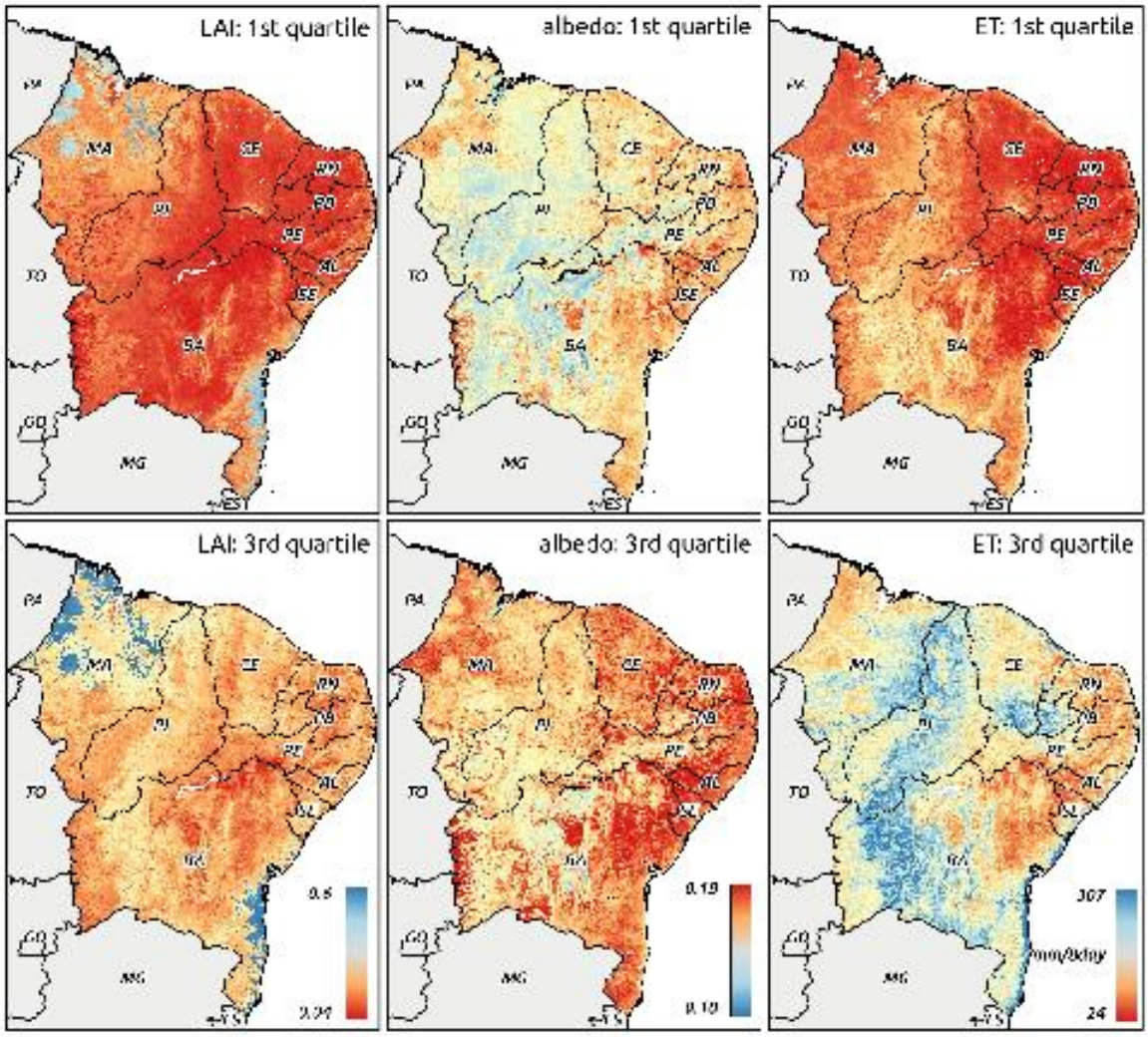

Figure 3.2: 1st and 3rd quartiles for LAI, albedo and ET considering the wet period from 2002 to 2016. The legends for each variable refer to both quartiles.

Evapotranspiration: The MODIS ET product (MOD16A2 and MYD16A2) is computed based on the Penman-Monteith equation by combining Monteith and Priestley-Taylor

methods for potential ET (PET) estimation, with albedo and LAI as input parameters for the surface energy balance partition algorithm (Mu et al., 2007, 2011). In the algorithm, LAI is used to derivate canopy conductance, whereas albedo is used to estimate reflected solar radiation and, therefore, net incoming solar radiation. The MODIS-ET version 6 (released in 2017) has an improvement in spatial resolution from 1000 m to 500 m, delivered at 8-day composites. As part of this study preprocessing, we held MYD16A2 (Aqua) as the main product and filled up the gaps with MOD16A2 whenever available for a given pixel-date.

3.4 Methodology

3.4.1 Precipitation analysis to map drought occurrence

Precipitation drives most of the phenomena analyzed in this study and there is extensive literature about drought occurrences in NEB. Marengo et al. (2016) presents a well-documented review of this matter. The authors emphasized the severity of the event that has started in 2012 for the majority of the region (also confirmed by Bretan and Engle (2017), and Marengo et al. (2017)), which is the only long-lasting drought in our studied period.

Although the drought is well documented, we preferred to run an exploratory analysis to have a more accurate spatiotemporal picture of the studied period. Taking advantage of the drought documentation, that the last five years are considered dry, we divided the entire period into three equal parts. For each of them, we calculated the sum of *z*-scores for the four wet months of each year. Cunha et al. (2015) mapped the region based on its 4-month rainy season; therefore, we based our precipitation *z*-scores and other subsequent analysis on these regions (Figure 3.3).

3.4.2 Mapping trends in remote sensing data

LAI is our primary component on LD prone areas mapping as it is immediately related to loss of biomass, which is understood to be directly affected by climate and human activities. Albedo and ET, in turn, are thought as to partially respond to biomass changes, comprehending part of the LD cycle, as presented by D'Odorico et al. (2013).

For all the MODIS data, we calculated *z*-scores (number of standard deviations from the mean in a data point) based on 40-day accumulation throughout the time-series (historical averages and standard deviations) for each 8-day period. Thus, a given *z*-score data point is calculated based on the historical average and standard deviation from the current date and its four immediate neighbor periods (two periods before and two after), where each period is 8-day long.

To detect trends in time series of MODIS *z*-scores data, we relied on a pixel-based Theil-Sen slope analysis, a non-parametric median based technique not subjected to the linear regression assumptions. The method calculates trends in sequential data and is often used in remote sensing studies (Higginbottom and Symeonakis, 2014). The fitted slope line indicates the rate at which the variable is changing over the timescale and, therefore, the intensity of the trend. As observed by Wessels et al. (2012), a considerable signal in an indicator (e.g., NDVI) is needed to produce a negative trend that can be characterized as LD. The initial and final years of a time series are likely to influence trend retrievals heavily; this is a limitation of our study due to the nonexistence of post-drought data. It is worth reminding the reader that the objective of this study is to detect trends within the analyzed period, assuming the limitations given by the backloading of drought at the end of our time series. That being said and taking advantage of the Theil-

Sen method's ability to deal with outliers; we can define the LD detection procedure regarding Theil-Sen slopes for this study as follows:

1. The most extreme value (either positive or negative) sets the range of the scale, therefore, the no-trend will be always centered at zero;
2. The data itself will determine the trends' thresholds. We define, for this study, that the values outside of the $\mu \pm \sigma$ are considered as trends for the side at what the distribution is skewed; then, the value is reflected into the other side of the distribution;
3. The slope is subject to the data and, to the time-series length - longer series may produce flatter slopes, as observed by Wessels et al. (2012). That is why we let the data distribution itself determine the trends' extremes.
4. The slope indicates the rate of change in *z*-scores, which facilitates the intercomparison between variables (LAI, albedo and ET).

Considering we separated the period of analysis into pieces according to precipitation distribution, we were able to focus on detecting monotonic trends within each period or a combination thereof. Finally, we restricted the datasets to the wet period (4 months) of each region (as described by Cunha et al. (2015) and shown in Figure 3.3) and, run the Theil-Sen algorithm. The processes were carried out twice for each variable: *i)* for the entire series (2003 to 2016) and, *ii)* for the period before the drought of 2012 (2003 to 2011). The analysis over the entire period gives us the panorama of degradation considering the last great drought, whereas the second analysis highlights areas that have shown degradation signals prior to the drought, indicating non-climate induced LD. Given our definition of LD detection for this study, the results are visually comparable, as

the color bars are tied to the extremes provided by the data and centered at zero (Figure 3.4). By visual analysis, in addition to the desertification nuclei, we highlighted regions where negative trends are strong and dense (avoiding salt-and-pepper pattern). Finally, we extracted time series data for the highlighted regions and the desertification nuclei for further analysis by averaging pixels values within these areas. The nuclei are given as groups of municipalities, so, the highlighted regions were also aggregated having municipalities as the smallest unit. Some degradation areas coincided with parts of the desertification nuclei, in these cases, we aggregated one to another.

3.4.3 Time series analysis

Working with *z*-scores eases the comparison between variables, takes into account the richness of a long time series, and removes seasonality. We extracted MODIS *z*-score times series for each of the regions mapped by the methods described in Section 3.4.2 and used them as input for the following procedures.

To test for the hypothesis of trend existence, we used the Mann-Kendall (MK) non-parametric test as a function of the ranks of observations, making it is less sensitive to outliers since the function is not based on the actual observations (de Jong et al., 2011). MK test outputs *z*-statistics and p-values; then it considers the ascending trend a $z \geq 1.96$ and descending trend a $z \leq 1.96$ at $\alpha = 0.05$ significance level, as recommended by Fensholt and Proud (2012) in a study with similar methods. We used MK tests to verify trends in time-series of LAI, albedo, and ET; however, we focused on LAI to lead the analysis as it is the primary indicator of LD, as we are interested in biomass reduction effects on land. Another particularity of this study was that the MK tests were performed

over all the data (not restricted to the wet season). We applied the MK tests for all variables for each chosen region for the 2002-2011 and 2002-2016 periods.

Both MK tests results and visual analysis of *z*-scores time series for all variables for each region underlie our analysis on LD processes taking place in NEB. We carefully interpreted these results and relied on the literature and local reports to support our findings.

3.4.4 Cattle population trend analysis

To support the discussion about human-induced LD, we designed a simple analysis of cattle population trends using yearly municipality data, ranging from 1991 to 2011. As stated by Lambin et al. (2001), *"rangeland has a natural carrying capacity for livestock, and exceeding this causes degradation especially in tropical and subtropical zones"*. It is noticeable that period of this analysis does not match the pre-drought period (2002 to 2011). The reason to consider earlier data (e.g., from 1991) is that headcount may not necessarily incur in immediate overgrazing, even in extensive ranching. However, in the long term, any existing trend, if present, tend to be more robust and not suffer from the limitations of analyzing trends in short time series. The period ranging from 1991 to 2011 has few drought occurrences reported for 1992-1993, 1997-1998, 2001-2002, 2005 and 2010; however, no long-lasting drought was reported for the period (Marengo et al., 2017). This allows us to understand cattle headcount trends as an effect of human activities, rather than climate. Our analysis consists of running MK test to detect and measure trends in cattle headcount from 1991 to 2011 at the municipality level. The resulting map was then used to support discussion on LD trend maps.

3.4.5 Impacts of vegetation loss on the LD cycle

To understand and measure how a loss of vegetation (as measured by trends in LAI) impacts other components of the LD cycle, we proceeded with a novel approach for multivariate time series analysis. ET is the indicator that aggregates most of the variables in the LD cycle and, therefore, is chosen as our ecosystem health indicator (Anderson and Kustas, 2008; Moran, 2003) - an indicator of the proper functioning of a complex ecosystem. This entire procedure was carried out over *z*-scores of LAI, albedo, precipitation, and ET to reduce autocorrelation and seasonality. For analyzing how LAI, albedo and precipitation impact ET, we used the Vector Autoregressive models (VAR) method. VAR is used for multivariate time series, where each variable is a linear function of past lags on itself and the other variables. The method has been widely used in Econometrics studies to analyze dynamic structures in multivariate time series, with the advantage over traditional Least Squares regression because it takes into account the relationships between variables through time, otherwise, correlations would be overestimated. The VAR approach for this study has Ordinary Least Squares (OLS) linear regression method under the hood; however, applied by lagging variables in relation to each other; an outline of the VAR method equations is presented in Mangiarotti et al. (2012). Once the appropriate VAR model was obtained, we proceeded with the Granger-causality and impulse response analysis (IR).

Causality is defined by Granger (1969) as *"if some other series y_t contains information in past terms that help in the prediction of x_t and if this information is contained in no other series used in the predictor, then y_t is said to cause x_t."* Literature often refers to this relationship as "*X* Granger causes *Y*", as this is just a mathematical causality relation which has yet to be assessed for each specific study. The Granger

method is an extension for time series analysis tools, such as the VAR method; an outline of the Granger causality mathematical derivation is in Detto et al. (2012). We used Granger analysis to assess causality existence of LAI, albedo and precipitation on ET.

Finally, we carried out an IR analysis, as Granger-causality may not be enough to describe how variables relate to each other. IR function measures the response of a variable to an impulse in another variable in a system involving other variables; in short, it shows the system's reaction to a shock (Lütkepohl, 2005). IR analysis can pairwise measure these impulse-response relations through time, allowing us to understand how ET is affected by LAI, albedo and precipitation for the desertification nuclei and the new regions mapped from the trend maps (Figure 3.4). For the IR analysis, the effects values were orthogonalized (uncorrelated), enabling us to assess the effect of each variable on ET independently from other variables, although we know that they are correlated (given the MODIS-ET algorithm design, which has LAI and albedo as input data). For an outline of how the IR analysis is implemented on the top a VAR model, the reader can refer to Fang et al. (2018).

For VAR, Granger-causality and IR analysis, we first resampled the time series data to weekly time-steps applying linear interpolation. The IR analysis was carried out for up to 15 periods (105 days), as that was a reasonable amount of time to capture lag effects between variables. We expressed IR orthogonalized values regarding standard deviation and also cumulative effects.

3.5 Results

3.5.1 Precipitation and drought occurrence

Precipitation was not evenly distributed throughout the analyzed period over the NEB region. Figure 3.3 depicts the accumulated *z*-scores from November to May for each year and the accumulated *z*-scores for each five-year period. As shown, the northern subregions (FMAM and JFMA) presented the most extreme years, either wet or dry as in 2009 and 2012, respectively. Overall, 2009 was the wettest year whereas 2012 was the driest and the latter marks the onset of the last long severe drought, as shown in the bottom-right map (2012-2016). It is worth noting that the CHIRPS *z* -score product showed a narrow range of variation, which is evident in Figure 3.7, when comparing to *z* -scores of MODIS based products. In fact, CHIRPS *z* -score product relies on a 30+ years time series whereas for MODIS we used 15 years, which might affect the *z* -scores' range of variation.

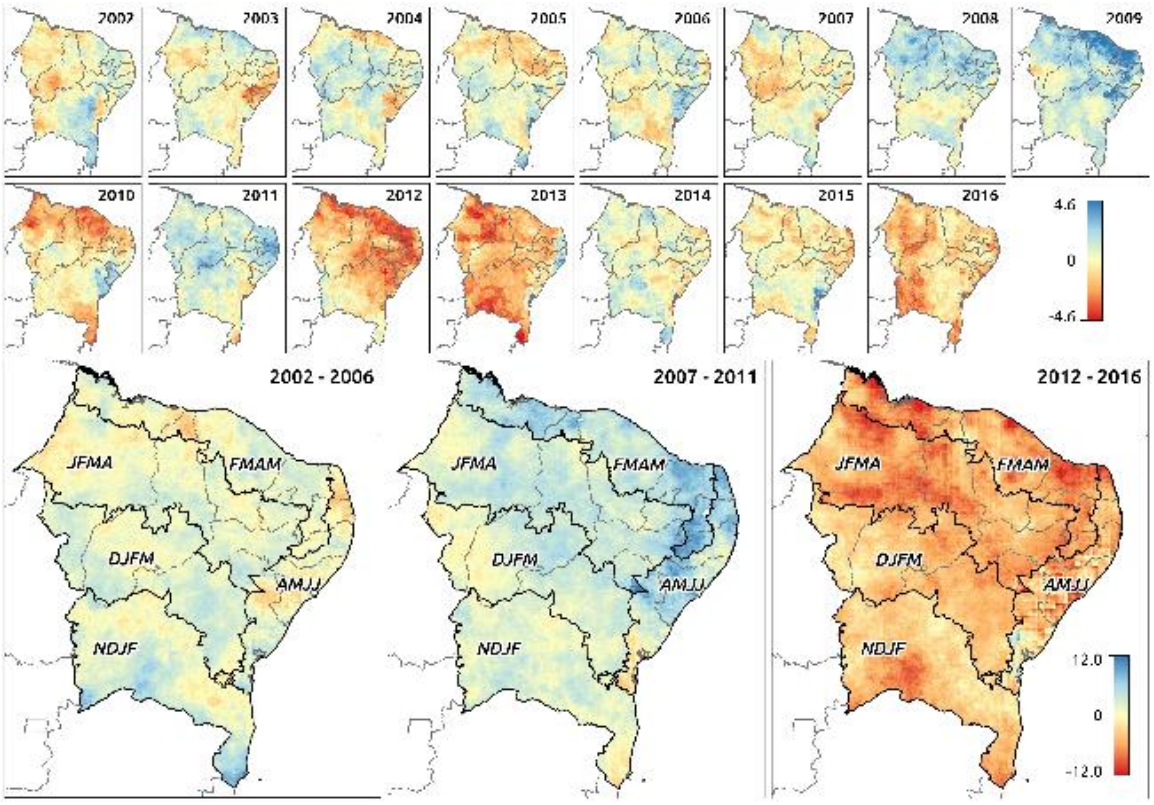

Figure 3.3: Annual maps of accumulated z-scores for the wet months (upper two rows). Five years accumulated monthly z-scores for the wet months. The regions were delimited by their wet season as proposed by Cunha et al. (2015), where the acronyms stand for the rainy months for each region.

As shown in Figure 3.3, the northern regions (FMAM and JFMA) were severely stricken by drought for the period starting in 2012, showing variability signals related to the ENSO cycle in the region. Although a dry year was detected in the second period (2010), it was followed by a wet year; therefore, the period ranging from 2007 to 2011 can still be considered wet on average. By combining the first two periods (2002 to 2011), no long-lasting drought occurrences were detected. Thus, these results are essential to our understanding of human-induced LD, since no substantial climate impacts were present. In short, the precipitation anomalies analysis agreed with the studies of (Brito et al., 2017; Marengo et al., 2016; Marengo et al., 2017).

It is known that the incidence of precipitation in the NEB is intrinsically related to the Ocean-Surface-Atmosphere interaction. These physical and dynamic interactions induce complex climatic systems in which they are mainly linked to the Sea Surface Temperature Dipole (SST Dipole) and are associated with events such as El Niño-Southern Oscillation (ENSO), the Intertropical Convergence Zone (ITCZ), Eastern Waves (EW), characteristic teleconnections, such as the Pacific Decadal Oscillation (PDO), the Atlantic Multidecadal Oscillation (AMO) and the Madden-Julian Oscillation (MJO). Finally, depending on their phase of positive or negative behavior, the average annual climatological precipitation level tends to be above or below the historical average, respectively (Marengo et al., 2013; Uvo et al., 1998). Additionally, in the NEB, dry conditions appeared in 2012/2013 due to an active role of the South Atlantic high-pressure system, which determined the low-level subsidence and anomalous downward motion that impacted the precipitation regime in the study region (Marengo et al., 2013; Rodrigues and McPhaden, 2014).

3.5.2 Trend maps and LD occurrence

Theil-Sen slope regression maps for the periods of 2003 to 2011 and 2003 to 2016 are presented in Figure 3.4. Additionally, Figure 3.6 shows the total detected areas by period based on *z*LAI trends. With an initial focus on *z*LAI maps, we identified few regions showing degradation trends before the 2012 drought, with BA1, BA2, PI1 and PI2 being the most evident and parts of ND2 and CERN [northeastern Ceará (CE), western Rio Grande do Norte (RN) and ND6]. These are the regions where we detected decreasing trends of *z*LAI prior to 2012, showing potential signs of human-induced LD. Although there are regions in northern MA and PI states showing negative *z*LAI trends,

we preferred to not include them in the further analysis due to their salt-and-pepper pattern, which can potentially be attributed to noise. The zLAI trend map matches what was observed by Redo et al., 2013 in a study ranging from 2001 to 2009 - gain of woody vegetation in most of the Caatinga, except for a few central regions in BA.

The zLAI trend map for the 2003-2016 period highlights the drought effects on vegetation, as can be seen in Figure 3.4 showing a widespread negative trend for zLAI in a large polygon comprehending all desertification nuclei and the newly highlighted areas (in BA and PI). In fact, a backload of drought in the time series led the trends to be negative; however, the slopes are less steep due to the longer time series (minimum of -0.087 in 2003-2011 and -0.035 for 2003-2016).

The same patterns were not observed in the albedo maps. When referring to Figure 3.2, for the mapped regions, LAI roughly ranges from 0.04 to 0.4 whereas albedo range is much narrower (0.1 to 0.19). The lack of variation in albedo incurs in a lower sensitivity to changes in the surface, leading us to conclude that the albedo response is dominated by soil reflectivity, given that LAI is predominantly low for the region; therefore, changes in LAI have minimal impact on albedo. In the case of ET, when including the dry period, the effects of LAI on ET are evident in the region delimited by an arc encompassing the CERN, ND3, ND4, and BA2 regions. zET trends map for this period has roughly the same range as the albedo map; however, its pattern matches the LAI map whereas the albedo does not. As observed in Figure 3.5 which pairwise relates variables trends for pixels within the analyzed areas, whenever albedo is involved, correlations are poor due to its positive kurtosis (narrow distribution). As in the Sahel, in our study area vegetation coverage is sparse and the net radiation attributed to

vegetation is low. Therefore, transpiration is more related to energy availability rather than canopy condition and stomatal conductance as described by Boegh et al. (1999), and, changes in albedo are more related to soil moisture/precipitation than vegetation coverage (Samain et al., 2008).

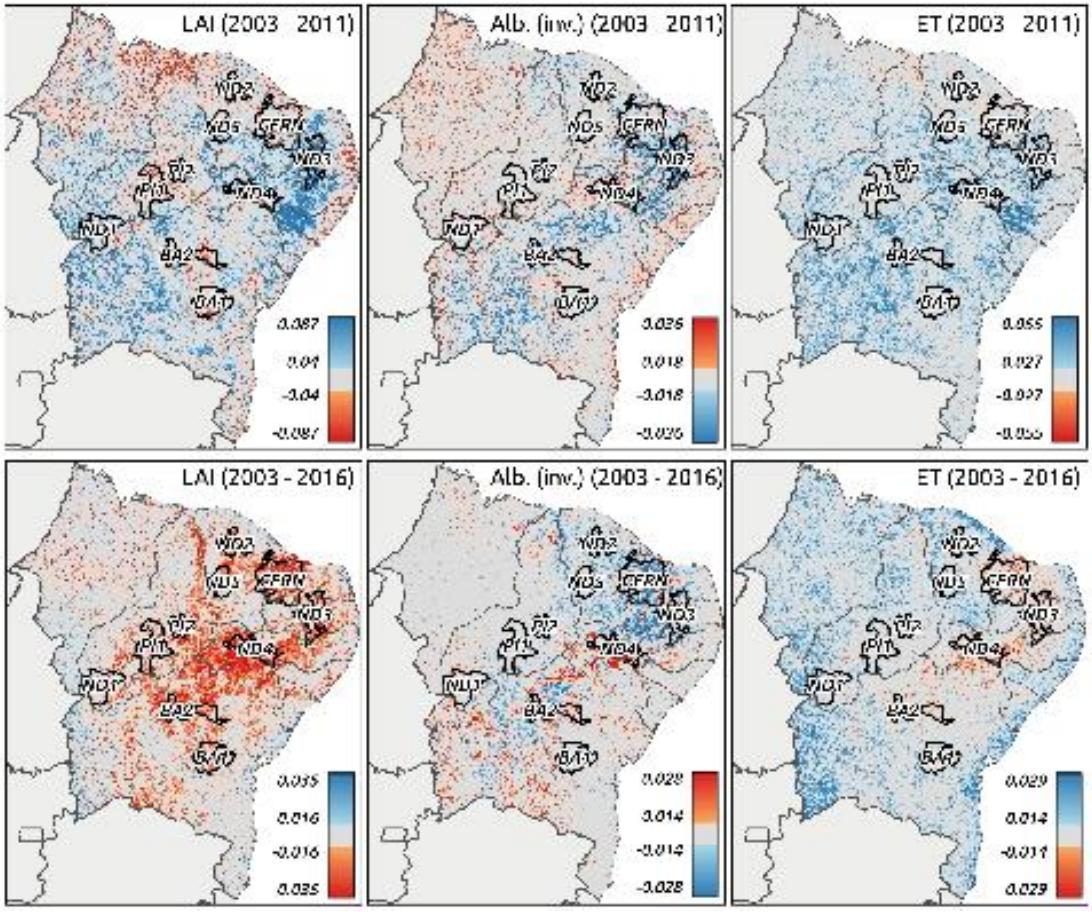

Figure 3.4: Theil-Sen slopes for LAI, albedo and ET z-scores. The color bars are stretched to fit the range of each regression, therefore, allowing comparison between maps. The non-significant trend pixels are masked in grey. Albedo scale is inverted to

ease interpretation.

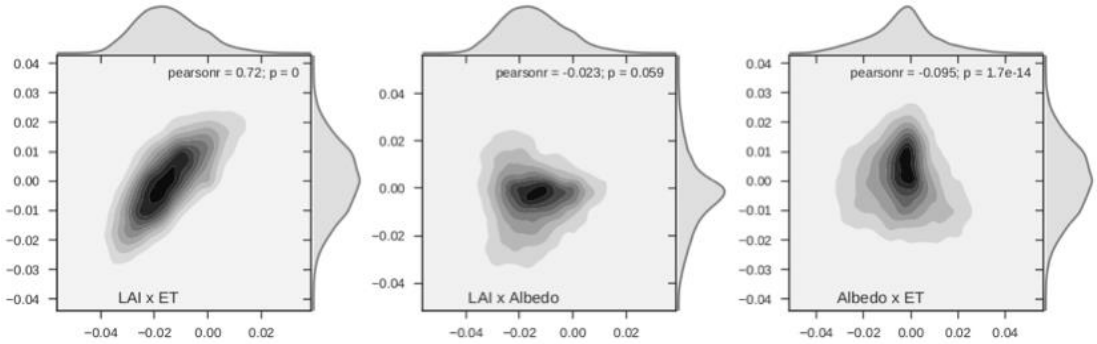

Figure 3.5: Scatterplots for pairs of variables trends within the analyzed areas. The distributions on the top refer to the terms of the left (LAI, LAI and albedo, respectively.

The changes in the median for absolute values for each variable were compared between the pre-drought and full periods, as presented in Table 3.1, values of ET and precipitation are computed as annual totals, and the median is obtained by considering all the years in a given period (pre-drought or full). The percentage change magnitude follows the pattern: ET > precipitation (P.) > LAI > albedo (negligible) for most of the regions, except for ND1 and BA1+BA2. In general, ET changes range from -13% to -26%, while precipitation ranges from -8% to -23% and, LAI ranges from -3% to -18%. ND1 and BA1+BA2 did not experience substantial changes in ET or precipitation; however, BA1+BA2 did experience a change in absolute LAI (-6.3%).

Table 3.1: Percentage changes in the median comparing the pre-drought to the full period.

Region	Period	ET (mm/y)	LAI	Albedo	P. (mm/y)
ND1	2003-2011	626.50	0.17	0.15	1110.94
	2003-2016	631.83	0.17	0.15	1039.15
	change	0.85%	-3.74%	0.40%	-6.46%
ND2	2003-2011	615.15	0.17	0.16	788.51
	2003-2016	472.09	0.15	0.16	647.31
	change	-23.26%	-12.96%	-0.43%	-17.91%
ND3	2003-2011	470.72	0.14	0.17	666.11
	2003-2016	354.46	0.11	0.17	511.97
	change	-24.70%	-18.09%	0.63%	-23.14%
ND4	2003-2011	417.86	0.22	0.15	538.49
	2003-2016	326.46	0.20	0.15	478.88
	change	-21.87%	-5.71%	1.02%	-11.07%
ND5	2003-2011	592.62	0.13	0.16	596.68
	2003-2016	487.19	0.12	0.16	497.99
	change	-17.79%	-11.59%	0.49%	-16.54%
ND6+CERN	2003-2011	598.37	0.17	0.16	802.56
	2003-2016	440.18	0.16	0.17	670.82
	change	-26.44%	-8.21%	1.80%	-16.41%
BA1+BA2	2003-2011	532.50	0.15	0.16	592.45
	2003-2016	508.65	0.14	0.16	577.54
	change	-4.48%	-6.31%	0.33%	-2.52%
PI1+PI2	2003-2011	674.24	0.19	0.15	853.58
	2003-2016	585.63	0.18	0.15	785.97
	change	-13.14%	-3.39%	-0.15%	-7.92%

3.5.3 Trending areas and cattle headcount

Figure 3.6 shows the *z*LAI trends total areas for both analyzed periods. We denoted 1 as a negative trend, 2 as no-trend and 3 as increasing; the tens refer to the 2003-2011 period and the ones to 2003-2016. In the NEB, only 23.43% of the area showed at least one trend occurrence. From the total trending area (23.43%), about 70% were areas that showed decreasing *z*LAI trend for the 2003-2016 period and no trend in 2003-2011. A few occurrences of decreasing *z*LAI were observed in PI1, BA1, and BA2, contributing

to a total of 3.46% of the trending area. Within the desertification nuclei, ND1, ND3, and ND5 presented occurrences of increasing *z*LAI for one or both periods.

The regions where LD indication was detected, as shown in Figure 3.4, overlap with the high susceptibility to degradation maps presented by Teixeira et al. (2006) and Vieira et al., 2015. By comparing our *z*LAI trend maps of 2003-2011 and 2003-2016, we noticed similar patterns in the increased area affected by drought (Cunha et al., 2015). The desertification nuclei in Ceará (ND2, ND5 and ND6), in PB (ND3), and PE (ND4) were the subject of many studies addressing LD and desertification (Alves et al., 2017; Petta et al., 2013) A characteristic of the northern part of NEB is the predominance of smallholder agriculture and human occupation that has historically driven land vulnerability to desertification (Sietz et al., 2006). However, these studies were carried out during periods before the drought of 2012/2013. Our findings highlight that the LD aggravation problem on these regions is mainly due to the lack of precipitation during the last five years of our analysis.

Zika and Erb (2009) globally mapped regions where human-induced LD had been reported. We found an agreement in the case of BA1+BA2, where the effects of human activities led the area to undergo severe and widespread loss of biomass during the prolonged drought. As shown in Figure 3.6, some municipalities in BA1, BA2 and PI1 showed an upward trend in cattle headcount for the 1991-2011 period, which may indicate that overgrazing is potentially leading to LD, further confirmed by some small red spots (decreasing *z*LAI for both periods). However, cattle headcount is a rough indicator for overgrazing, provided that obtaining information regarding cattle management from the field is unfeasible and, therefore, out of the scope of our study. To

date, these areas have not been labeled as desertification nuclei and are simultaneously heavily occupied by cattle as reported in Parente et al. (2017) and observed in our maps. These facts should alarm decision-makers to take action towards mitigating the drought effects and susceptibility to degradation. For most of the desertification nuclei, no decreasing zLAI trends were observed in the 2003-2011 period, although the cattle headcount increased, which might indicate that increasing headcount no longer play a significant role on human-induced LD for these regions. Therefore, one can attribute LD in these areas to climate factors.

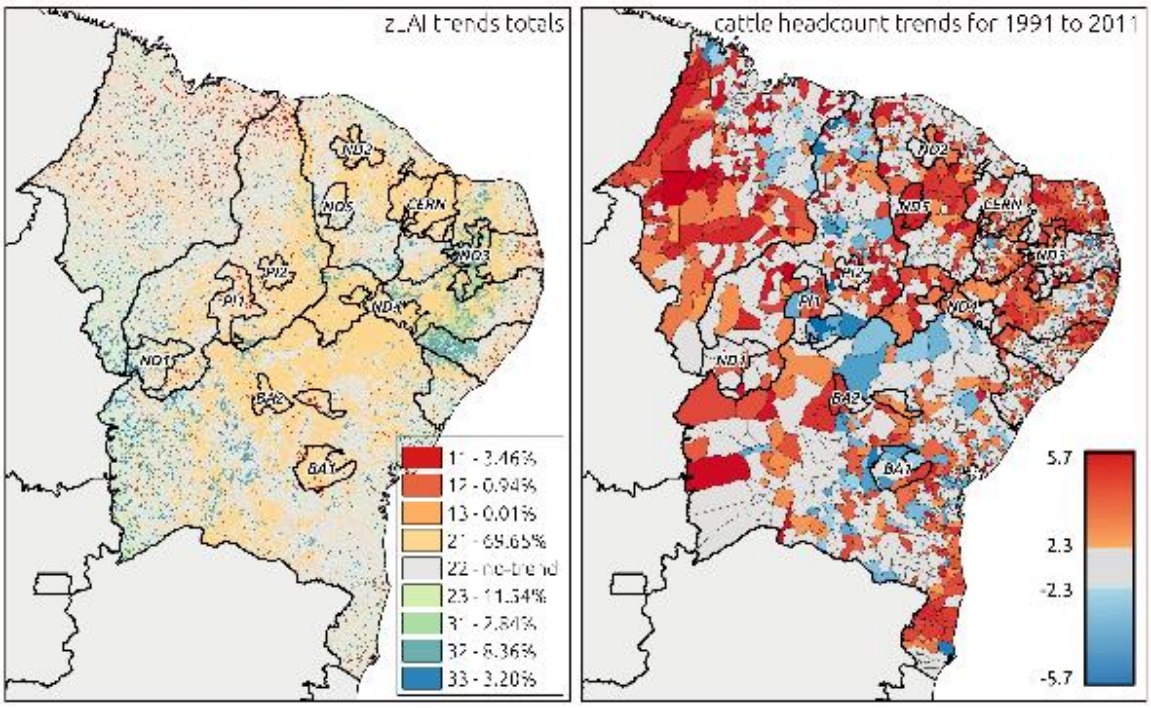

Figure 3.6: zLAI trends for the two analyzed periods on the left. 1 is decreasing trend, 2 is no-trend and 3 is increasing; the tens refer to the period from 2003 to 2011 whereas the ones refer to 2003 to 2016 (*e.g.*, 12 means decreasing trend in 2003-2011whereas the ones refer to 2003 to 2016 (*e.g.*, 12 means decreasing trend in 2003-2011 and no trend in 2003-2016). The percentages refer only to the total trending area, the "22 no-trend" was excluded, corresponding to 76.57% of the total NEB area. On the right panel, the cattle

headcount MK trends from 1991 to 2011 are presented at the municipality level, non-significant trend occurrences are masked in grey.

3.5.4 Time-series analysis

The regions highlighted in Figure 3.4 were submitted to further time series analysis. The MK test results for trend significance are presented in Table 3.2, where $z \geq 1.96$ is increasing, $z \leq 1.96\$$ is decreasing, otherwise, no-trend was detected (*p-value*>0.05).

Table 3.2: Mann-Kendall test results for trend detection in time series.

Region	Period	z-LAI		z-Albedo		z-ET	
		p-value	z stats	p-value	z stats	p-value	z stats
ND1	2002-2011	0.38	0.88	0.36	-0.91	<0.05	4.77
	2002-2016	<0.05	-6.72	<0.05	5.74	<0.05	2.97
	2012-2016	0.09	1.69	<0.05	8.56	0.19	1.29
ND2	2002-2011	0.27	1.09	<0.05	-2.03	0.14	1.47
	2002-2016	<0.05	-6.20	<0.05	-4.30	0.28	-1.08
	2012-2016	<0.05	3.81	<0.05	-2.41	<0.05	2.71
ND3	2002-2011	<0.05	9.31	<0.05	-6.78	<0.05	6.11
	2002-2016	<0.05	-2.13	<0.05	-3.00	<0.05	-2.25
	2012-2016	<0.05	2.35	0.06	1.91	<0.05	2.35
ND4	2002-2011	<0.05	7.69	<0.05	-4.53	<0.05	4.77
	2002-2016	<0.05	-4.13	<0.05	4.33	<0.05	-2.36
	2012-2016	<0.05	3.31	0.08	-1.75	<0.05	3.14
ND5	2002-2011	<0.05	2.59	<0.05	-2.03	<0.05	3.18
	2002-2016	<0.05	-4.75	<0.05	-2.37	0.41	-0.81
	2012-2016	<0.05	5.57	<0.05	-4.83	<0.05	2.12
ND6+CERN	2002-2011	<0.05	5.29	<0.05	-5.18	<0.05	4.72
	2002-2016	<0.05	-4.26	<0.05	-2.83	0.09	-1.67
	2012-2016	0.15	-1.41	<0.05	-3.49	0.17	-1.36
BA1+BA2	2002-2011	<0.05	-2.21	<0.05	-7.44	<0.05	3.89
	2002-2016	<0.05	-9.15	<0.05	4.34	<0.05	-2.72
	2012-2016	<0.05	5.29	<0.05	-5.00	<0.05	5.22
PI1+PI2	2002-2011	0.15	1.43	<0.05	-3.01	<0.05	4.71
	2002-2016	<0.05	-6.87	<0.05	-3.51	<0.05	-2.02
	2012-2016	<0.05	6.14	0.14	1.47	<0.05	3.33

As shown in Table 3.2, all the regions showed decreasing trends for zLAI when considering the entire period, whereas BA1+BA2 were the only regions showing decreasing trend prior to the drought. zAlbedo, in turn, in the pre-drought period showed

decreasing or no-trend for all the regions as expected; however, increasing trends for the entire period were not observed for most of the regions, which falls into the already discussed issue related to the small range at which albedo varies for the region - loss of vegetation may not necessarily incur in albedo increase, as the LAI influence on albedo response in the area is minimal. Therefore, care should be taken on drawing conclusions about the albedo behavior as noise might play a significant role in this study. Regarding zET trends, we found a good agreement with zLAI, as expected considering what was observed in the maps in Figure 3.4. An interesting disagreement was found in BA1+BA2 for the pre-drought period when zLAI decreased while zET showed an upward trend, which can potentially indicate that loss of vegetation is not driving ET.

To better understand the unexpected behavior presented in Table 3.2 we visually analyzed the *z*-scores time series depicted in Figure 3.7. As shown in Figure 3.7 and Table 3.2, the overall behavior is that zLAI, zET, and *z*Prec follow the same pattern whereas zAlbedo has an inverse relation to thereof. The plots are divided into two shaded areas, before and after 2012 to ease interpretation and mark the drought effects onset. Hereafter, we proceed with the events descriptions by breaking them into two periods separated by 2012, having zLAI as the guiding reference and all other variables mentioned whenever necessary.

Figure 3.7: Z-scores time series for ET, LAI, albedo and precipitation for the regions detected in the LD mapping process. The plot area highlighted on the left (blue) refers to 2003-2011 period whereas the right (orange) is related to 2012-2016.

3.5.4.1 2002 to 2011: detecting signs of human-induced land degradation

To ease visual interpretation of the time series in Figure 3.7, henceforth, we refer to years as pairs to capture the summer season in the Southern Hemisphere (*e.g.*, 2009/2010 refers to the wet season starting in 2009 and finishing in 2010). Further, we considered as dry/wet years CHIRPS *z*-scores outside of the [-0.25,0.25] range, for reasons already mentioned in Section 3.5.1. For MODIS data, we considered as extreme values *z* -scores outside of the [-0.75,0.75] range.

For most of the analyzed regions, the first five years show no apparent extremes, except *z*LAI peaks in 2006/2007 for PI1+PI2, BA1+BA2 and CERN and, another peak for BA1+BA2 in 2005/2006. Stability concerning *z*Prec marked this first period. The following five years were marked by the highest peaks for all the regions in 2009/2010 and 2011/2012, again, with BA1+BA2 as an exception regarding *z* LAI response. This confirms what was observed by Redo et al. (2013) in central Bahia (BA1+BA2), where vegetation was lost without any apparent drought occurrence (as we observed in the precipitation analysis on Section 3.5.1). Most of the regions presented increasing trends as result of these latter year peaks. However, the regions ND1 and ND2 on western Ceará and PI1+PI2 showed no significant trend (Table 3.2) due to their fluctuation behavior throughout the early years and low *z*LAI in the year of 2010/2011. As observed in Figure 3.4, these regions showed a heterogeneous distribution of increasing and predominantly no-trending areas, which may have contributed to an overall no-trending behavior.

The case of BA1+BA2 is the only one that showed a decreasing trend in *z*LAI and *z*Albedo, although *z*Prec fluctuated closely to 0, indicating no drought occurrences and precipitation influence on albedo response, which masks the loss of vegetation effects on

the trend. The period from 2003 to 2007 was marked by three consecutive zLAI peaks followed by a slightly decreasing behavior every year within the period before 2012. BA1+BA2 and PI1+PI2 are the only regions where we detected negative biomass trends in a hydrologically stable period, highlighting the human-induced LD. In fact, the cattle headcount analysis showed increasing trend in some municipalities within BA1+BA2 and PI1, which may indicate that an increase in overgrazing has been preventing herbaceous vegetation regrowth, characterized by the negative zLAI trends.

3.5.4.2 2012 to 2016: the long drought

The period spanning from 2012 to 2016 was marked by a long and drought with its onset on 2012/2013 (Figure 3.3), at what all the regions presented their lowest zLAI values (Figure 3.7). The year of 2013/2014 was regular regarding precipitation; however, zLAI levels remained low for most of the regions, with a subsequent decrease on the slightly dry year of 2015/2016 and dropped even further on the dry year of 2016/2017. For all the regions, the backloaded drought in the time series led to a decreasing trend in zLAI when considered the entire period (2002-2016). During the last five years period, even having normal and moderately dry years (2014/2015 and 2015/2016, respectively), the vegetation was not able to recover to normal levels of zLAI and, with another drought event (2016/2017), vegetation dropped almost to the 2012/2013 levels for most of the regions. An exception was the BA1+BA2 region, where the drought was not severe after 2012/2013, and the vegetation shows signals of recovering.

In the considered period of study, the apparent inability of the vegetation to recover even under regular precipitation regimes poses a tricky question: are these areas degrading or not? We do not have post-drought data to provide a proper answer, as

already stated in the limitations of this study and, the case of Sahel with its recent re-greening occurrences led us to be cautious about drawing any firm conclusion. On the other hand, the decreasing *z*LAI trends and, for most of the cases, decreasing in *z*ET (except for ND1) indicates that these are LD prone regions, given the last 15 years observed trends.

3.5.5 Linking ET to land degradation

The Granger causality analysis results are presented in Table 3.3 at $\alpha = 0.05$ significance level. The independent variable *z*Albedo Granger causes *z*ET in all regions, and *z*Prec also Granger causes *z*ET, except for ND1 (borderline *p-value* of 0.057). Regarding vegetation, the regions of ND6+CERN, PI1+PI2 and ND5 (borderline *p-value* of 0.073) are the negative cases of *z*LAI Granger causing *z*ET. We expected that all the variables would Granger cause *z*ET, as the computation of ET is based on a radiation balance model, which has LAI and albedo as input and, precipitation indirectly affects these variables, as it is known that precipitation is the main driver for vegetation condition in NEB as reported by Barbosa et al. (2016). The cases of PI1+PI2 and ND6+CERN, however, raise questions about which factors play a role in driving ET, as PI1+PI2 apparently presents human-induced LD signals and, ND6+CERN shows strong negative *z*LAI trends (Figure 3.4), indicating that vegetation no longer plays a role in the latter, as its LAI is negligible (close to 0). To further address such issues, we investigated cause-effect relations in a lagged manner to understand how these variables interact having time as a factor, through the IR analysis.

Table 3.3: Granger causality analysis test results.

Region	p-value (Gc or nc)		
	zLAI on zET	zAlbedo on zET	zPrec on zET
ND1	0 (Gc)	0 (Gc)	0.05 (nc)
ND2	0 (Gc)	0 (Gc)	0 (Gc)
ND3	0 (Gc)	0 (Gc)	0 (Gc)
ND4	0.01 (Gc)	0 (Gc)	0 (Gc)
ND5	0.07 (nc)	0 (Gc)	0 (Gc)
ND6+CERN	0.57 (nc)	0 (Gc)	0 (Gc)
BA1+BA2	0 (Gc)	0 (Gc)	0 (Gc)
PI1+PI2	0.59 (nc)	0 (Gc)	0 (Gc)

Significance level set at $\alpha = 0.05$, Gc is Granger causality and nc is no-causality.

Figure 3.8 shows the results of the IR analysis for independent variables impulse on *z*ET throughout 15 weeks for the entire study period, where the y-axis is expressed in standard deviation (*e.g.*, *variable A* causes *y* standard deviations on *variable B* at the *n*-weeks lag). For most of the analyzed regions, *z*Albedo, *z*LAI and *z*Prec had their highest impulse on *z*ET at four to six weeks period. *z*LAI apparently did not impact *z*ET on ND1 and PI1+PI2 regions, whereas in BA1+BA2 and ND6+CERN the impulses were just marginal. In fact, by analyzing the 2003-2016 trend maps in Figure 3.4, we can observe a mismatch between LAI and ET for these regions and, on the other hand, a good match for ND2, ND3, and ND4, which presented the highest impulses from *z*LAI. These regions were also the ones that presented visually stronger signals of LD trends. Concerning *z*Albedo, the IR analysis expressed its results as expected - *z*Albedo negatively impacting *z*ET with short memory after the peak (steep curve towards zero) for most regions; ND3 and PI1+PI2 were less impacted by albedo, as this variable has a small amplitude in these areas (Figure 3.2). Finally, the *z*Prec impulse on *z*ET was clear for all the regions, being ND6+CERN the most sensitive and BA1+BA2, PI1+PI2, ND1 and ND4 the less impacted.

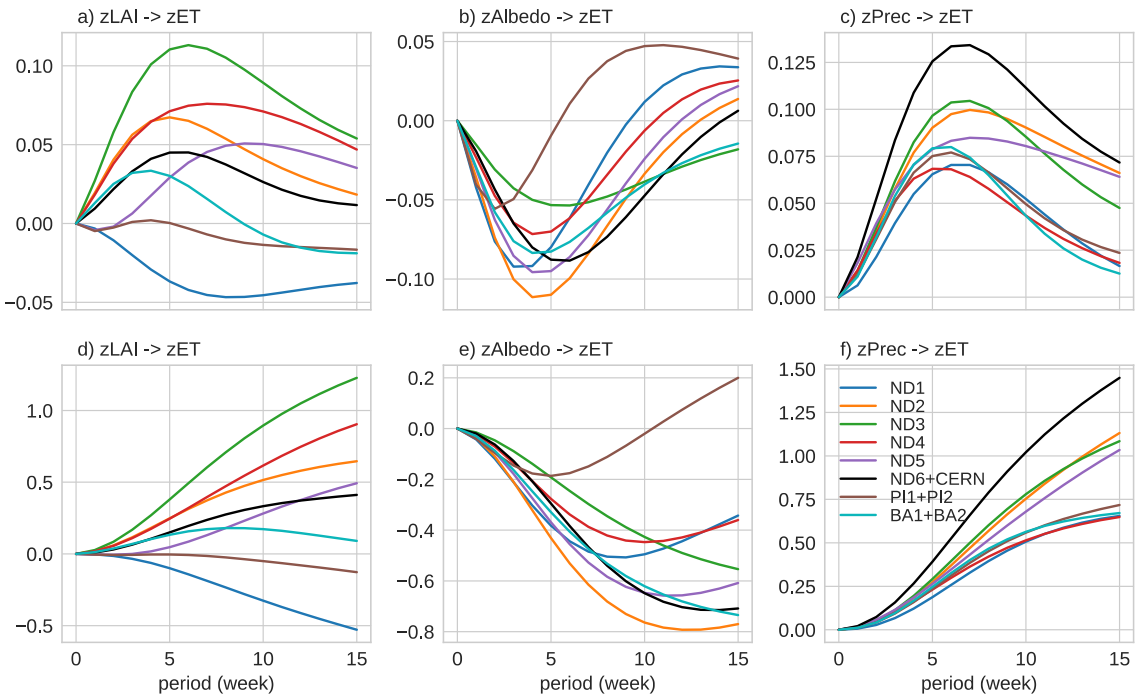

Figure 3.8: Impulse response analysis results. The y-axis is expressed in standard deviation change that one variable cause to the other, remembering that the IR analysis was performed over z-scores. The upper row ((a), (b) and (c)) shows the impulse response res response results for each independent variable to zET, the lower ((d), (e) and (f)) shows the cumulative impulses thereof.

Surface energy balance-based ET models are highly responsive to biomass and surface conditions, as they are critical drivers for surface heat exchange (Li et al., 2016; Rajan et al., 2015; Yuan et al., 2010). However, as we observed in the NEB, LAI levels are low and, therefore, albedo exerts high influence on surface-related data inputs on the ET model. Furthermore, albedo has a narrow range of variation (0.10 to 0.19), and its role on ET, although being a key factor, remains nearly constant. That led us to conclude that ET is driven mostly by precipitation, as presented in Figure 3.8 and other factors not measured in this study (*e.g.*, temperature). According to Oyama and Nobre (2004), in the NEB, LD leads to an increase in albedo and surface temperature as result of biomass loss. In turn, cloudiness decreases from precipitation reduction if a large spatial scale scenario

is considered. Regarding the cumulative effects of impulse-response (Figure 3.8 *d*, *e* and *f*), our results indicate that biomass loss (cumulative impulse-response up to 1.2 after 15 weeks) along with albedo (up to -0.8) increase have altered ET dynamics in all the regions at different levels, although precipitation plays a major role (up to 1.4). That further confirms the overall trend of decreasing ET as an effect of not only precipitation anomalies but also LD. Although we statistically decoupled the weight of factors affecting ET, this separation is not straightforward given the climatological system complexity of NEB and the partial dependency that one variable exerts on another. The results hereby presented give us strong indication that LD due to drought and human activities are leading to ET reduction, which in turn, can potentially feedback the LD cycle.

3.6 Discussion

This research study aimed at identifying hotspots of LD prone areas caused either by drought or human activities. For that, we used trend analysis of LAI from MODIS sensors covering the entire NEB region. Furthermore, we investigated how vegetation removal affects the LD feedback cycle by analyzing changes in land surface albedo and ET, also from MODIS. The study was temporally designed based on precipitation anomalies from 2002 to 2016; notably, the last five years of the period were marked by a long-lasting drought, with a severely dry start in 2012/2013. That allowed us to understand LD under normal and drought conditions and, therefore, decouple climate from human-induced LD. Finally, by relying on Granger causality and IR analysis, we investigated how LD affects the ecosystem health (as measured by ET), which is potentially a driver for the degradation cycle itself.

Under reasonable confidence thresholds, we found that 23.4% of the region showed at least one type of trend for *z*LAI. From this total, about 4.5% presented decreasing trend due to human activities and 73% experienced drought-related trends in vegetation. We relied on LAI to delimit LD prone areas finding that most of the degradation hotspots coincided with the desertification nuclei and surroundings, historically problematic regions of NEB where authorities draw particular attention. However, our results detected new hotspots in the states of Piauí and Bahia, where we found evidence of human-induced degradation which can partially be attributed to overgrazing, as the hotspots were already evident before the prolonged drought that started in 2012/2013. Further, the cattle headcount trend analysis also showed an increase in population for few municipalities within these regions. Although cattle headcount is a rough proxy for overgrazing, it is still the most accessible data that relates extensive human intervention on altering the landscape in the NEB, which is historically managed using low levels of technology.

For all the desertification nuclei, LAI decreasing trends were detected only when the drought period was included in the analysis, showing that this climate hazard impacted vegetation conditions. As mentioned by Moura et al. (2013), shrubs may increase soil fertility and moisture acting as buffers against radiation and high temperatures, also determining seedling survival ratio. Similar patterns of trends were observed in ET, although, not as pronounced as LAI; in fact, according to Santos et al. (2014), leaf loss and woody vegetation suppression (commonly used as fuel source in the NEB) are likely to imply in increased soil evaporation during the dry season. Albedo trends, on the other hand, matched poorly with LAI or ET. The range of variation of these variables are small: LAI ranges from 0.04 to 0.4, and albedo ranges from 0.10 to 0.19,

which demonstrates how changes in LAI barely affect albedo, due to the already dominant response of the soil. That being said, we concluded that albedo is not suitable to map LD in the NEB and, its minimal changes (given its positive kurtosis) may not produce a signal strong enough to characterize a significant trend. Further, albedo changes might be due to precipitation/soil moisture conditions rather than vegetation coverage for the NEB, which is the similar case of Sahel (Nicholson et al., 1998).

In our analysis relating impulse-response between variables having time as a factor, we found causality between pairs of variables in most the cases. In fact, LAI, albedo, ET, and precipitation are all connected, and causality is expected. Further, LAI and albedo are input data for the MODIS-ET algorithm and, precipitation affects all these three variables. However, the degrees to which variables affect ET are lag and region-specific. The IR analysis showed that all variables have their peak impulse on ET at four to six weeks lag. The correlation between drought indicators (precipitation and ET-based) to biomass-related variables is particularly high in semi-arid regions globally (Huang et al., 2016), with their peak occurring at less than 3 months lag time, as observed in the southwestern US, the majority of Australia, southern Argentina and a variety of sub-Saharan regions, which falls into the lag period observed in our study (Vicente-Serrano et al., 2013). Among the variables considered, precipitation plays a significant role in ET, whereas LAI and albedo cause a slightly smaller response. In a study carried out by Anderson et al. (2015), ET anomalies had a higher correlation with LAI than precipitation had for the NEB, which is in agreement with our results and expected for semiarid regions globally. Regions where the LD trends are more evident show higher LAI and lower albedo influence on ET, leading us to conclude that in such areas, loss of

vegetation is affecting ET and, possibly contributing to alter the hydrological cycle. At this point, we raise the concern about whether the reduction on ET will further reduce precipitation, catalyzing the LD cycle, as indicated by Oyama and Nobre (2004). This latter conjecture opens an avenue of investigation to date not explored in-depth for the NEB: impacts in the hydrological cycle due to changes in vegetation coverage.

The reader might have noticed that we did not mention the word "desertification" throughout our results and discussion and, we preferred the term "LD prone areas" rather than "degraded areas." To confirm that LD in fact occurred, we would need post-drought data, which is to date a limitation of our study, rather, we indicated LD prone areas based on loss of vegetation trends and changes in ET, which might potentially feedback the LD cycle. Lessons learned from the Sahel case make us cautious on drawing conclusions about LD in the NEB. The Sahel has been experiencing some cases of regreening, due to land management and changes in the local climate, although, there is an intense debate about the region's dynamics. In our study, we found some signs of vegetation recovering in BA1+BA2 after a severe drought; however, for this region, the drought was not as prolonged as for the northern regions of the studied area. Finally, as Marengo et al. (2016) warned, considering climate change projections, the NEB is likely to undergo increases in temperature and precipitation reduction, leading to higher frequency and intensity of dry spells. These findings and cited literature draw a scenario of imminent LD, which is partially confirmed by our study.

3.7 Conclusions

Our study indicates an overall negative trend in biomass due mostly to a lengthy drought in the NEB, as the last third of the 15 years period was remarkably dry. In few

regions, a negative trend was detected even in a normal precipitation period, indicating human-induced LD, possibly as a result of herd increase, leading to overgrazing. To date, the latter regions are not classified as desertification nucleus and might be subjected to further surveillance by local authorities to prevent LD. As compared to albedo, LAI showed itself as a better indicator for LD assessment due to a wider range of variation, also showing a higher correlation with ET. When comes to ET causation, albedo had a slightly weaker impulse than LAI on ET whereas precipitation played a major role. In areas where LD was more intense, the link between LAI/albedo to ET was stronger. These findings highlight the fact that ET is affected by LD; however, precipitation still being the main driver on ET anomalies. The capacity of LD on partially affecting ET indicates a potential impact on the hydrological cycle, which feedbacks the LD cycle.

Claiming LD occurrence in our study is precipitated, we rather indicated LD prone areas due to the absence of post-drought data. Assessing vegetation resilience and better understanding the NEB hydrological cycle feedback under LD occurrence are, therefore, subjects for future studies. Monitoring and detecting LD prone areas is just the first step on providing valuable information for decision makers to mitigate effects and prevent climate disasters by establishing policies regarding land exploration and occupation. We advocate for the authorities to draw particular attention to the areas mapped in this study, as a significant portion of the Brazilian population will be affected by LD and a looming desertification disaster.

CHAPTER 4.

DROUGHT IMPACTS ON CROP YIELDS, WILDFIRE OCCURRENCE, AND THE CARBON BUDGET IN THE SOUTHEASTERN AMAZON

Abstract:

The Xingú Indigenous Park (PIX) region, in the southeastern portion of the Amazon forest, is characterized by the intense conversion of natural vegetation (Amazon and Cerrado biomes) into agricultural enterprises whose expansion decelerated in the recent years. We studied the effects of drought in the region, as the period of 2003 to 2017 was marked by climate extremes including a prolonged drought from a Standardized Precipitation Evapotranspiration Index (SPEI) standpoint, with two critical episodes, one in 2005/2006 and, the most severe in 2015/2016. We analyzed how these events impacted the region in various aspects: soybean yield loss, fire occurrence, forest resilience loss, and the carbon budget, thus, characterizing the PIX degradation cycle. Soybeans yield decreased severely during the highlighted drought events, being particularly affected by above-normal temperatures and evaporative stress during the reproductive/grain-filling phase. Fire occurrences showed abnormally high occurrences within the PIX borders, a protected area, due to a loss of resilience to drought events. This effect may be attributed to the vegetation breeze, which desiccates the forest interface with clearing/agricultural areas. Hotspots of forest disturbance and resilience loss (high yearly gross primary productivity (GPP) variance) were mapped within the borders using the MODIS-based GPP modeled product (MOD17A2H). Moreover, an increased GPP variance near rivers

in the PIX were detected, where part of the indigenous population (53% growth in 10 years) dwells, increasing the pressure for resources. We observed post-drought declines in total GPP (*e.g.,* 16% reduction of forest GPP in 2016), suggesting that, if the degradation spreads, forest contribution to total GPP might decline even further in future drought events, therefore, impacting the local climate, which is likely to increase in drought frequency. Based on this scenario, agriculture can be negatively impacted by climate change, which can threat its viability, therefore, we close the PIX degradation cycle concluding that agricultural expansion represents a potential threat to itself and on native population livelihood.

4.1 Introduction

Drought is becoming more frequent in the Amazon biome, as shown by a trend of drought occurrences over the last fifteen years (Lopes et al., 2016; Marengo et al., 2018). In the southern Amazon, the increase in dry-days frequency during the wet season is associated with the northern Atlantic Ocean warming and reduced water vapor flux from the tropical Atlantic, partially explaining these trends in a synoptic scale (Espinoza et al. (2018). Concomitantly, many land use changes (LUC) have been observed along the borders of the Amazon forest, predominantly by deforestation followed by a conversion into pasture and, in many cases followed by crops like soybeans and corn (Coe et al., 2013). Replacing tropical forests with pastures or degraded grass leads to increase in temperature and decrease in ET (Shukla et al., 1990) and, LUC associated with other sources of greenhouse gases emissions can also alter precipitation distribution (Costa et al. (2007).

The deforestation cycle is observed in the Indigenous Xingu Park (Parque Indígena do Xingú - PIX) region, which is covered by evergreen forest and surrounded by cerrado, a particular variation of savanna. Forest-to-crop and forest-to-pasture transitions together were responsible for an increase in land surface temperature (LST) of 0.3 ºC, and evapotranspiration (ET) reduction of 32% in the 2000s (Silvério et al., 2015). The cerrado biome, which is where most of the conversion happened, is composed of a mosaic of semi-decidual forest and grasslands. It has undergone a substantial transformation in the recent past and nowadays is a main soybean production region (Rada, 2013). In the eastern Amazon, forest-to-crop and cerrado-to-crop conversion accounted for about 30% of the carbon emissions from 2003 to 2013 (Noojipady et al., 2017). Lima et al. (2019) suggest that agricultural expansion, represented by these conversions, is not sustainable due to the intensification of drought.

The impacts on agriculture expressed through yield loss are partially due to a decrease in local-scale moisture advecting from the nearby forest to the soybean production areas in the north of the state of Mato Grosso, led by an increase in the atmospheric vapor pressure deficit (VPD), which dries the local environment, consequently reducing long-term ET rates, due to the depletion of moisture drawn from adjoint forest canopies. The "robbed" moisture also contributes to ephemerous cloud formation over the clearing area, however, the precipitation is short-lived because of the increased distance from forests, as deforestation advances and forest border dries (Cochrane and Laurance, 2008; Khanna et al., 2017; Numata et al., 2017). The phenomenon, as depicted in Figure 4.1, is known as vegetation-breeze, which leads to forest dehydration on the interfaces with agricultural or clearing area, causing

desiccation, which increases flammability. This is a scenario once simulated by Sampaio et al. (2007) and later confirmed by António Sumila et al. (2017) in the eastern part of the forest and the PIX, which nowadays corresponds to the southeast corner of the Amazon forest. ET is also an important source of water for the local precipitation formation, therefore, its reduction due to LUC further exacerbate the degradation effects on the local climate (Fisher et al., 2009; Harper et al., 2014).

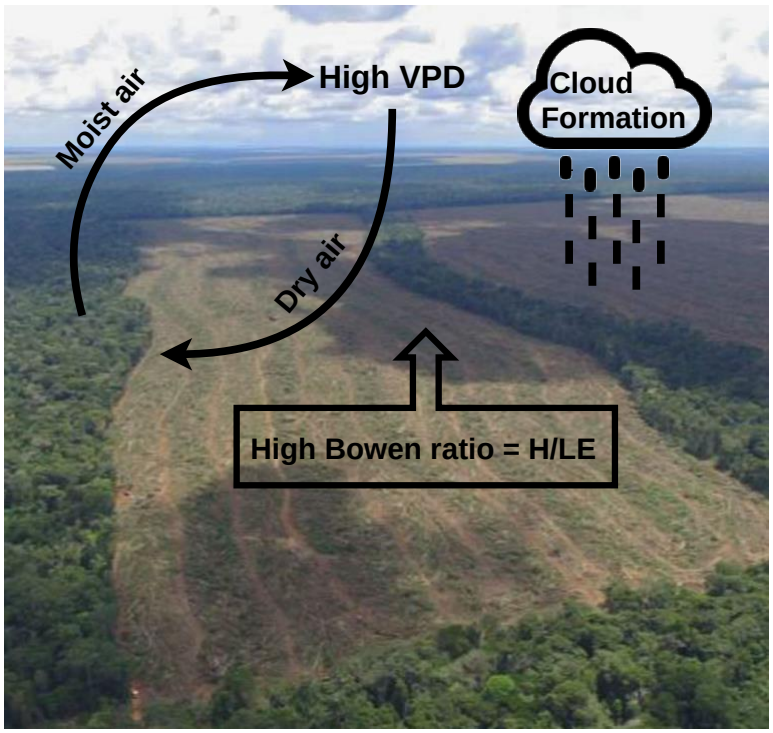

Figure 4.1: The vegetation breeze (Cochrane and Laurance, 2008). Photo source: (www.ibama.gov.br).

As a result of these transformations, the forest has had its resilience reduced, which was observed during an extreme drought during the El Niño period of 2015/2016 (Anderson et al., 2018). For our study, the concept of resilience is defined as *"the capacity of an ecosystem to return to the original state following a perturbation, maintaining its essential*

characteristic taxonomic composition, structures, ecosystem functions, and process rates (Holling, 1973)." The reported drought episode is of great importance, especially because as simulated by Marengo et al. (2018), the frequency of droughts shows a trend of increase since anthropogenic activities began to play a more-than-usual role in the region's biophysical dynamic. There is a the long history of the native population using fire as a tool for land preparation purposes in the context of their traditional agriculture (Serrão et al., 1996), however, recent LUC associated with climate change lead to an increase in fire risk in Amazon (Le Page et al., 2017). Moreover, wildfires, when not severe, can favor lower vegetation growth due to a higher incidence of radiation on the surface (Uhl et al., 1988). During a drought, the temperature increases, relative humidity decreases and the vegetation gets drier and flammable. As a result, the risk of wildfires increases contributing to tree mortality, Brando et al. (2014) verified an up to four-fold increment in fire-induced tree mortality during a severe drought event, with declines in canopy cover favoring the dispersion of highly flammable grasses on the nowadays Amazon-Cerrado southern interfaces of the PIX. Repetitive disturbances including fire associated with increased border effects (due to fragmentation), are responsible for species richness decrease, which makes the forest more sensitive to drought, implying in biomass loss (Anderegg et al., 2018; Laurance et al., 2011). Understory fueled fires lead to a more persistent and broad reduction in biomass (Rappaport et al., 2018), characterizing what we could call an anthropo-climatic land degradation (LD).

Droughts in the Amazon region associated with LD intensification has a direct impact on the carbon budget, gradually converting the land from sink to source. As observed by Gatti et al. (2014), measurements of CO_2 and CO during a dry and a wet

year, the region acted as a carbon source in the dry year and neutral on the next year. Aragão et al. (2018) point out the increase in the number of active fire counts detected in 2015, a dry year regardless of the decrease in deforestation rates as the gross emissions from wildfires surpassed those from deforestation by 50% during this drought. Anderson et al. (2018) and Yang et al. (2018) also noticed a post-drought decline in Amazon's role of carbon sink. Baccini et al. (2019), however, found patches where the forest has become a source of carbon in southern Amazon as result of repeated droughts and local disturbances, adding to the debate about the carbon source or sink role of the forest. These studies alert for the outcomes of increasing frequency of droughts, where the moisture anomaly will pose a restriction to vegetation development and increase wildfire occurrences, thus reducing forest's carbon sequestration capacity. To date, the ability of the forest to deal with repeated droughts is not yet fully known since there is not enough post-event data (and time) to address this question. In fact, loss of resilience is part of the forest degradation cycle, where climatic and anthropogenic factors are the overall impelling forces (Coe et al., 2013). The loss of forest resilience associated with changes in climate and increased exposure to risks (border effects) pose a severe threat to the ecosystem health; a study indicates that drought impacts are surpassing hydrological and biochemical cycles natural variability, thus, suggesting that some of these analyzed areas have reached a tipping point at where forests might not recover even under favorable hydrothermal conditions (Davidson et al., 2012).

Economic forces push land changes forward (Hargrave and Kis-Katos, 2013; Richards et al., 2012) on the surroundings of the PIX, converting Amazon forest and Cerrado into agricultural enterprises. As an immediate result, the native population of the

park has to cope and adapt to this new scenario, where the microclimate is affected, thus drying the borders of the forest out. In the long-run, drought becomes more frequent threatening the forest health and its resilience, increasing wildfire occurrences, altering the carbon balance and, leading to crop yield loss. We hypothesize that such alterations have positive feedback in the degradation cycle of the PIX region, leading to crop yield reduction and forest resilience losses, thus compromising agricultural profitability and people's livelihood. Our objective is to analyze the extreme drought event of 2015/2016 in the context of the 2002-2018 period to understand these losses and how their positive feedback on the region's degradation cycle. To account for that, we analyze yearly crop yields, LUC, active wildfire occurrences and carbon balance supported by drought indicators.

4.2 Spatio-temporal domain

The study region is located in the northeastern part of the state of Mato Grosso and, includes the PIX and the surrounding mosaic of evergreen forest (Amazon), savanna (Cerrado) and croplands (mostly soybeans in the Summer). We delimited a rectangle totaling roughly 170000 km^2, whose composition is 62% of evergreen forest, 5% of deciduous forest, 21% of grasslands and, 12% of crops, as of 2017 according to the MCD12Q1 Type-5 land cover product, as presented in Figure 4.2. The PIX is composed mainly of semideciduous evergreen and rainforest, the latter is also the predominant physiognomy in the Amazon biome. The evergreen and semideciduous blend characterize the transitional aspect of these two biomes. Vegetation is highly adapted to the local climate, which has a short dry and twice longer wet seasons, although these proportions are not permanent as pointed out by recent studies indicating prolongation of

dry season most likely due to LUC, which makes up for grasslands (21%) and crop (12%) areas in our study region (Marengo et al., 2018; Rao et al., 2016).

It is also worth mentioning a change in the PIX demographics from 2000 to 2010, based on census data, showing an increase in the indigenous population of the municipalities that are within the PIX from 2892 to 4413 (53.2% increase) inhabitants (Villas-Bôas, 2012). The PIX and its population play a fundamental role in hampering the LUC advance toward the forest, as the region is legally protected (Nepstad et al., 2006; Schwartzman et al., 2013).

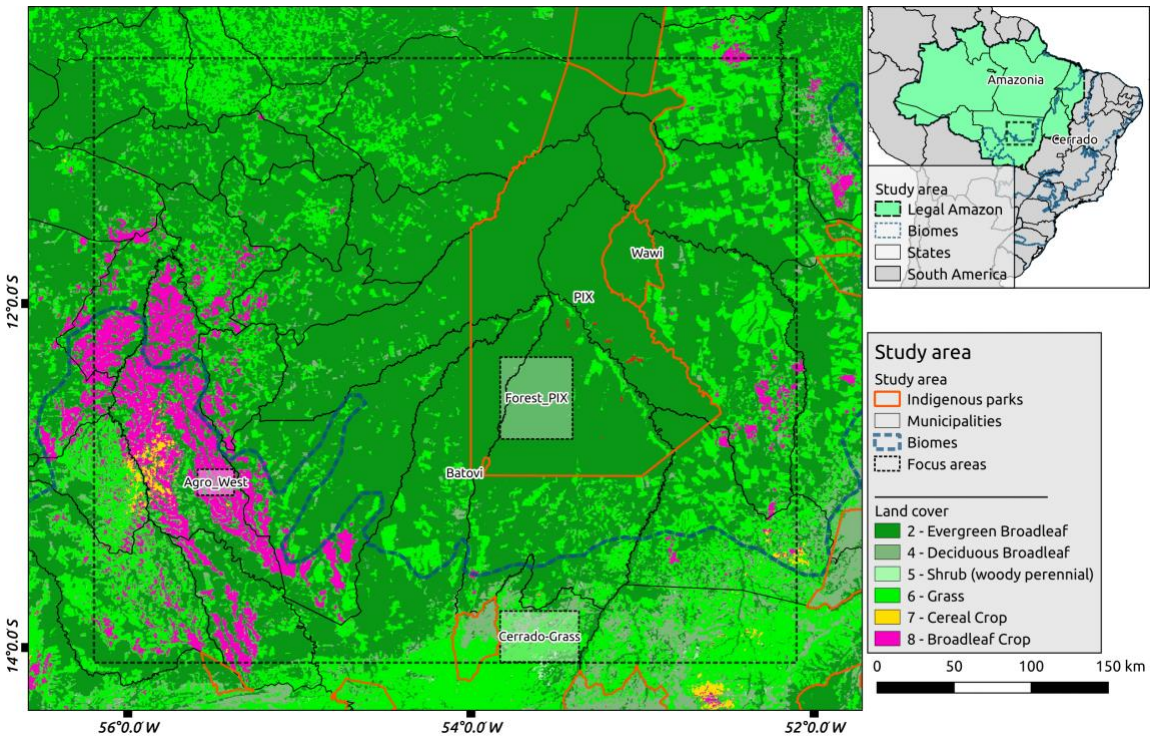

Figure 4.2: Land cover in 2017 (MCD12Q1) for the study region. The large dashed rectangle comprehends the whole study area, the small shaded rectangles indicates the focus areas (Forest_PIX, Cerrado-Grass and Agro_West).

The current research focus on the widely studied and documented drought of 2015/2016, which was remarkably hot and dry over some regions, including our study area (Aragão

et al., 2018; Jimenez et al., 2018; Leitold et al., 2018; Yang et al., 2018). The period was characterized by a strong El Niño event associated with unprecedented warming and soil moisture deficit (Garcia et al., 2018; Jimenez et al., 2018). The current study, however, relies on past events for short-term climatology comparisons and discussion we associate "short-term" with the availability of MODIS-Aqua data, launched on 2002; therefore, our historical averages for MODIS data are based on the period spanning from 2003 to 2018.

4.3 Data and methods

4.3.1 Land use change

Understanding the LUC of the region is crucial to delineating our research and explain much of what is observed in the other topics of our study. To depict yearly land cover and compute the change rates we relied on the MODIS land cover product (MCD12Q1 Type 5) from 2003 to 2017. We further simplified the dataset classes and combined them into Agriculture (Broadleaf Crop + Cereal Crop), Cerrado_Grass (Deciduous Broadleaf + Shrub + Grass) and Forest (Evergreen Broadleaf). Figure 4.2 shows the original classes of our study area as of the year 2017.

We quantified the total area of each class per year to present a time-series to verify the forest-to-crop and cerrado-to-crop conversion rates. This exploratory analysis is fundamental to pick representative regions as described below and to contextualize the region within the last two decades to support our discussion. We compared 2017 to 2003 to detect areas that presented no substantial LUC throughout the period. Then we picked a sizeable homogeneous area of each class to perform more detailed time-series analysis, as presented in Section 4.3.3 and described as follows: Forest_PIX - a large sample totaling 2480 km^2 of evergreen forest in the PIX, 19 km from the park's southern border,

Agro_West - a much smaller area of agriculture totaling 396 km^2 where soybean is the predominant crop during the Summer (part of the wet season) and, Cerrado-Grass - an intermediate size sample of Cerrado physiognomy composed of semideciduous forest and grass totaling 1682 km^2, located at 87 km south of the PIX.

4.3.2 Drought classification

Drought classification supports the entire study and, therefore, consolidates the base for subsequential topics. We addressed drought levels during the dry (June to September) and wet seasons (October to May). The delimitation of these periods is based on what was observed from the precipitation dataset (Section 4.3.3). Although numerous papers are addressing the drought of 2015/2016 in Amazon, we are analyzing a smaller region in greater detail and, therefore, this wet/dry period scheme does not follow the literature as these thresholds vary between locations and years. The strategy helps us to tailor the analysis for crops, active fires occurrences (AFO) and carbon budget in a way that each period has its relevance more closely linked to each of these topics, for example, AFO are more intense in the dry period whereas agriculture crop production takes place during the wet period.

We quantified drought intensity over these periods using the Standardised Precipitation-Evapotranspiration Index (SPEI, Vicente-Serrano et al., 2010), which represents a climatic water balance of the difference between precipitation and potential ET (PET); these differences are then transformed into standardized anomalies considering the chosen accumulation window that. For the current study, the 12-month scale was chosen for being less subject to short-term variations. We used an online tool (SPEI Global Drought Monitor - spei.csic.es) to retrieve the monthly average SPEI-12 for

the study area. With this procedure we are able to compare drought events in a broad perspective by applying the classification thresholds based on Nam et al. (2015), as follows: <-2: extremely dry, [-2,-1.5): severe, [-1.5,1.0): moderate, [-1.0, -0.5): mild and, [-0.5,0.5]: normal.

4.3.3 Time-series analysis for the subsets

Vegetation of the three land use classes considered have different Enhanced Vegetation Index (EVI) temporal signatures, being our reference for vegetation status and, health when compared in terms of *z*-scores, as our chosen representation of anomaly. Our data source is the product MOD (Terra) and MYD13A1 (Aqua) (MODIS Vegetation Indices at 500 m spatial and, 8-day temporal resolution when combining Terra and Aqua). To take into account the water exchanges between land and atmosphere, as a comprehensive proxy for drought, but in a perspective closer to vegetation by relying on the Evaporative Stress Index [ESI, Anderson et al. (2007)] as presented in Equation 4.1:

$$ESIr = 1 - ET/PET \tag{4.1}$$

$$ESI = \frac{ESIr - \mu}{\sigma}$$

where PET is the potential ET, we call it ESIr with *r* for raw, which ranges from 0 to 1, the higher, the dryer the environment. It represents the failure of ET to reach its potential, indicating whether soil moisture is meeting the plant's demand or not and maintaining the temporal signature closely associated with EVI. To allow intercomparability, the index is finally converted into z-scores, as shown in the second part of Equation 4.1, where μ and σ are the mean and standard deviation of ESIr for a given central 8-day in a 40-day window period (for smoothening) considering all the years; in

short, it is a z-score with a moving window to make historical averages less noisy. As data source, we used the MYD16A2 product (Mu et al., 2011), which provides ET and PET at 500 m spatial and 8-day temporal resolution.

Changes in ET are attributed partially to water availability associated with radiation and temperature, although prevailing wind, VPD levels, and surface roughness are also components connected to ET variability. To account for changes in temperature, we analyzed daytime land surface temperature (LSTday) from the product MYD11A2 at 1000 m spatial and 8-day temporal resolution. To account for the primary water source for the study region, we considered the estimates of accumulated precipitation, as provided by the Climate Hazards Group InfraRed Precipitation with Station [CHIRPS-v.2, (Funk et al., 2015)], delivered at 5 km spatial resolution every five days (resampled to 8 days to match all the MODIS based data) and already tested for the Amazon basin (Wongchuig et al., 2017).

With a focus on the drought of 2015/2016, we analyzed how EVI, zESI, zLSTday and precipitation were distributed for Amazon, Cerrado/Grass, and Agriculture plots. The spatial-temporal data were extracted and averaged for each of the three regions, thus establishing our time-series of standardized anomalies.

4.3.4 Agricultural drought

To assess the impacts of drought on agriculture we utilized the IBGE yearly crop yield and planted area data (soybeans) by municipality (IBGE, 2018b). We focus on soybeans due to its predominance during the summer for the study area, which is when most of precipitation is distributed and, for its importance as the main product in the

agricultural enterprises portfolio. Figure 4.3 shows the yearly soybean acreage for the region, yield and total production.

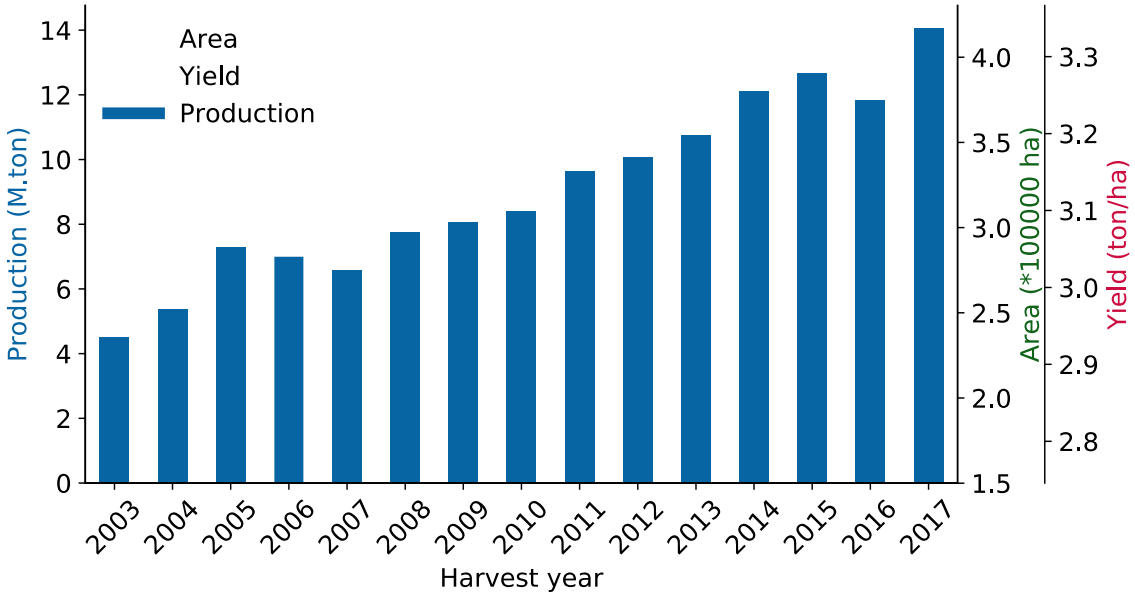

Figure 4.3: Soybean area, yield and production for the study area.

Rainfed agriculture is heavily dependent on the timing of precipitation to meet crop needs. For soybeans, the stages of emergence/germination and flowering/grain filling are extremely critical on water demand and, therefore, drought during these specific stages is likely to affect biomass and yield negatively (Carmello and Neto, 2016). Other factors also have an impact on soybean yield, such as temperature are reflected by changes in ET (Anderson et al., 2016; Battisti and Sentelhas, 2015; Melo et al., 2008). To account for the effects of drought on soybean yield we considered three periods in the soybean development as follows: (1) emergence, greening onset -mid September to mid-October, (2) vegetative phase -to late-November and, (3) the reproductive and grain-filling phase of the plant ending in early January. Periods 1 and 3 are known for their critical demand for water from a final yield standpoint (Arvor et al., 2011; Vera-Diaz et

al., 2008). For this procedure, the explanatory variables were normalized to facilitate intercomparison. We calculated the average values for all pixels classified as crops and from the time-series of EVI, ESIr, and LSTd, the averages for each variable for these periods were computed, totaling nine explanatory variables in the initial model. Finally, the effect of each of the significant factors and periods was evaluated within the growing season on final soybean yields.

4.3.5 Mapping the fire

Fire is a cause and effect of drying climate associated with LUC. Increased number of fire occurrences lead to a more flammable forest around the burned area, which loses resilience due to an increased posterior presence of grasses and other small profile vegetation, now favored by more light availability (Davidson et al., 2012). By mapping the fire occurrences, we can track how the PIX, a legally protected area, is being affected by successive drought events and surrounding LUC, thus, spatializing the loss of resilience. This task is made possible through the Fire Data Base of the National Institute for Space Research - Brazil (BDQueimadas - INPE), which monitors AFO using a set of satellites, providing rich spatiotemporal information to precisely track these events (Carranza et al., 2014; Rodrigues et al., 2019). We restricted our AFO data to MODIS-Aqua-afternoon for being this the primary reference covering the whole study period for both biomes allowing temporal analysis (Aragão et al., 2018).

4.3.6 Carbon budget

MODIS Gross Primary Productivity (GPP) (MOD17A2H, Running et al., 2006) has as inputs the fraction of photosynthetically active radiation (FPAR), leaf area index (LAI), temperature, incoming solar radiation, VPD and, light conversion efficiency, a

plant-functional-group related parameter in the model. GPP is the chosen indicator for forest state as a way to assess its resilience in the wake of disturbances caused by human actions and climate extremes. We could have considered EVI for this purpose, but there is a debate about its ability to represent mature forest state (Samanta et al., 2010). We took a similar approach of Phillips et al. (2009), which associates changes in net biomass as a proxy for forest state (comprehensively related to vegetation structures, species composition, height, density and layers for mature forests (Thompson et al., 2009). By measuring its state over time, we can map the loss of resilience, accomplished by computing the variance of accumulated yearly GPP per pixel, as disturbances in mature forests might imply in GPP increased variability. It is worth noting that, GPP is modeled, but there is a debate about the quality, implying that these products have to be improved (Joiner et al., 2018).

4.4 Results

4.4.1 LUC analysis for contextualization

Figure 4.3 shows the increase of soybean acreage for the region, where in 15 years the total area occupied by these crops increased nearly three-fold, from 1.5 to about 4 million ha. The average yield and overall production increased two-fold, currently at 3.3 ton/ha totaling 14 million ton of soybeans in 2017. From a spatial standpoint, the agricultural expansion is shown as shaded areas in Figure 4.6, further discussed in Section 4.4.4, where we assess impacts of drought in agriculture. The expansion slows down in 2014 and even further after the 2015/2016 drought event. However, we do not have a post-event means to analyze if this behavior is due to less available area for expansion, public policies or discouragement due to the recent drought event. In terms of

yield, the increasing trend is primarily associated with the transformation process that land goes through during the conversion into agriculture rather than technology improvement, although the latter plays some role. During the transformation, soil organic matter is increased due to crop rotation and no-till techniques, providing better conditions for crops to grow and reach higher yields (Corbeels et al., 2006; Nagy et al., 2018).

4.4.2 Drought occurrence

Using SPEI-12 we classified each year and season of our study period in terms of drought intensity. Since mid '90s, SPEI levels for the region entered in a quasi-permanent drought condition with few episodes of normal seasons (Figure 4.4), as opposed to the previous three decades. Thus, at this point, we are analyzing drought events within a near two-decade extended drought that, to date, has not return to the normal SPEI (near zero) levels. Similar patterns of extended drought were simulated for Rondônia-Brazil on the southwest side of the Amazon forest, a region that underwent intense deforestation in the last four decades (Khanna et al., 2017). Table 4.1 shows an almost permanent dry condition, with very few occurrences of normal years.

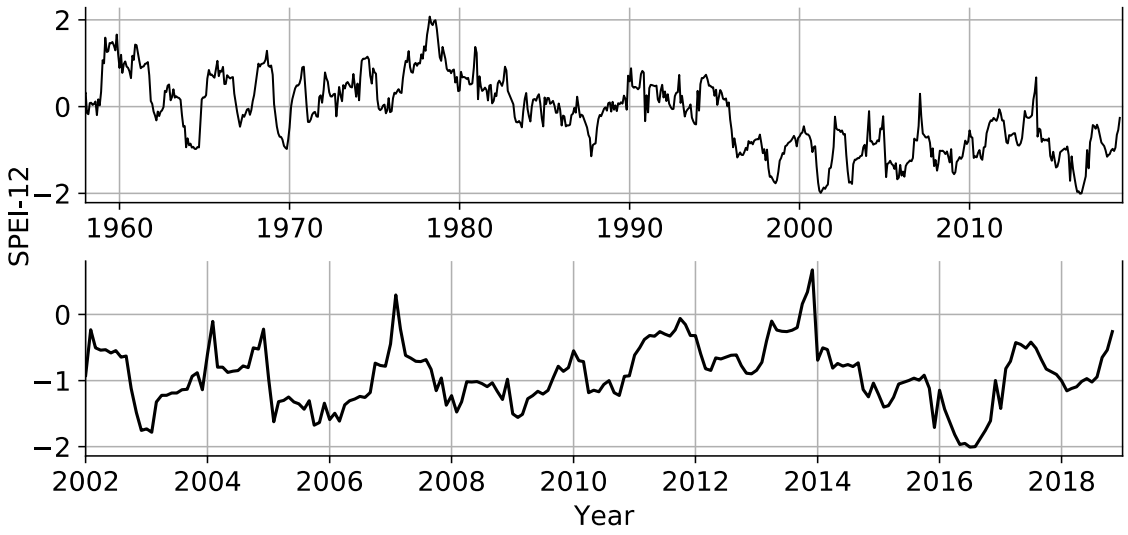

Figure 4.4: Monthly SPEI-12 for all the available data (top chart) and, for our study period (bottom) with the rainy seasons highlighted in grey.

Table 4.1: Averages of SPEI-12 for drought classification by period, (First year) is the (dry) season and the pair refers to the wet season.

Year	(Dry) season	Wet season
(2002)/2003	-0.6 Mild dry	-1.5 Moderately dry
(2003)/2004	-1.2 Moderately dry	-0.8 Mild dry
(2004)/2005	-0.8 Mild dry	-1.0 Mild dry
(2005)/2006	-1.4 Moderately dry	-1.5 Severely dry
(2006)/2007	-1.2 Moderately dry	-0.5 Normal
(2007)/2008	-0.7 Mild dry	-1.2 Moderately dry
(2008)/2009	-1.0 Moderately dry	-1.3 Moderately dry
(2009)/2010	-1.1 Moderately dry	-0.8 Mild dry
(2010)/2011	-1.1 Moderately dry	-0.7 Mild dry
(2011)/2012	-0.3 Normal	-0.5 Normal
(2012)/2013	-0.6 Mild dry	-0.6 Mild dry
(2013)/2014	-0.2 Normal	-0.3 Normal
(2014)/2015	-0.8 Mild dry	-1.2 Moderately dry
(2015)/2016	-1.0 Mild dry	-1.5 Moderately dry
(2016)/2017	-2.0 Severely dry	-1.0 Moderately dry
(2017)/2018	-0.5 Mild dry	-1.0 Mild dry

In Table 4.1, it is worth noting that the wet season is twice longer than the dry; therefore, the averaged SPEI for these periods have a sample size proportion of 2:1 ratio. The dry seasons (June-September) were predominantly classified as mild dry and, during the El Niño period of 2015/2016 it transitioned into a severe drought (2016: -2.0). The wet seasons (October to May) were mostly mildly dry having only one severe year (2005/2006: -1.5, further discussed in Jimenez et al. (2018). For the recent El Niño, all the years were at least moderately dry; in short, 2014 to 2018 can be considered a period of extended drought in the PIX region. SPEI-12 values for the 2015/2016 drought went to its lowest in the series (-2) (Figure 4.4), and it is the critical year within the extended drought period. (Garcia et al., 2018) highlight the extreme above-normal temperatures in this period as both partially cause and consequence of drought exacerbation. The impacts of the extreme event are analyzed in terms of agriculture (Section 4.4.4), wildfires (Section 4.4.5) and carbon balance (Section 4.4.6).

4.4.3 Time series analysis

Figure 4.5 shows the time-series of precipitation and z-scores of EVI, ESI and LSTday for the three plots (Forest_PIX, Cerrado-Grass, and Agro_West). It is worth noting that these areas were not affected by fire during the studied period presented on Figure 4.5, that comprehends the extended drought of 2014-2018 and, the z-scores refer to the whole series (2003-2018). The average total precipitation for these regions was 2051 mm (2014/2015), 1475 mm (2015/2016), 2822 mm (2016/2017) and, 1865 mm is the average for 2004-2018 wet periods.

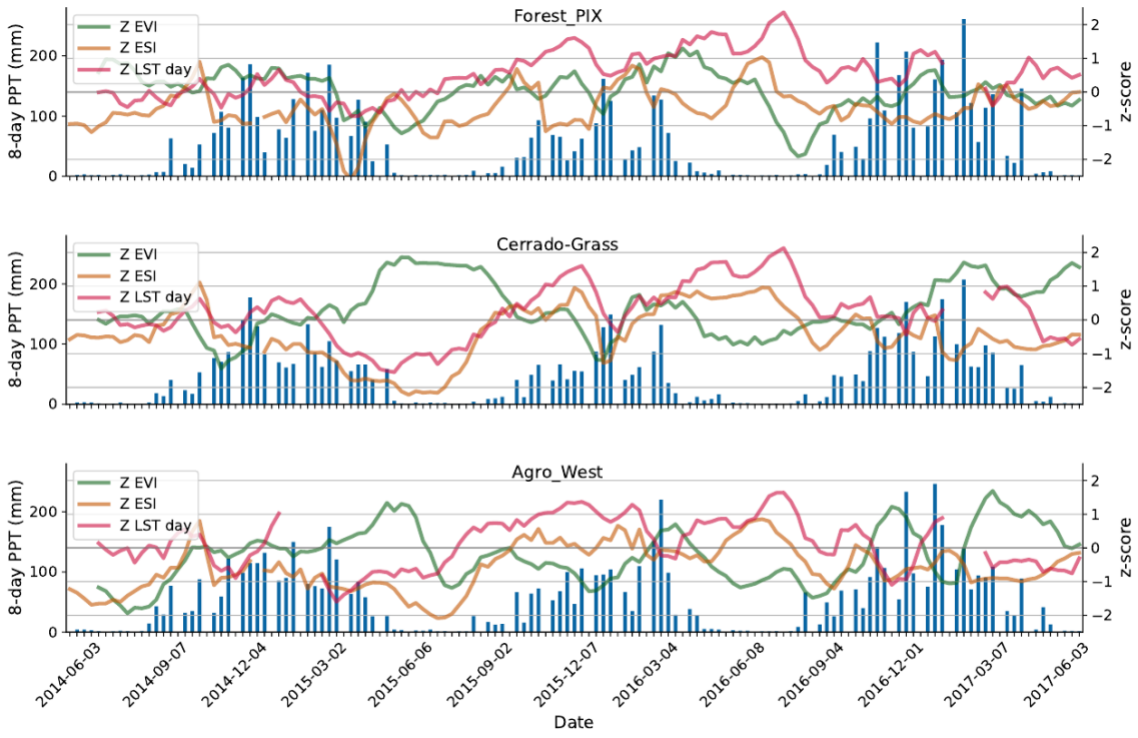

Figure 4.5: Time-series of z-scores for EVI, ESI and LSTday for the focus areas capturing the drought of 2015/2016. The blue bars indicate the accumulated precipitation in 8-day periods.

As shown in Figure 4.5, in 2015/2016 zEVI values were lower for agriculture than of Cerrado, while forest remained stable, highlighting how the natural vegetation is more resistant to drought events than agriculture is. Temperatures were above normal for all the regions most of the time and continuously high for agriculture. zESI (the higher, the more stressed) were remarkably high during the following dry season (June and July of 2016), when LSTday reached the highest values for all the classes. Higher temperatures can be both cause and effect of evaporative stress, whereas precipitation only causes it. The anomalously high LSTday for this period can also be partially attributed to the creeping drying effect coming from below-normal precipitation levels. Drought effects have different outcomes on each of the vegetation types covered in this

study, and the time-series here presented help on examining what is observed in agriculture and natural environments.

4.4.4 Agricultural drought

Table 4.1 shows periods of intense drought, in 2005/2006 and on consecutive years around 2015, at the same time that Figures 4.3 and 4.6 indicate relative crop yield losses per municipality. The drop in 2006 was large, however, in parts of the region, agriculture was still in its initial years, not yet benefiting from organic matter accumulation in the soil (as a result of years of agriculture) (Cerri et al., 2007). Thus, the expected yields were not high to start with and, in 2006 we observed yields 40% below the previous and next years average. After the drought of 2005/2006, the region experienced a substantial yearly increase in yield, but this climbing halted in 2012, which started to show signs of drought (dry season of 2012 had SPEI of -0.6). Besides the normal year of 2013/2014, the region finally entered in an extended drought, leading to consecutive yield loss culminating with a drastic drop in 2016.

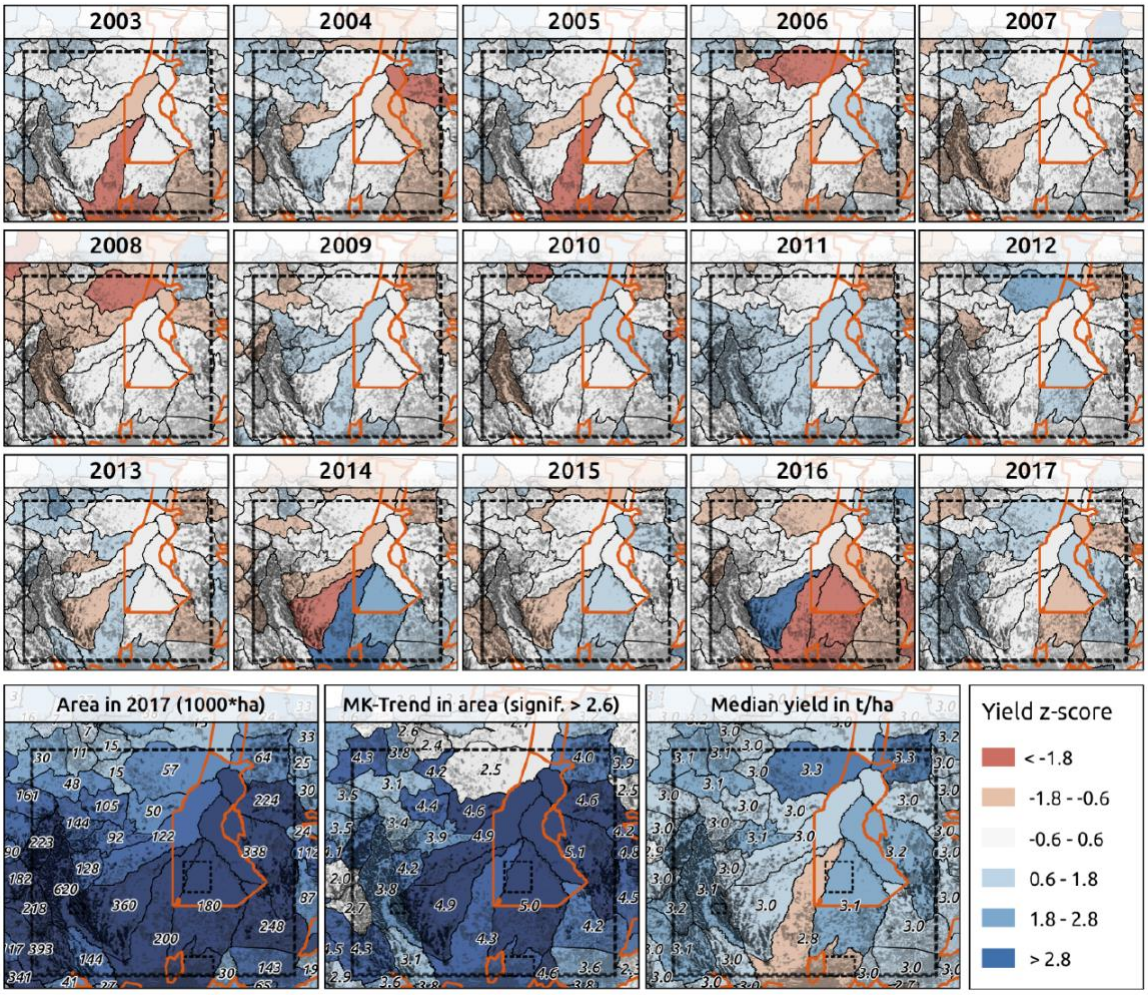

Figure 4.6: Z-scores for soybean yield by municipality (small maps) and descriptive statistics about quantitative and qualitative geographical distribution of crops in the study region. The yearly maps refer to the harvest year. The shaded masks refer to the soybean areas for each year in the yearly maps and, for 2017 in the bottom maps.

We modeled soybean yield (kg/ha) based on remote sensing indicators of temperature (LSTday), evaporative stress (ESIr) and green biomass (EVI) divided into three periods within the emergence-grain filling continuum of the soybean cycle, as the water needs for each period vary. After performing parameters elimination based on higher *p-values*, we obtained the model shown in Equation 4.2, with adjusted r^2 of 0.70. LSTday had a significant impact on vegetative (2) and reproductive/grain-filling (3) phases, whereas

ESIr was significant for the latter. The negative coefficients on phase 3 indicate how water stress and high temperatures are catastrophic for the final yield (Sentelhas et al., 2015). Decoupling these effects is hard due to their reciprocity, as soybean plants have the ability to regulate stomata aperture under high temperatures; therefore, impacting ET rates. The non-significant EVI indicates how apparently normal canopies (green biomass) does not represent yield, as it is possible for the crop to have regular green biomass accumulation (through efficient stomatal regulation), but unable to keep up with the prolonged drought, which unfolds into flower abortion, deficient pod formation and insufficient grain filling (Rafael Battisti et al., 2017).

$$Yield = 3241.8 + 353.5 * LSTd2 - 377.8 * LSTd3 - 398.3 * ESIr3 \quad (4.2)$$

As shown in Figure 4.6, not all the observed results can be explained by the drought-yield assessment, as many other factors not measured in this study are determinant on final yields, such as crop management, technology and soil condition, which changes throughout years of agricultural activity in this relatively new frontier in the Brazilian territory. Moreover, our study period is predominantly dry, which can bias the analysis. Regardless of the limitations, the results indicate how drought impacts soybean yields in the region and, how these effects are pronounced during the reproductive phase. Not all drought occurrences led to severe yield losses, as the timing and intensity of drought are determinant on the impacts. Still, we can see, for example, the drastic yield loss in the municipalities comprising the southern region of the PIX in 2016, which are more recently converted. It is possible that these regions get better soil

conditions in the forthcoming few years, yet, the local microclimate is being affected too and, it can impede sustainable rainfed agriculture.

4.4.5 Fire

Figure 4.8 shows the number of AFO per biome during the study period. Fire is used as a tool for forest clearing and expansion of agricultural enterprises. Crop area more than doubled in Mato Grosso from 2001 to 2006 (Galford et al., 2010), which is also when most of the AFO were detected in our study period. When considering the whole study region, the AFO number seems unrelated to the drought level, but rather to human activities, which also occur mostly during the dry seasons. The total AFO number slows its rate as the region is transformed, reaching a plateau for both biomes, as depicted in Figure 4.8. The analysis can be misleading, as one would say that "the yearly AFO number is decreasing, regardless of drought frequency and intensity," which is incomplete, as we show next.

Forest fire is likely to occur in the vicinity of previously cleared (either burned or logged) area, as flammability increases on the interfaces due to a combination of various edge effects. Due to vegetation elimination, there is an increase in the Bowen ratio on the clearing area altering the interface's microclimate, which gradually causes forest desiccation reaching up to 2.7 km from the edge, as moisture is drawn by the "thirsty" atmosphere (high VPD and vegetation breeze, as depicted in Figure 4.1) of the cleared area (Briant et al., 2010). With more light reaching the lower layers of the forest edge due to opened canopies, comes the proliferation of vines and other small profile vegetation that, later on, is likely to turn into highly flammable material further increasing fire risk (Camargo and Kapos, 1995). From year to year, we can see the AFO taking place around

the same areas of previous years, a pattern depicted in Figure 4.7. On the first five years of our study period, we observed intense fire activity on the far-west and close-east of the PIX, regions where agriculture and pastures are, nowadays, the dominant landscapes. The AFO reduction on the same areas after a few years is, therefore, due to no forest left to burn. So we can track the AFO shifting to other regions, like in the south of PIX border. Inside the PIX, however, AFO are recurrent, but in low number and happening mostly where the native population lives, usually, near rivers, as fire is used a traditional agricultural tool. What is concerning is the increase in AFO on the southern border of the PIX, a region that has typically no fire incidence, denoting no indigenous activity. The area is protected and, fire is probably due to the increased flammability resulting from the clearing on the south of the PIX, which loses resilience as marked by the intense AFO in the drought of 2015/2016.

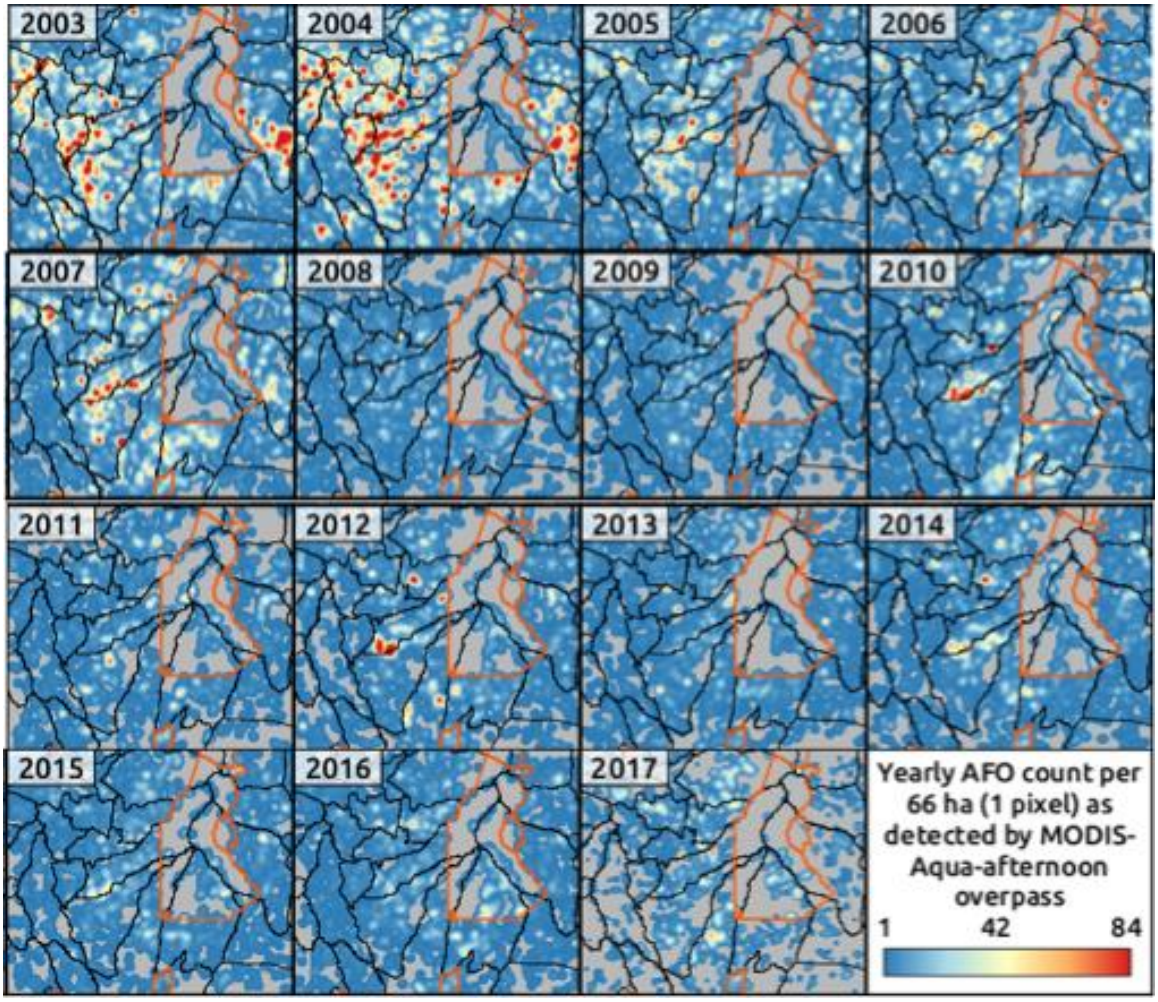

Figure 4.7: Spatialized yearly AFO, areas in grey registered no occurrences. Each pixel corresponds to 66 ha, therefore, the color bar numbers are associated to the AFO count in a given pixel.

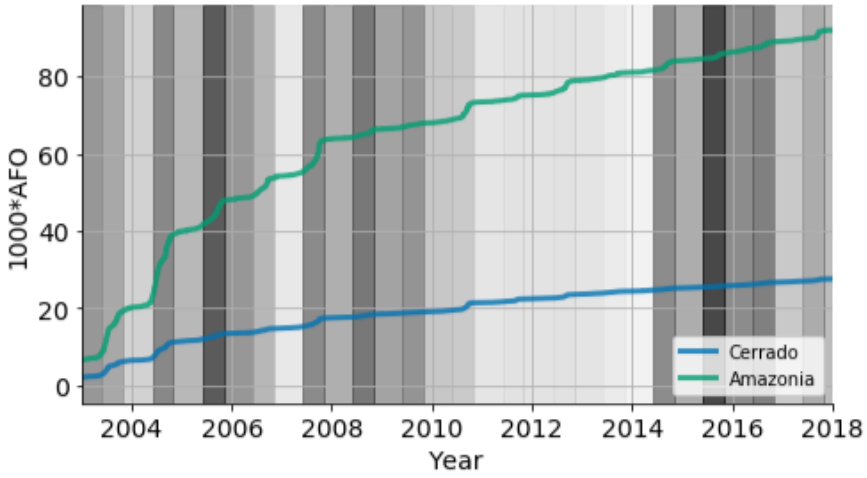

Figure 4.8: Cumulative active fire occurrences by biome in the study area as detected by MODIS Aqua-afternoon. The grey shaded areas correspond to the average SPEI during the dry (July to October) and wet (November to June). The grey scale refers to the range of S SPEI considering only the period of 2003-2018 (Figure 4.4): the darker the area, the lower the SPEI (indicating dryer periods). Refer to Table 4.1 for the actual SPEI-12 average values.

Back to the non-accurate statement about AFO decrease, we observed that the unprotected areas (outside the PIX) are what is burned and transformed, therefore, the reduction in AFO number is mostly due to legal restrictions (lack of "legal" areas to convert). With the increasing drought trend, patterns like those observed in 2015/2016 on the PIX borders are liked to become recurrent, which will cause forest degradation, regardless of legal protection against deforestation. The PIX becomes, thus, less resilient to drought and less prepared to the projected trends.

4.4.6 Carbon budget

The study area generally presented post-drought total GPP declines, highlighting the event in 2006/2007 and, the most extreme in 2015/2016, as shown in Figure 4.9. Forest height and biomass decrease and, consequently GPP loss, as a result of extreme or severe droughts. In this mosaic of agriculture, Cerrado and forests, the latter presented considerable carbon loss, as an effect of both the areal contribution (62%) and, most importantly, drought effects on forest health (Aragão et al., 2018; Feldpausch et al., 2016; Yang et al., 2018). Considering the period average yearly GPP per class, forest and Cerrado experienced losses of 7.6% and 10.4% in 2007, respectively. For the drought of 2015/2016, both classes presented a GPP reduction of 9% in 2015 and, 16% (Forest) and 12.5% (Cerrado) in 2016.

We further detailed the spatial distribution of the carbon loss on the PIX region as shown in Figure 4.10. In the time-series of maps, we noticed that rather than just post-drought, the region suffers "at drought" disturbances, as we can observe in 2005/2006, 2007/2008, 2010/2011 and the most severe in 2015/2016. The eastern and southern sides of the PIX presented the lower contributions to regional GPP, whereas the park presents the highest. By observing the variance map, we observe many regions with high variance, which can indicate two facts: indigenous population increase and resilience loss on the PIX southern borders.

Indigenous population increase: With a 53% indigenous population increase from 2000 to 2010 partially as a result of improved living conditions and access to healthcare, it is expected an increase in the pressure for local resources. In Figure 4.10 (areas 1 and 2) we observed hotspots of high variance near the rivers inside the PIX, where the indigenous population is concentrated. There is a steady low amount of AFO on these areas (Figure 4.7), reflecting the sustainable character of the use of fire by the native population. That generates a variance in the series of annual GPP, but not showing any noticeable increase in area. The pattern indicated in area 1 is intriguing, as the AFO seems to oscillate from low to null inside the PIX, whereas fire activity was usually high on the west of the border, a region of recent agricultural expansion. However, due to the proximity of indigenous population and the expansion area, the interaction of these actors has to be further studied and, unfortunately, we do not have enough data to indicate a loss of resilience, despite the high variance.

Resilience loss on the PIX southern borders: High variance in forest state was detected on the southern borders of the PIX (areas 3 and 4), where we also observed high

AFO number in the park in 2016, indicating a loss of resilience. LUC in the vicinity of the park exerted a degradation effect in the protected area leading to forest desiccation and increased flammability. What we observed on area 4 is similar to 1, with indigenous population dwelling near the PIX border with agricultural enterprises laying on the park limits. However, the high variance area extent spreads beyond one focal point, which indicates that forest degradation due to proximity with the interface with grasslands and agriculture begins to show its widespread effects. Thus, the edges of the park appear to be affected by the vegetation breeze. Zemp et al. (2017) modeled similar effects but at a much larger study scale, with projections indicating possible alterations in forest structure due to changes in the local climate. What our study does, however, is to suggest that these alterations are already happening on a small scale, closely related to local human activity rather than just regional changes in the climate. At the plot level, Silva et al. (2018) show that forest recovery is severely affected by fire, which increases mortality of all trees (including old-growth forests) and, therefore, leading to biomass reduction. Similar effects are expected in our study region due to fire occurrences. The PIX is, therefore, undergoing increased internal pressure for resources, microclimatological alterations on the borders and, potentially inserted in a context of regional climate change, which can accelerate the degradation process. Although the disturbance areas are considerably small in the context of the park, their proliferation and expansion has the potential to alter the local carbon balance, which has a positive feedback in the degradation cycle (Soares-Filho et al., 2012).

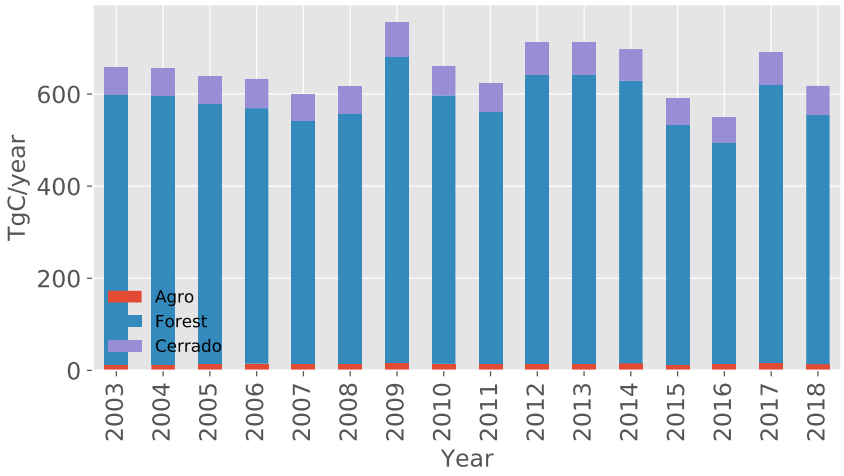

Figure 4.9: Yearly Tg of carbon in the region with all the classes combined as estimated by MODIS-GPP.

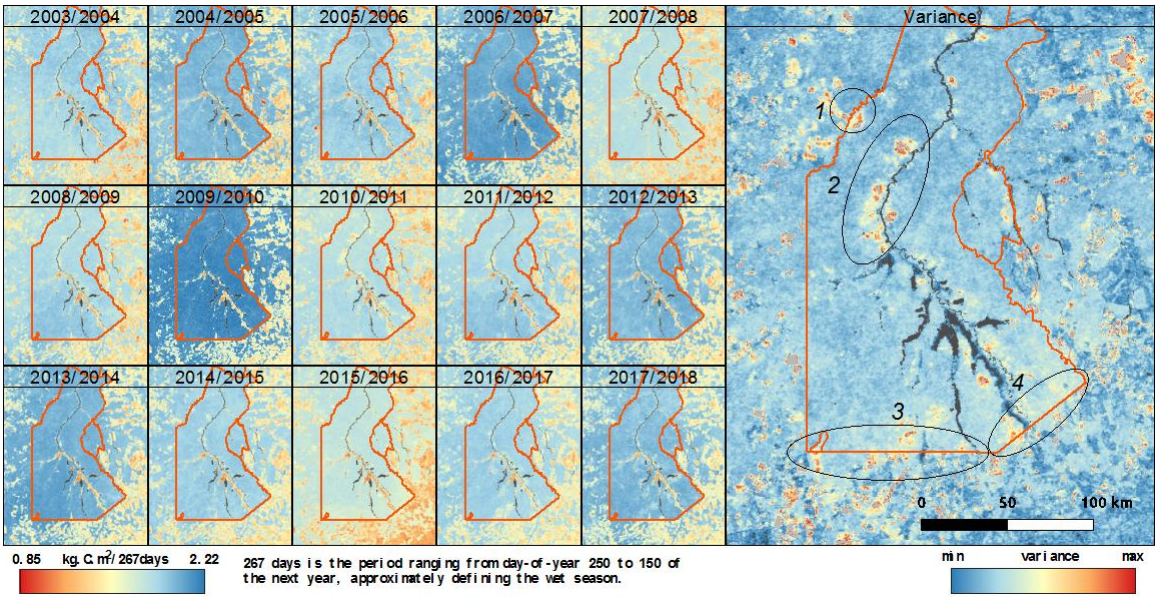

Figure 4.10: Temporal analysis of accumulated GPP on the rainy seasons (DOY 250-150) for the study period. On the Variance map, the areas (1-4) are further discussed in this study.

4.5 Discussion and Conclusion

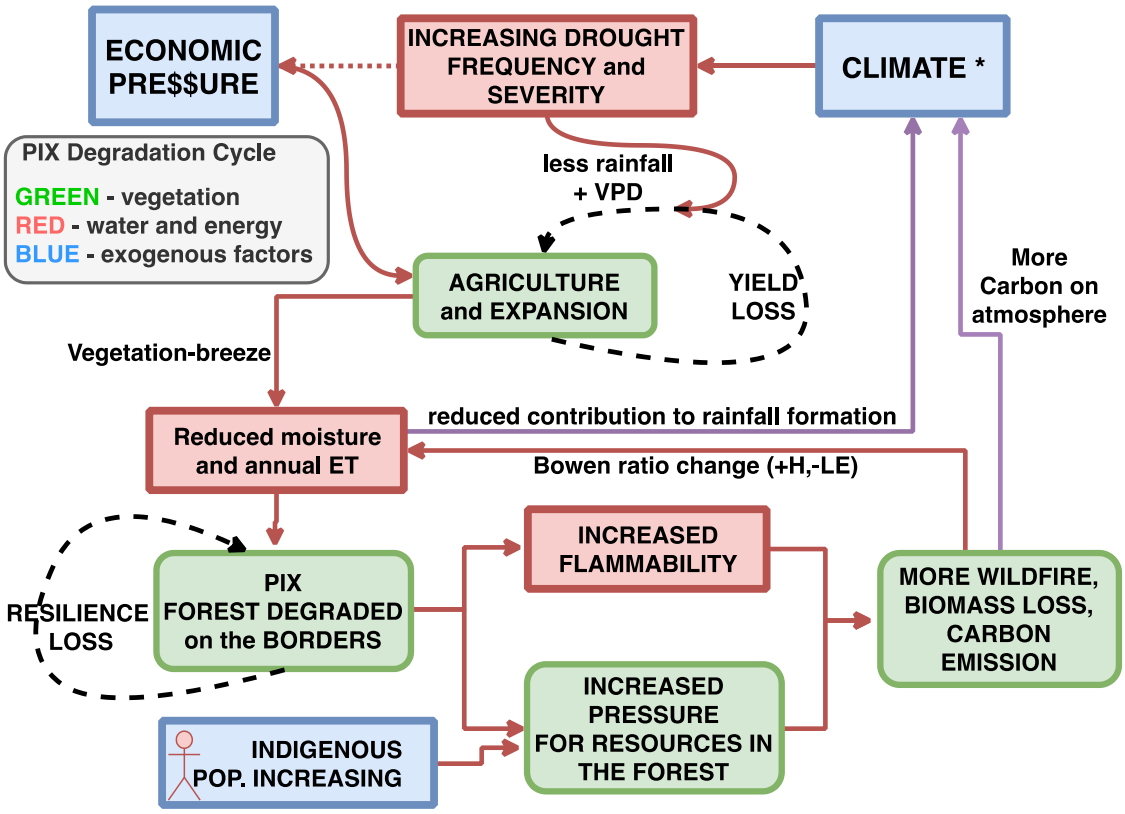

Figure 4.11: PIX degradation cycle. * indicates a factor that is both exogenous and endogenous.

Global population increase is leading to higher demand for food, which turns into the globalization of food commodities, finally, pushing agricultural expansion to new lands (Boerema et al., 2016). This poses the Economic Pressure indicated in Figure 4.11, which shows the interconnectedness of human, land and climate factors on the PIX degradation cycle. The background of our study is a period of continuous drought, with SPEI levels below the average since the late '90s. This dreadful scenario deserves further investigation and raises questions: is this SPEI inversion a local and isolated phenomenon or is that a sign that Amazon is reaching the tipping point of its hydrothermal sustainability, as suggested by Davidson et al. (2012)? The fact is, the study period

presented two major drought events, one centered in 2005/2006 and the more severe and extended in 2015/2016.

During the same period (2003-2017), we witnessed a fast-paced agricultural expansion driven by commodities price boom and government incentives (Hargrave and Kis-Katos, 2013). LUC slowed down in the last years due to legal restrictions (proximity to protected areas), Brazilian environmental agencies enforcement efforts and, climatological adverse conditions. The latter led to astounding crop yield loss in 2005/2006 and even more in 2015/2016, as soybean cannot cope with an extended drought. More specifically, the soybean crop is highly sensitive to environmental conditions in the reproductive phase (flowering, pod formation, and grain filling). Droughts are characterized by high temperatures (LSTday) and evaporative stress (ESI), thus hurdling soybean production, which suggests that local climate anomalies can be an impediment to this economic activity for this economic activity. ET rates are altered by LUC and repeated droughts (Lathuillière et al., 2012), which can lead to a reduction in the water source for precipitation formation (Fisher et al., 2009, 2017), representing a long-term threat for the local agriculture.

The agricultural expansion can be tracked by fire occurrences, as mapped in Figure 4.7. Andela et al. (2017) found decreasing trends in the human-driven global burned area, which is in agreement with what we observed. Is the expansion deceleration due to human consciousness or just the lack of areas to convert? In our case, the second possibility seems more plausible. As shown in Figure 4.7, there is a shifting of fire occurrences toward the PIX borders and, as in 2016, an above normal number of AFO in

legally protected areas, indicating the vegetation breeze effects increasing forest flammability and, therefore, fire risk.

Brazil experienced economic growth during the period, which reflected on enhanced indigenous welfare and led to population growth (Schwartzman et al., 2013; Villas-Bôas, 2012). The natives traditionally make sustainable use of fire in their subsistence agriculture (Uhl et al., 1988), however, with increased pressure for resources inside the PIX associated with repeated droughts, their way of living is also put under threat. As forest desiccation encroaches the park indicating loss of resilience on the forest/agriculture interfaces (Figure 4.10), we observe inwards and outwards degradation signs represented by high yearly GPP variance, although firm conclusions can be overstated due to significant uncertainties on GPP estimations (Joiner et al., 2018). Our study suggests that forest resilience loss has, therefore, positive feedback (dashed line in Figure 4.11), which initially unfolds into a harsh prospect for the local environment with long-term consequences at a larger scale.

Post-drought GPP totals decrease are evident (Figure 4.9, when Cerrado and forest have their contribution to the local carbon balance reduced. The Amazon is a large terrestrial carbon sink, however, at small scales, as pointed out by Espírito-Santo et al. (2014), there are hotspots of higher tree dieback, slowly shifting the area from carbon sink to neutral, a behavior also demonstrated by Baccini et al. (2019) on the eastern and southern portions of the forest. We mapped hotspots of intense forest disturbance and shifting patterns; although these spots are not big enough yet to significantly change the carbon sink role of Amazon, the expansion of these weakened areas is just another cog in the land degradation engine. The changes in carbon balance, also catalyzed by frequent

droughts (thus, ET reduction), imply in an increase in greenhouse gases released to the atmosphere, potentially leading to changes in the climate (purple arrows in Figure 4.11) (Cai et al., 2014; Huntingford et al., 2013). That being said, we do not see how the SPEI levels will again fluctuate close to the historical average. With this scenario being drawn, we consider that agriculture is facing a climate-related potential yield loss as the PIX degradation cycle advances.

Protected areas (like the PIX) are effective in hampering LUC and, therefore, maintaining the ecosystem stability (Carranza et al., 2014). We observed the increasing effects of vegetation breeze on forest resilience and, the chain-reaction on climate and consequently in agriculture sustainability. Breaking the stability implies shocks to an increasingly weakened ecosystem. Freitas et al. (2018), in a study on federal and state level relaxation of policies for land tenure consolidation for illegal farmers and loggers, indicate that we are moving away from the deforestation reduction (signed) global agreements. Improved regulation and governance fostering vertical intensification of cropland and pasture is a way to increase productivity and, therefore, relieve the pressure for LUC (Garrett et al., 2018).

We concluded that agricultural expansion is, therefore, a threat to itself and to the economic sustainability it strives for. Consequences of LUC are ubiquitous, ranging from forest disturbances to changes in the climate. Actions to mitigate the effects of repeated drought occurrences are needed; they can be partially addressed by reaching tighter adaptation to drought and, verticalization of the already converted areas to increase productivity. The whole system would benefit from forest conservation endeavors, leading to better management of the pressure for resources, improving indigenous wellbeing and

forest resilience. Long term results of them would likely reflect on the local carbon balance and hopefully, reduction of climate anomalies frequency bringing stability to the ecosystem.

Future research can help answer questions raised in this study, improve the understanding of the PIX degradation cycle intricacies and, local climate changing. The persistent SPEI negative anomalies is a phenomenon that has to be investigated on the entire Amazon biome to detect possible land degradation related changes in the climate. Another interesting research subject is the mapping of forest disturbance using the GPP variance technique. Further, there is a clear need for human dimension data, especially when it comprehends demographics and economics related to forest dwellers.

CHAPTER 5.

FINAL REMARKS AND OUTLOOK

The three studies compiled in this document are based on data from the 2000s and, all the regions covered presented above normal drought occurrences with unprecedent impacts. The availability of high-quality RS data, especially those from the MODIS series, allowed us to design innovative techniques and approach some underexplored subjects in drought impacts assessment. These two aspects have to be highlighted: the high availability of data and the high number and intensity of drought events. Climate variability is on the rise and, our studies point to an intriguing question: is drought the new normal?

In the south of Brazil, anticipating agricultural drought impacts in soybean based on "within growing season" data seems possible, but far from trivial. To date, the freely available RS data with spatial and temporal resolution to address the retrieval of such information is still a limiting factor for robust systems to operate. Nevertheless, our study presented on Chapter 2indicates that we can move on this direction with reasonably good results, delivering new and valuable information for agriculture value chain stakeholders. A similar approach might have better results on the Brazilian midwestern agriculture, with larger and more homogeneous agricultural areas. The results presented on Chapter 4 indicate the possibility of modeling soybean yields with r^2 of 0.7, with higher sensitivity to thermal based data from the reproduction/grain-filling phase. Both studies provide possible solutions for yield assessment, which might have increasing importance as drought frequency also increases.

Time-series of RS data allowed us to understand the unfolding of land degradation (LD) in regions where drought is repeated and, in some cases, also extended. The studies about northeast Brazil and southeastern Amazon (Chapters 3 and 4, respectively) brought new insights on how drought leads to LD and are often catalyzed by human actions. The

case of Xingú Indigenous Park (PIX) is emblematic: land use changes leading to forest resilience loss even in protected areas, as an impact of local microclimate alteration promoting forest desiccation and, therefore, increasing flammability. Another question surfaces: is the same happening in other parts of Amazon or, going even further, is this phenomenon happening at a much larger scale? The concept of drought in the Anthropocene is, thus, taken to another level, with humans not relegated to cause only direct hydrological impacts, rather, as positive feedback in a cycle encompassing land use changes impacting the climate. On top of the LD feedback on climate, there is also the increased pressure on the ecosystem posed by increasing population and demand for resources.

All the rhetorical questions presented here, sometimes as post-realizations, can turn into valid scientific questions, thus, directing future research. Here are listed these unanswered questions and suggestions:

- Is something like the PIX LD cycle happening in other parts of Amazon and possibly in other tropical forest/non-forest interfaces?
- Is the to date apparently persistent drought (from a SPEI standpoint) happening in other areas in Amazon, indicating the reach of a "tipping point", as suggested by Davidson et al. (2012)?
- What is the economic value of information of agricultural drought predictions?
- There is a need for better understanding the feedbacks of LD on climate for Brazil, not only in the studied places, but the whole country.
- There is also a need for better human dimensions data. Such information will lead to improved use of RS data for assessing drought impacts and also understand feedback mechanisms.

As emphasized, RS-based studies focusing on social problems requires more data on the human side. This is key for making science more applied and tangible. However, there is

one factor that brings even more uncertainties: political decisions. At the same time that I write these conclusions, science and climate research are being defunded in the United States and, to a more severe degree in Brazil. Political decisions, unfortunately, often fail to follow scientific evidence. There is a debate in Earth sciences about "tipping points": the thawing of the Greenland and Antarctica, Amazon as a carbon source, changes in the oceanic streams like the deceleration of the Thermohaline Circulation (W. Liu, Xie, Liu, & Zhu, 2017), methane release from the bottom of warming oceans to the atmosphere, to name few. What are the tipping points we have to reach to prevent self-destructive political decisions?

REFERENCES

Adegoke, J. O., & Carleton, A. M. (2002). Relations between Soil Moisture and Satellite Vegetation Indices in the U.S. Corn Belt. *Journal of Hydrometeorology*, *3*(4), 395–405. https://doi.org/10.1175/1525-7541(2002)003<0395:RBSMAS>2.0.CO;2

AghaKouchak, A., Farahmand, A., Melton, F. S. S., Teixeira, J., Anderson, M. C. C., Wardlow, B. D. D., & Hain, C. R. R. (2015). Remote sensing of drought: Progress, challenges and opportunities. *Reviews of Geophysics*, *53*(2), 452–480. https://doi.org/10.1002/2014RG000456

Albrecht, L. P., Krenchinski, F. H., Gomes, A. D. O., Albrecht, A. J. P., Mattiuzzi, M. D., & Cassol, M. (2018). Performance of fall and winter crops in a no tillage system in west Paraná State. *Acta Scientiarum. Agronomy*, *40*(1), 34999. https://doi.org/10.4025/actasciagron.v40i1.34999

Alliprandini, L. F., Abatti, C., Bertagnolli, P. F., Cavassim, J. E., Gabe, H. L., Kurek, A., … Steckling, C. (2009). Understanding Soybean maturity groups in Brazil: environment, cultivar classification, and stability. *Crop Science*, *49*(3), 801. https://doi.org/10.2135/cropsci2008.07.0390

Alves, T. L. B., de Azevedo, P. V., & Costa dos Santos, C. A. (2017). Influence of climate variability on land degradation (desertification) in the watershed of the upper Paraíba River. *Theoretical and Applied Climatology*, *127*(3–4), 741–751. https://doi.org/10.1007/s00704-015-1661-1

Andela, N., Morton, D. C., Giglio, L., Chen, Y., van der Werf, G. R., Kasibhatla, P. S., … Randerson, J. T. (2017). A human-driven decline in global burned area. *Science*, *356*(6345), 1356–1362. https://doi.org/10.1126/science.aal4108

Anderegg, W. R. L., Konings, A. G., Trugman, A. T., Yu, K., Bowling, D. R., Gabbitas, R., … Zenes, N. (2018). Hydraulic diversity of forests regulates ecosystem resilience during drought. *Nature*, *561*(7724), 538–541. https://doi.org/10.1038/s41586-018-0539-7

Anderson, L. O., Ribeiro Neto, G., Cunha, A. P., Fonseca, M. G., Mendes de Moura, Y., Dalagnol, R., … de Aragão, L. E. O. E. C. (2018). Vulnerability of Amazonian forests to repeated droughts. *Philosophical Transactions of the Royal Society of London. Series B, Biological Sciences*, *373*(1760). https://doi.org/10.1098/rstb.2017.0411

Anderson, M. C., Hain, C., Otkin, J., Zhan, X., Mo, K., Svoboda, M., … Pimstein, A. (2013). An Intercomparison of Drought Indicators Based on Thermal Remote Sensing and NLDAS-2 Simulations with U.S. Drought Monitor Classifications. *Journal of Hydrometeorology*, *14*(4), 1035–1056. https://doi.org/10.1175/JHM-D-12-0140.1

Anderson, M. C., Norman, J. M., Mecikalski, J. R., Otkin, J. a., & Kustas, W. P. (2007a).

A climatological study of evapotranspiration and moisture stress across the continental United States based on thermal remote sensing: 1. Model formulation. *Journal of Geophysical Research*, *112*(D10), D10117. https://doi.org/10.1029/2006JD007506

Anderson, M. C., Norman, J. M., Mecikalski, J. R., Otkin, J. a., & Kustas, W. P. (2007b). A climatological study of evapotranspiration and moisture stress across the continental United States based on thermal remote sensing: 2. Surface moisture climatology. *Journal of Geophysical Research*, *112*(D11), D11112. https://doi.org/10.1029/2006JD007507

Anderson, M. C., Zolin, C. A., Hain, C. R., Semmens, K., Tugrul Yilmaz, M., & Gao, F. (2015). Comparison of satellite-derived LAI and precipitation anomalies over Brazil with a thermal infrared-based Evaporative Stress Index for 2003–2013. *Journal of Hydrology*, *526*, 287–302. https://doi.org/10.1016/j.jhydrol.2015.01.005

Anderson, M. C., Zolin, C. A., Sentelhas, P. C., Hain, C. R., Semmens, K., Tugrul Yilmaz, M., … Tetrault, R. (2016). The Evaporative Stress Index as an indicator of agricultural drought in Brazil: An assessment based on crop yield impacts. *Remote Sensing of Environment*, *174*, 82–99. https://doi.org/10.1016/j.rse.2015.11.034

Anderson, M., & Kustas, W. (2008). Thermal remote sensing of drought and evapotranspiration. *Eos*, *89*(26), 233–234. https://doi.org/10.1029/2008EO260001

Anderson, W., Seager, R., Baethgen, W., & Cane, M. (2018). Trans-Pacific ENSO teleconnections pose a correlated risk to agriculture. *Agricultural and Forest Meteorology*, *262*(November 2017), 298–309. https://doi.org/10.1016/j.agrformet.2018.07.023

António Sumila, T. C., Pires, G. F., Fontes, V. C., & Costa, M. H. (2017). Sources of Water Vapor to Economically Relevant Regions in Amazonia and the Effect of Deforestation. *Journal of Hydrometeorology*, *18*(6), 1643–1655. https://doi.org/10.1175/JHM-D-16-0133.1

Aragão, L. E. O. C., Anderson, L. O., Fonseca, M. G., Rosan, T. M., Vedovato, L. B., Wagner, F. H., … Saatchi, S. (2018). 21st Century drought-related fires counteract the decline of Amazon deforestation carbon emissions. *Nature Communications*, *9*(1), 1–12. https://doi.org/10.1038/s41467-017-02771-y

Arvor, D., Jonathan, M., Meirelles, M. S. P., Dubreuil, V., & Durieux, L. (2011). Classification of MODIS EVI time series for crop mapping in the state of Mato Grosso, Brazil. *International Journal of Remote Sensing*, *32*(22), 7847–7871. https://doi.org/10.1080/01431161.2010.531783

Avissar, R., & Werth, D. (2005). Global Hydroclimatological Teleconnections Resulting from Tropical Deforestation. *Journal of Hydrometeorology*, *6*(2), 134–145. https://doi.org/10.1175/JHM406.1

Awange, J. L., Mpelasoka, F., & Goncalves, R. M. (2016). When every drop counts: Analysis of Droughts in Brazil for the 1901-2013 period. *Science of the Total Environment*, *566–567*, 1472–1488. https://doi.org/10.1016/j.scitotenv.2016.06.031

Baccini, A., Walker, W., Carvalho, L., Farina, M., & Houghton, R. A. (2019). Response to Comment on "Tropical forests are a net carbon source based on aboveground measurements of gain and loss." *Science*, *363*(6423), eaat1205. https://doi.org/10.1126/science.aat1205

Bajgain, R., Xiao, X., Wagle, P., Basara, J., & Zhou, Y. (2015). Sensitivity analysis of vegetation indices to drought over two tallgrass prairie sites. *ISPRS Journal of Photogrammetry and Remote Sensing*, *108*, 151–160. https://doi.org/10.1016/j.isprsjprs.2015.07.004

Barbosa, H. A., & Lakshmi Kumar, T. V. (2016). Influence of rainfall variability on the vegetation dynamics over Northeastern Brazil. *Journal of Arid Environments*, *124*, 377–387. https://doi.org/10.1016/j.jaridenv.2015.08.015

Battisti, R., & Sentelhas, P. C. (2015). Drought Tolerance of Brazilian Soybean Cultivars Simulated By a Simple Agrometeorological Yield Model. *Experimental Agriculture*, *51*(2), 285–298. https://doi.org/10.1017/S0014479714000283

Battisti, Rafael, Sentelhas, P. C., Boote, K. J., Gil, G. M., Farias, J. R. B., & Basso, C. J. (2017). Assessment of soybean yield with altered water-related genetic improvement traits under climate change in Southern Brazil. *European Journal of Agronomy*, *83*, 1–14. https://doi.org/10.1016/j.eja.2016.11.004

Beck, H. E., Vergopolan, N., Pan, M., Levizzani, V., van Dijk, A. I. J. M., Weedon, G. P., … Wood, E. F. (2017). Global-scale evaluation of 22 precipitation datasets using gauge observations and hydrological modeling. *Hydrology and Earth System Sciences*, *21*(12), 6201–6217. https://doi.org/10.5194/hess-21-6201-2017

Behrangi, A., Fetzer, E. J., & Granger, S. L. (2016). Early detection of drought onset using near surface temperature and humidity observed from space. *International Journal of Remote Sensing*, *37*(16), 3911–3923. https://doi.org/10.1080/01431161.2016.1204478

Berlato, M. A., Farenzena, H., & Fontana, D. C. (2005). Associação entre El Niño Oscilação Sul e a produtividade do milho no Estado do Rio Grande do Sul. *Pesquisa Agropecuária Brasileira*, *40*(5), 423–432. https://doi.org/10.1590/S0100-204X2005000500001

Boegh, E., Soegaard, H., Hanan, N., Kabat, P., & Lesch, L. (1999). A remote sensing study of the NDVI-T(s) relationship and the transpiration from sparse vegetation in the sahel based on high-resolution satellite data. *Remote Sensing of Environment*, *69*(3), 224–240. https://doi.org/10.1016/S0034-4257(99)00025-5

Boerema, A., Peeters, A., Swolfs, S., Vandevenne, F., Jacobs, S., Staes, J., & Meire, P.

(2016). Soybean trade: Balancing environmental and socio-economic impacts of an intercontinental market. *PLoS ONE*, *11*(5), 1–13. https://doi.org/10.1371/journal.pone.0155222

Bolten, J. D., & Crow, W. T. (2012). Improved prediction of quasi-global vegetation conditions using remotely-sensed surface soil moisture. *Geophysical Research Letters*, *39*(19). https://doi.org/10.1029/2012GL053470

Bolton, D. K., & Friedl, M. A. (2013). Forecasting crop yield using remotely sensed vegetation indices and crop phenology metrics. *Agricultural and Forest Meteorology*, *173*, 74–84. https://doi.org/10.1016/j.agrformet.2013.01.007

Brando, Paulo M, Paolucci, L., Ummenhofer, C. C., Ordway, E. M., Hartmann, H., Cattau, M. E., … Balch, J. (2019). Droughts, Wildfires, and Forest Carbon Cycling: A Pantropical Synthesis. *Annual Review of Earth and Planetary Sciences*, *47*(1), 555–581. https://doi.org/10.1146/annurev-earth-082517-010235

Brando, Paulo Monteiro, Balch, J. K., Nepstad, D. C., Morton, D. C., Putz, F. E., Coe, M. T., … Soares-Filho, B. S. (2014). Abrupt increases in Amazonian tree mortality due to drought-fire interactions. *Proceedings of the National Academy of Sciences of the United States of America*, *111*(17), 6347–6352. https://doi.org/10.1073/pnas.1305499111

Brandt, M., Romankiewicz, C., Spiekermann, R., & Samimi, C. (2014). Environmental change in time series - An interdisciplinary study in the Sahel of Mali and Senegal. *Journal of Arid Environments*, *105*, 52–63. https://doi.org/10.1016/j.jaridenv.2014.02.019

Bretan, E., & Engle, N. L. (2017). Drought Preparedness Policies and Climate Change Adaptation and Resilience Measures in Brazil: An Institutional Change Assessment. In J. I. Uitto, J. Puri, & R. D. van den Berg (Eds.), *Evaluating Climate Change Action for Sustainable Development* (pp. 305–326). Cham: Springer International Publishing. https://doi.org/10.1007/978-3-319-43702-6_17

Briant, G., Gond, V., & Laurance, S. G. W. (2010). Habitat fragmentation and the desiccation of forest canopies: A case study from eastern Amazonia. *Biological Conservation*, *143*(11), 2763–2769. https://doi.org/10.1016/j.biocon.2010.07.024

Brito, S. S. B., Cunha, A. P. M. A., Cunningham, C. C., Alvalá, R. C., Marengo, J. A., & Carvalho, M. A. (2017). Frequency, duration and severity of drought in the Semiarid Northeast Brazil region. *International Journal of Climatology*, *529*(August 2017), 517–529. https://doi.org/10.1002/joc.5225

Caccamo, G., Chisholm, L. a., Bradstock, R. a., & Puotinen, M. L. (2011). Assessing the sensitivity of MODIS to monitor drought in high biomass ecosystems. *Remote Sensing of Environment*, *115*(10), 2626–2639. https://doi.org/10.1016/j.rse.2011.05.018

Cai, W., Borlace, S., Lengaigne, M., Van Rensch, P., Collins, M., Vecchi, G., … Jin, F. F. (2014). Increasing frequency of extreme El Niño events due to greenhouse warming. *Nature Climate Change*, *4*(2), 111–116. https://doi.org/10.1038/nclimate2100

Camargo, J. L. C., & Kapos, V. (1995). Complex edge effects on soil moisture and microclimate in central Amazonian forest. *Journal of Tropical Ecology*, *11*(2), 205–221.

Carmello, V., & Neto, J. L. S. (2016). Rainfall Variability and Soybean Yield in Paraná State , Southern Brazil. *International Journal of Environmental & Agriculture Research*, *2*(1), 86–97.

Carranza, T., Balmford, A., Kapos, V., & Manica, A. (2014). Protected area effectiveness in reducing conversion in a rapidly vanishing ecosystem: The Brazilian Cerrado. *Conservation Letters*, *7*(3), 216–223. https://doi.org/10.1111/conl.12049

Castelhano, F. J., Pinheiro, G. M., & Roseghini, W. F. F. (2017). Correlação entre precipitação estimada por satélite e dados de superfície para apliacação em estudos climatológicos. *Geosul*, *32*(64), 179–192.

Cerri, C. E. P., Easter, M., Paustian, K., Killian, K., Coleman, K., Bernoux, M., … Cerri, C. C. (2007). Predicted soil organic carbon stocks and changes in the Brazilian Amazon between 2000 and 2030. *Agriculture, Ecosystems and Environment*, *122*(1), 58–72. https://doi.org/10.1016/j.agee.2007.01.008

Charney, J., Quirk, W. J., Chow, S., & Kornfield, J. (1977). A Comparative Study of the Effects of Albedo Change on Drought in Semi–Arid Regions. *Journal of the Atmospheric Sciences*. https://doi.org/10.1175/1520-0469(1977)034<1366:ACSOTE>2.0.CO;2

Cirino, P. H., Féres, J. G., Braga, M. J., & Reis, E. (2015). Assessing the Impacts of ENSO-related weather effects on the Brazilian Agriculture. *Procedia Economics and Finance*, *24*(15), 146–155. https://doi.org/10.1016/S2212-5671(15)00635-8

Cochrane, M. A., & Laurance, W. F. (2008). Synergisms among Fire, Land Use, and Climate Change in the Amazon. *Ambio*, *37*(7/8), 522–527. https://doi.org/https://www.jstor.org/stable/25547943

Coe, M. T., Marthews, T. R., Costa, M. H. ei., Galbraith, D. R., Greenglass, N. L., Imbuzeiro, H. M. A., … Wang, J. (2013). Deforestation and climate feedbacks threaten the ecological integrity of south-southeastern Amazonia. *Philosophical Transactions of the Royal Society of London. Series B, Biological Sciences*, *368*(1619), 20120155. https://doi.org/10.1098/rstb.2012.0155

Corbeels, M., Scopel, E., Cardoso, A., Bernoux, M., Douzet, J. M., & Neto, M. S. (2006). Soil carbon storage potential of direct seeding mulch-based cropping systems in the Cerrados of Brazil. *Global Change Biology*, *12*(9), 1773–1787. https://doi.org/10.1111/j.1365-2486.2006.01233.x

Costa, M. H., Yanagi, S. N. M., Souza, P. J. O. P., Ribeiro, A., & Rocha, E. J. P. (2007). Climate change in Amazonia caused by soybean cropland expansion, as compared to caused by pastureland expansion. *Geophysical Research Letters*, *34*(7), 2–5. https://doi.org/10.1029/2007GL029271

Crouzeilles, R., Feltran-Barbieri, R., Ferreira, M. S., & Strassburg, B. B. N. (2017). Hard times for the Brazilian environment. *Nature Ecology & Evolution*, *1*(September), 2017. https://doi.org/10.1038/s41559-017-0303-7

Crow, W. T., Berg, A. A., Cosh, M. H., Loew, A., Mohanty, B. P., Panciera, R., … Walker, J. P. (2012). Upscaling sparse ground-based soil moisture observations for the validation of coarse-resolution satellite soil moisture products. *Reviews of Geophysics*, *50*(2), 1–20. https://doi.org/10.1029/2011RG000372

Cunha, A. P. M., Alvalá, R. C., Nobre, C. A., & Carvalho, M. A. (2015). Monitoring vegetative drought dynamics in the Brazilian semiarid region. *Agricultural and Forest Meteorology*, *214–215*, 494–505. https://doi.org/10.1016/j.agrformet.2015.09.010

D'Odorico, P., Bhattachan, A., Davis, K. F., Ravi, S., & Runyan, C. W. (2013). Global desertification: Drivers and feedbacks. *Advances in Water Resources*, *51*, 326–344. https://doi.org/10.1016/j.advwatres.2012.01.013

da Rocha, H. R., Manzi, A. O., Cabral, O. M., Miller, S. D., Goulden, M. L., Saleska, S. R., … Maia, J. F. (2009). Patterns of water and heat flux across a biome gradient from tropical forest to savanna in Brazil. *Journal of Geophysical Research*, *114*(1), G00B12. https://doi.org/10.1029/2007JG000640

Dai, A. G. (2013). Increasing drought under global warming in observations and models. *Nature Climate Change*, *3*(1), 52–58. https://doi.org/10.1038/nclimate1633

Dardel, C., Kergoat, L., Hiernaux, P., Mougin, E., Grippa, M., & Tucker, C. J. (2014). Re-greening Sahel: 30 years of remote sensing data and field observations (Mali, Niger). *Remote Sensing of Environment*, *140*, 350–364. https://doi.org/10.1016/j.rse.2013.09.011

Das, N. N., Entekhabi, D., & Njoku, E. G. (2011). An algorithm for merging SMAP radiometer and radar data for high-resolution soil-moisture retrieval. *IEEE Transactions on Geoscience and Remote Sensing*, *49*(5), 1504–1512. https://doi.org/10.1109/TGRS.2010.2089526

Davidson, E. A., de Araújo, A. C., Artaxo, P., Balch, J. K., Brown, I. F., C. Bustamante, M. M., … Wofsy, S. C. (2012). The Amazon basin in transition. *Nature*, *481*(7381), 321–328. https://doi.org/10.1038/nature10717

de Jong, R., de Bruin, S., de Wit, A., Schaepman, M. E., & Dent, D. L. (2011). Analysis of monotonic greening and browning trends from global NDVI time-series. *Remote Sensing of Environment*, *115*(2), 692–702. https://doi.org/10.1016/j.rse.2010.10.011

Detto, M., Molini, A., Katul, G., Stoy, P., Palmroth, S., & Baldocchi, D. (2012). Causality and Persistence in Ecological Systems: A Nonparametric Spectral Granger Causality Approach. *The American Naturalist*, *179*(4), 524–535. https://doi.org/10.1086/664628

Dias, L. C. P. P., Pimenta, F. M., Santos, A. B., Costa, M. H., & Ladle, R. J. (2016). Patterns of land use, extensification, and intensification of Brazilian agriculture. *Global Change Biology*, *22*(8), 2887–2903. https://doi.org/10.1111/gcb.13314

Dinku, T., Funk, C., Peterson, P., Maidment, R., Tadesse, T., Gagain, H., & Ceccato, P. (2018). Validation of the CHIRPS Satellite Rainfall Estimates over Eastern of Africa. *Quarterly Journal of the Royal Meteorological Society*, 1–24.

Draper, C., Reichle, R., de Jeu, R., Naeimi, V., Parinussa, R., & Wagner, W. (2013). Estimating root mean square errors in remotely sensed soil moisture over continental scale domains. *Remote Sensing of Environment*, *137*, 288–298. https://doi.org/10.1016/j.rse.2013.06.013

Dubovyk, O., Menz, G., Conrad, C., Kan, E., Machwitz, M., & Khamzina, A. (2013). Spatio-temporal analyses of cropland degradation in the irrigated lowlands of Uzbekistan using remote-sensing and logistic regression modeling. *Environmental Monitoring and Assessment*, *185*(6), 4775–4790. https://doi.org/10.1007/s10661-012-2904-6

Eberhardt, I. D. R., Schultz, B., Rizzi, R., Sanches, I. D. A., Formaggio, A. R., Atzberger, C., … Luiz, A. J. B. (2016). Cloud cover assessment for operational crop monitoring systems in tropical areas. *Remote Sensing*, *8*(3), 1–14. https://doi.org/10.3390/rs8030219

Eckert, S., Hüsler, F., Liniger, H., & Hodel, E. (2015). Trend analysis of MODIS NDVI time series for detecting land degradation and regeneration in Mongolia. *Journal of Arid Environments*, *113*, 16–28. https://doi.org/10.1016/j.jaridenv.2014.09.001

Espinoza, J. C., Ronchail, J., Marengo, J. A., & Segura, H. (2018). Contrasting North–South changes in Amazon wet-day and dry-day frequency and related atmospheric features (1981–2017). *Climate Dynamics*, *0*(0), 0. https://doi.org/10.1007/s00382-018-4462-2

Espinoza, J. C., Ronchail, J., Marengo, J. A., & Segura, H. (2019). Contrasting North–South changes in Amazon wet-day and dry-day frequency and related atmospheric features (1981–2017). *Climate Dynamics*, *52*(9–10), 5413–5430. https://doi.org/10.1007/s00382-018-4462-2

Espírito-Santo, F. D. B., Gloor, M., Keller, M., Malhi, Y., Saatchi, S., Nelson, B., … Phillips, O. L. (2014). Size and frequency of natural forest disturbances and the Amazon forest carbon balance. *Nature Communications*, *5*(1), 3434. https://doi.org/10.1038/ncomms4434

Esquerdo, J. C. D. M. D. M., Zullo, J., Antunes, J. F. G. G., Zullo Júnior, J., & Antunes, J. F. G. G. (2011). Use of NDVI/AVHRR time-series profiles for soybean crop monitoring in Brazil. *International Journal of Remote Sensing*, *32*(13), 3711–3727. https://doi.org/10.1080/01431161003764112

Evans, J., & Geerken, R. (2004). Discrimination between climate and human-induced dryland degradation. *Journal of Arid Environments*, *57*(4), 535–554. https://doi.org/10.1016/S0140-1963(03)00121-6

Fang, C., Luo, K., Kong, Y., Lin, H., & Ren, Y. (2018). Evaluating Performance and Elucidating the Mechanisms of Collaborative Development within the Beijing–Tianjin–Hebei Region, China. *Sustainability*, *10*(2), 471. https://doi.org/10.3390/su10020471

Fang, H., Liang, S., & Hoogenboom, G. (2011). Integration of MODIS LAI and vegetation index products with the CSM-CERES-Maize model for corn yield estimation. *International Journal of Remote Sensing*, *32*(4), 1039–1065. https://doi.org/10.1080/01431160903505310

Farias, J. R. B., Assad, E. D., de Almeida, I. R., Evangelista, B. A., Lazzarotto, C., Neumaier, N., & Nepomuceno, A. L. (2001). Caracterização de risco de déficit hídrico nas regiões produtoras de soja no Brasil. *Revista Brasileira de Agrometeorologia*, *9*(3), 415–421.

Feldpausch, T. R., Phillips, O. L., Brienen, R. J. W., Gloor, E., Lloyd, J., Lopez-Gonzalez, G., … Vos, V. A. (2016). Amazon forest response to repeated droughts. *Global Biogeochemical Cycles*, *30*(7), 964–982. https://doi.org/10.1002/2015GB005133

Fensholt, R., & Proud, S. R. (2012). Evaluation of earth observation based global long term vegetation trends - Comparing GIMMS and MODIS global NDVI time series. *Remote Sensing of Environment*, *119*, 131–147. https://doi.org/10.1016/j.rse.2011.12.015

Fensholt, R., Sandholt, I., & Rasmussen, M. S. (2004). Evaluation of MODIS LAI, fAPAR and the relation between fAPAR and NDVI in a semi-arid environment using in situ measurements. *Remote Sensing of Environment*, *91*(3–4), 490–507. https://doi.org/10.1016/j.rse.2004.04.009

Filho, A. R., & Pereira, L. C. (1999). Aptidão agrícola das terras do Brasil. Rio de Janeiro, RJ, Brazil: Emprapa Solos.

Fisher, J. B., Malhi, Y., Bonal, D., Da Rocha, H. R., De Araújo, A. C., Gamo, M., … Von Randow, C. (2009). The land-atmosphere water flux in the tropics. *Global Change Biology*, *15*(11), 2694–2714. https://doi.org/10.1111/j.1365-2486.2008.01813.x

Fisher, J. B., Melton, F., Middleton, E., Hain, C., Anderson, M., Allen, R., … Wood, E. F. (2017). The future of evapotranspiration: Global requirements for ecosystemfunctioning, carbon and climate feedbacks, agriculturalmanagement, and water resources. *Water Resources Research*, *10.1002/20*, 2618–2626.

https://doi.org/10.1002/2016WR020175.Received

Franchini, J. C., Balbinot Junior, A. A., Debiasi, H., & Nepomuceno, A. L. (2017). Root growth of soybean cultivars under different water availability conditions. *Semina: Ciências Agrárias*, *38*(2), 715. https://doi.org/10.5433/1679-0359.2017v38n2p715

Freitas, F. L. M., Sparovek, G., Berndes, G., Persson, U. M., Englund, O., Barretto, A., & Mörtberg, U. (2018). Potential increase of legal deforestation in Brazilian Amazon after Forest Act revision. *Nature Sustainability*, *1*(11), 665–670. https://doi.org/10.1038/s41893-018-0171-4

Fu, R., Yin, L., Li, W., Arias, P. A., Dickinson, R. E., Huang, L., … Myneni, R. B. (2013). Increased dry-season length over southern Amazonia in recent decades and its implication for future climate projection. *Proceedings of the National Academy of Sciences*, *110*(45), 18110–18115. https://doi.org/10.1073/pnas.1302584110

Funk, C., Peterson, P., Landsfeld, M., Pedreros, D., Verdin, J., Shukla, S., … Michaelsen, J. (2015). The climate hazards infrared precipitation with stations - a new environmental record for monitoring extremes. *Scientific Data*, *2*, 150066. https://doi.org/10.1038/sdata.2015.66

Galford, G. L., Melillo, J., Mustard, J. F., Cerri, C. E. P., & Cerri, C. C. (2010). The Amazon frontier of land-use change: Croplands and consequences for greenhouse gas emissions. *Earth Interactions*, *14*(15). https://doi.org/10.1175/2010EI327.1

Garcia, B. N., Libonati, R., & Nunes, A. M. B. (2018). Extreme drought events over the Amazon Basin: The perspective from the reconstruction of South American Hydroclimate. *Water (Switzerland)*, *10*(11). https://doi.org/10.3390/w10111594

Garrett, R. D., Koh, I., Lambin, E. F., le Polain de Waroux, Y., Kastens, J. H., & Brown, J. C. (2018). Intensification in agriculture-forest frontiers: Land use responses to development and conservation policies in Brazil. *Global Environmental Change*, *53*(September), 233–243. https://doi.org/10.1016/j.gloenvcha.2018.09.011

Gatti, L. V., Gloor, M., Miller, J. B., Doughty, C. E., Malhi, Y., Domingues, L. G., … Lloyd, J. (2014). Drought sensitivity of Amazonian carbon balance revealed by atmospheric measurements. *Nature*, *506*(7486), 76–80. https://doi.org/10.1038/nature12957

Gelcer, E., Fraisse, C., Dzotsi, K., Hu, Z., Mendes, R., & Zotarelli, L. (2013). Effects of El Niño Southern Oscillation on the space-time variability of Agricultural Reference Index for Drought in midlatitudes. *Agricultural and Forest Meteorology*, *174–175*, 110–128. https://doi.org/10.1016/j.agrformet.2013.02.006

Granger, C. W. J. (1969). Investigating Causal Relations by Econometric Models and Cross-spectral Methods. *Econometrica*, *37*(3), 424. https://doi.org/10.2307/1912791

Grzegozewski, D. M., Johann, J. A., Uribe-Opazo, M. A., Mercante, E., & Coutinho, A. C.

(2016). Mapping soya bean and corn crops in the State of Paraná, Brazil, using EVI images from the MODIS sensor. *International Journal of Remote Sensing*, *37*(6), 1257–1275. https://doi.org/10.1080/01431161.2016.1148285

Guindin-Garcia, N., Gitelson, A. A., Arkebauer, T. J., Shanahan, J., & Weiss, A. (2012). An evaluation of MODIS 8- and 16-day composite products for monitoring maize green leaf area index. *Agricultural and Forest Meteorology*, *161*, 15–25. https://doi.org/10.1016/J.AGRFORMET.2012.03.012

Gusso, A. (2013). Integração de imagens NOAA/AVHRR: Rede de cooperação para monitoramento nacional da safra de soja. *Revista Ceres*, *60*(2), 194–204. https://doi.org/10.1590/S0034-737X2013000200007

Gusso, A., Ducati, J. R., Veronez, M. R., Sommer, V., & Silveira Junior, L. G. da. (2014). Monitoring Heat Waves and Their Impacts on Summer Crop Development in Southern Brazil. *Agricultural Sciences*, *05*(04), 353–364. https://doi.org/10.4236/as.2014.54037

Gutiérrez, A. P. A., Engle, N. L., De Nys, E., Molejón, C., & Martins, E. S. (2014). Drought preparedness in Brazil. *Weather and Climate Extremes*, *3*, 95–106. https://doi.org/10.1016/j.wace.2013.12.001

Hargrave, J., & Kis-Katos, K. (2013). Economic Causes of Deforestation in the Brazilian Amazon: A Panel Data Analysis for the 2000s. *Environmental and Resource Economics*, *54*(4), 471–494. https://doi.org/10.1007/s10640-012-9610-2

Harper, A., Baker, I. T., Denning, A. S., Randall, D. A., Dazlich, D., & Branson, M. (2014). Impact of evapotranspiration on dry season climate in the Amazon forest. *Journal of Climate*, *27*(2), 574–591. https://doi.org/10.1175/JCLI-D-13-00074.1

Hein, L., & de Ridder, N. (2006). Desertification in the Sahel: a reinterpretation. *Global Change Biology*, *12*(5), 751–758. https://doi.org/10.1111/j.1365-2486.2006.01135.x

Herrmann, S. M., Anyamba, A., & Tucker, C. J. (2005). Recent trends in vegetation dynamics in the African Sahel and their relationship to climate. *Global Environmental Change*, *15*(4), 394–404. https://doi.org/10.1016/j.gloenvcha.2005.08.004

Higginbottom, T. P., & Symeonakis, E. (2014). Assessing land degradation and desertification using vegetation index data: Current frameworks and future directions. *Remote Sensing*, *6*(10), 9552–9575. https://doi.org/10.3390/rs6109552

Hlavinka, P., Trnka, M., Semerádová, D., Dubrovský, M., Žalud, Z., & Možný, M. (2009). Effect of drought on yield variability of key crops in Czech Republic. *Agricultural and Forest Meteorology*, *149*(3–4), 431–442. https://doi.org/10.1016/j.agrformet.2008.09.004

Hobbins, M. T., Wood, A., McEvoy, D. J., Huntington, J. L., Morton, C., Verdin, J., … Hain, C. (2016). The Evaporative Demand Drought Index. Part I: Linking Drought

Evolution to Variations in Evaporative Demand. *Journal of Hydrometeorology*, *17*(6), 1745–1761. https://doi.org/10.1175/JHM-D-15-0121.1

Holling, C. S. (1973). Resilience and Stability of Ecological Systems. *Annual Review of Ecology and Systematics*, *4*(1), 1–23. https://doi.org/10.1146/annurev.es.04.110173.000245

Holmes, T. R. H., Crow, W. T., Hain, C., Anderson, M. C., & Kustas, W. P. (2015). Diurnal temperature cycle as observed by thermal infrared and microwave radiometers. *Remote Sensing of Environment*, *158*, 110–125. https://doi.org/10.1016/j.rse.2014.10.031

Huang, J., Yu, H., Dai, A., Wei, Y., & Kang, L. (2017). Drylands face potential threat under 2°C global warming target. *Nature Climate Change*, *7*(6), 417–422. https://doi.org/10.1038/nclimate3275

Huang, J., Yu, H., Guan, X., Wang, G., & Guo, R. (2015). Accelerated dryland expansion under climate change. *Nature Climate Change*, *6*(October), 1–22. https://doi.org/10.1038/nclimate2837

Huang, L., He, B., Chen, A., Wang, H., Liu, J., Lu, A., & Chen, Z. (2016). Drought dominates the interannual variability in global terrestrial net primary production by controlling semi-arid ecosystems. *Scientific Reports*, *6*(November 2015), 1–7. https://doi.org/10.1038/srep24639

Hulley, G. C., Malakar, N. K., Islam, T., & Freepartner, R. J. (2018). NASA's MODIS and VIIRS Land Surface Temperature and Emissivity Products: A Long-Term and Consistent Earth System Data Record. *IEEE Journal of Selected Topics in Applied Earth Observations and Remote Sensing*, *11*(2), 522–535. https://doi.org/10.1109/JSTARS.2017.2779330

Hunt, E. D., Hubbard, K. G., Wilhite, D. A., Arkebauer, T. J., & Dutcher, A. L. (2009). The development and evaluation of a soil moisture index. *International Journal of Climatology*, *29*(5), 747–759. https://doi.org/10.1002/joc.1749

Huntingford, C., Zelazowski, P., Galbraith, D., Mercado, L. M., Sitch, S., Fisher, R., … Cox, P. M. (2013). Simulated resilience of tropical rainforests to CO 2 -induced climate change. *Nature Geoscience*, *6*(4), 268–273. https://doi.org/10.1038/ngeo1741

IBGE. (2002). *Série Relatórios Metodológicos - Pesquisas agropecuárias* (Vol. 6). Rio de Janeiro, RJ, Brazil. Retrieved from ftp://ftp.ibge.gov.br/Producao_Agricola/Metodologia_da_pesquisa/PesquisasAgropecuarias2002.pdf

IBGE. (2017). *Tabela 3939 - Efetivo dos rebanhos, por tipo de rebanho*. Brasília, DF, Brazil: Instituto Brasileiro de Geografia e Estatística. Retrieved from https://sidra.ibge.gov.br/tabela/3939#/

IBGE. (2018a). Tabela 1612 - Área plantada, área colhida, quantidade produzida, rendimento médio e valor da produção das lavouras temporárias. Brasília, DF, Brazil: Instituto Brasileiro de Geografia e Estatística. Retrieved from https://sidra.ibge.gov.br/tabela/1612

IBGE. (2018b). *Tabela 1612 - Área plantada, área colhida, quantidade produzida, rendimento médio e valor da produção das lavouras temporárias*. Brasília, DF, Brazil: Instituto Brasileiro de Geografia e Estatística. Retrieved from https://sidra.ibge.gov.br/tabela/1612#/

Ji, L., & Peters, A. J. (2003). Assessing vegetation response to drought in the northern Great Plains using vegetation and drought indices. *Remote Sensing of Environment*, *87*(1), 85–98. https://doi.org/10.1016/S0034-4257(03)00174-3

Jiang, L., & Hardee, K. (2011). How do Recent Population Trends Matter to Climate Change? *Population Research and Policy Review*, *30*(2), 287–312. https://doi.org/10.1007/s11113-010-9189-7

Jimenez, J. C., Barichivich, J., Mattar, C., Takahashi, K., Santamaría-Artigas, A., Sobrino, J. A., & Malhi, Y. (2018). Spatio-temporal patterns of thermal anomalies and drought over tropical forests driven by recent extreme climatic anomalies. *Philosophical Transactions of the Royal Society of London. Series B, Biological Sciences*, *373*(1760). https://doi.org/10.1098/rstb.2017.0300

Jimenez, J. C., Libonati, R., & Peres, L. F. (2018). Droughts Over Amazonia in 2005, 2010, and 2015: A Cloud Cover Perspective. *Frontiers in Earth Science*, *6*(December), 1–7. https://doi.org/10.3389/feart.2018.00227

Johnson, D. M. (2014). An assessment of pre- and within-season remotely sensed variables for forecasting corn and soybean yields in the United States. *Remote Sensing of Environment*, *141*. https://doi.org/10.1016/j.rse.2013.10.027

Joiner, J., Yoshida, Y., Zhang, Y., Duveiller, G., Jung, M., Lyapustin, A., … Tucker, C. J. (2018). Estimation of terrestrial global gross primary production (GPP) with satellite data-driven models and eddy covariance flux data. *Remote Sensing*, *10*(9), 1–38. https://doi.org/10.3390/rs10091346

Kalma, J. D., McVicar, T. R., & McCabe, M. F. (2008). Estimating land surface evaporation: A review of methods using remotely sensed surface temperature data. *Surveys in Geophysics*, *29*(4–5), 421–469. https://doi.org/10.1007/s10712-008-9037-z

Kerr, Y. H. (2007). Soil moisture from space: Where are we? *Hydrogeology Journal*, *15*(1), 117–120. https://doi.org/10.1007/s10040-006-0095-3

Khanna, J., Medvigy, D., Fueglistaler, S., & Walko, R. (2017). Regional dry-season climate changes due to three decades of Amazonian deforestation. *Nature Climate Change*, *7*(3), 200–204. https://doi.org/10.1038/nclimate3226

Kim, J., & Hogue, T. S. (2012). Improving Spatial Soil Moisture Representation Through Integration of AMSR-E and MODIS Products. *IEEE Transactions on Geoscience and Remote Sensing*, *50*(2), 446–460. https://doi.org/10.1109/TGRS.2011.2161318

Kinley, R. (2017). Climate change after Paris: from turning point to transformation. *Climate Policy*, *17*(1), 9–15. https://doi.org/10.1080/14693062.2016.1191009

Lambin, E. F., Turner, B. L., Geist, H. J., Agbola, S. B., Angelsen, A., Bruce, J. W., … Xu, J. (2001). The causes of land-use and land-cover change: Moving beyond the myths. *Global Environmental Change*, *11*(4), 261–269. https://doi.org/10.1016/S0959-3780(01)00007-3

Lathuillière, M. J., Johnson, M. S., & Donner, S. D. (2012). Water use by terrestrial ecosystems: Temporal variability in rainforest and agricultural contributions to evapotranspiration in Mato Grosso, Brazil. *Environmental Research Letters*, *7*(2). https://doi.org/10.1088/1748-9326/7/2/024024

Laurance, W. F., Camargo, J. L. C., Luizão, R. C. C., Laurance, S. G., Pimm, S. L., Bruna, E. M., … Lovejoy, T. E. (2011). The fate of Amazonian forest fragments: A 32-year investigation. *Biological Conservation*, *144*(1), 56–67. https://doi.org/10.1016/j.biocon.2010.09.021

Lavinas, L. (2017). How Social Developmentalism Reframed Social Policy in Brazil. *New Political Economy*, *22*(6), 628–644. https://doi.org/10.1080/13563467.2017.1297392

Le Page, Y., Morton, D., Hartin, C., Bond-Lamberty, B., Pereira, J. M. C., Hurtt, G., & Asrar, G. (2017). Synergy between land use and climate change increases future fire risk in Amazon forests. *Earth System Dynamics*, *8*(4), 1237–1246. https://doi.org/10.5194/esd-8-1237-2017

Leitold, V., Morton, D. C., Longo, M., dos-Santos, M. N., Keller, M., & Scaranello, M. (2018). El Niño drought increased canopy turnover in Amazon forests. *New Phytologist*, *219*(3), 959–971. https://doi.org/10.1111/nph.15110

Li, Z., Chen, Y., Wang, Y., & Fang, G. (2016). Dynamic changes in terrestrial net primary production and their effects on evapotranspiration. *Hydrology and Earth System Sciences*, *20*(6), 2169–2178. https://doi.org/10.5194/hess-20-2169-2016

Lima, M., Silva Junior, C. A. da, Rausch, L., Gibbs, H. K., & Johann, J. A. (2019). Demystifying sustainable soy in Brazil. *Land Use Policy*, *82*(December 2018), 349–352. https://doi.org/10.1016/J.LANDUSEPOL.2018.12.016

Liu, W. T., & Kogan, F. (2002). Monitoring Brazilian soybean production using NOAA/AVHRR based vegetation condition indices. *International Journal of Remote Sensing*, *23*(March 2015), 1161–1179. https://doi.org/10.1080/01431160110076126

Liu, W., Xie, S. P., Liu, Z., & Zhu, J. (2017). Overlooked possibility of a collapsed atlantic meridional overturning circulation in warming climate. *Science Advances*, *3*(1), 1–8.

https://doi.org/10.1126/sciadv.1601666

Lobell, D. B., Roberts, M. J., Schlenker, W., Braun, N., Little, B. B., Rejesus, R. M., & Hammer, G. L. (2014). Greater sensitivity to drought accompanies maize yield increase in the U.S. Midwest. *Science*, *344*(6183), 516–519. https://doi.org/10.1126/science.1251423

Loew, A., Stacke, T., Dorigo, W., de Jeu, R., & Hagemann, S. (2013). Potential and limitations of multidecadal satellite soil moisture observations for selected climate model evaluation studies. *Hydrology and Earth System Sciences*, *17*(9), 3523–3542. https://doi.org/10.5194/hess-17-3523-2013

Lopes, A. V., Chiang, J. C. H., Thompson, S. A., & Dracup, J. A. (2016). Trend and uncertainty in spatial-temporal patterns of hydrological droughts in the Amazon basin. *Geophysical Research Letters*, *43*(7), 3307–3316. https://doi.org/10.1002/2016GL067738

Lütkepohl, H. (2005). VAR Processes with Parameter Constraints. In *New introduction to multiple time series analysis* (pp. 193–231). Berlin: Springer Science & Business Media.

Magrin, G. O., Marengo, J. A., Boulanger, J. P., Buckeridge, M. S., Castellanos, E., Poveda, G., … Vicuña, S. (2014). *Impacts, adaptation, and vulnerability: central and South America. Climate change 2014: Impacts, adaptation, and vulnerability. Part B: Regional aspects. Contribution of working group II to the fifth asessment report of the intergovernmental panel on climate change.* New York, NY, USA,.

Mangiarotti, S., Sekhar, M., Berthon, L., Javeed, Y., & Mazzega, P. (2012). Causality analysis of groundwater dynamics based on a Vector Autoregressive model in the semi-arid basin of Gundal (South India). *Journal of Applied Geophysics*, *83*, 1–10. https://doi.org/10.1016/j.jappgeo.2012.04.003

Marengo, José A., Alves, L. M., Alvala, R. C. ., Cunha, A. P., Brito, S., & Moraes, O. L. L. (2017). Climatic characteristics of the 2010-2016 drought in the semiarid Northeast Brazil region. *Anais Da Academia Brasileira de Ciências*, (0), 1–13. https://doi.org/10.1590/0001-3765201720170206

Marengo, Jose A., Alves, L. M., Soares, W. R., Rodriguez, D. A., Camargo, H., Riveros, M. P., & Pabló, A. D. (2013). Two contrasting severe seasonal extremes in tropical South America in 2012: Flood in Amazonia and drought in Northeast Brazil. *Journal of Climate*, *26*(22), 9137–9154. https://doi.org/10.1175/JCLI-D-12-00642.1

Marengo, Jose A., & Bernasconi, M. (2015). Regional differences in aridity/drought conditions over Northeast Brazil: present state and future projections. *Climatic Change*, *129*(1–2), 103–115. https://doi.org/10.1007/s10584-014-1310-1

Marengo, Jose A., Souza, C. A., Thonicke, K., Burton, C., Halladay, K., Betts, R. A., … Soares, W. R. (2018). Changes in Climate and Land Use Over the Amazon Region:

Current and Future Variability and Trends. *Frontiers in Earth Science*, *6*(December). https://doi.org/10.3389/feart.2018.00228

Marengo, Jose A., Torres, R. R., & Alves, L. M. (2016). Drought in Northeast Brazil - past, present, and future. *Theoretical and Applied Climatology*, 1–12. https://doi.org/10.1007/s00704-016-1840-8

Mariano, Denis A., Santos, C. A. C. dos, Wardlow, B. D., Anderson, M. C., Schiltmeyer, A. V., Tadesse, T., & Svoboda, M. D. (2018). Use of remote sensing indicators to assess effects of drought and human-induced land degradation on ecosystem health in Northeastern Brazil. *Remote Sensing of Environment*, *213*(April), 129–143. https://doi.org/10.1016/j.rse.2018.04.048

Mariano, Denis Araujo. (2015). *Detecção e Avaliação de Seca Agronômica através da análise de séries temporais de dados MODIS e PERSIANN*. *Instituto Nacional de Pesquisas Espaciais*. National Institute for Space Research, Brazil. Retrieved from http://mtc-m21b.sid.inpe.br/col/sid.inpe.br/mtc-m21b/2015/02.12.20.29/doc/publicacao.pdf

Martens, B., Miralles, D. G., Lievens, H., Van Der Schalie, R., De Jeu, R. A. M., Fernández-Prieto, D., … Verhoest, N. E. C. (2017). GLEAM v3: Satellite-based land evaporation and root-zone soil moisture. *Geoscientific Model Development*, *10*(5), 1903–1925. https://doi.org/10.5194/gmd-10-1903-2017

Martínez-Fernández, J., González-Zamora, A., Sánchez, N., & Gumuzzio, A. (2015). A soil water based index as a suitable agricultural drought indicator. *Journal of Hydrology*, *522*, 265–273. https://doi.org/10.1016/j.jhydrol.2014.12.051

Martínez-Fernández, J., González-Zamora, A., Sánchez, N., Gumuzzio, A., & Herrero-Jiménez, C. M. M. (2016). Satellite soil moisture for agricultural drought monitoring: Assessment of the SMOS derived Soil Water Deficit Index. *Remote Sensing of Environment*, *177*, 277–286. https://doi.org/10.1016/J.RSE.2016.02.064

Mckee, T. B., Doesken, N. J., & Kleist, J. (1993). The relationship of drought frequency and duration to time scales. In *Eighth Conference on Applied Climatology* (pp. 17–22). Anaheim, California: American Meteorological Society.

Melo, R. W. De, Fontana, D. C., Berlato, M. A., & Ducati, J. R. (2008). An agrometeorological-spectral model to estimate soybean yield, applied to southern Brazil. *International Journal of Remote Sensing*, *29*(14), 4013–4028. https://doi.org/10.1080/01431160701881905

Millen, D. D., Pacheco, R. D. L., Meyer, P. M., Rodrigues, P. H. M., & De Beni Arrigoni, M. (2011). Current outlook and future perspectives of beef production in Brazil. *Animal Frontiers*, *1*(2), 46–52. https://doi.org/10.2527/af.2011-0017

Mishra, A. K., Ines, A. V. M., Das, N. N., Prakash Khedun, C., Singh, V. P., Sivakumar, B., & Hansen, J. W. (2014). Anatomy of a local-scale drought: Application of

assimilated remote sensing products, crop model, and statistical methods to an agricultural drought study. *Journal of Hydrology*, *526*, 15–29. https://doi.org/10.1016/j.jhydrol.2014.10.038

Mladenova, I. E., Bolten, J. D., Crow, W. T., Anderson, M. C., Hain, C. R., Johnson, D. M., & Mueller, R. (2017). Intercomparison of Soil Moisture, Evaporative Stress, and Vegetation Indices for Estimating Corn and Soybean Yields Over the U.S. *IEEE Journal of Selected Topics in Applied Earth Observations and Remote Sensing*, *10*(4), 1328–1343. https://doi.org/10.1109/JSTARS.2016.2639338

Moran, M. S. (2003). Thermal infrared measurement as an indicagtor of plant ecosystem health. In D. A. Quatrocchi & J. Luvall (Eds.), *Thermal Remote Sensing in Land Surface Processes* (pp. 257–282). Philadelphia, PA: Taylor & Francis.

Moura, F. de B. P., Mendes Malhado, A. C., & Ladle, R. J. (2013). Nursing the caatinga back to health. *Journal of Arid Environments*, *90*, 67–68. https://doi.org/10.1016/j.jaridenv.2012.10.010

Mu, Q., Heinsch, F. A., Zhao, M., & Running, S. W. (2007). Development of a global evapotranspiration algorithm based on MODIS and global meteorology data. *Remote Sensing of Environment*, *111*(4), 519–536. https://doi.org/10.1016/j.rse.2007.04.015

Mu, Q., Zhao, M., Kimball, J. S., McDowell, N. G., & Running, S. W. (2013). A remotely sensed global terrestrial drought severity index. *Bulletin of the American Meteorological Society*, *94*(1), 83–98. https://doi.org/10.1175/BAMS-D-11-00213.1

Mu, Q., Zhao, M., & Running, S. W. (2011). Improvements to a MODIS global terrestrial evapotranspiration algorithm. *Remote Sensing of Environment*, *115*(8), 1781–1800. https://doi.org/10.1016/j.rse.2011.02.019

Myneni, R. B., Hoffman, S., Knyazikhin, Y., Privette, J. L., Glassy, J., Tian, Y., … Running, S. W. (2002). Global products of vegetation leaf area and fraction absorbed PAR from year one of MODIS data. *Remote Sensing of Environment*, *83*(1–2), 214–231. https://doi.org/10.1016/S0034-4257(02)00074-3

Nagy, R. C., Porder, S., Brando, P., Davidson, E. A., Figueira, A. M. e. S., Neill, C., … Trumbore, S. (2018). Soil Carbon Dynamics in Soybean Cropland and Forests in Mato Grosso, Brazil. *Journal of Geophysical Research: Biogeosciences*, *123*(1), 18–31. https://doi.org/10.1002/2017JG004269

Nam, W. H., Hayes, M. J., Svoboda, M. D., Tadesse, T., & Wilhite, D. A. (2015). Drought hazard assessment in the context of climate change for South Korea. *Agricultural Water Management*, *160*, 106–117. https://doi.org/10.1016/j.agwat.2015.06.029

Nemani, R. R. (2003). Climate-Driven Increases in Global Terrestrial Net Primary Production from 1982 to 1999. *Science*, *300*(5625), 1560–1563. https://doi.org/10.1126/science.1082750

Nepstad, D., Schwartzman, S., Bamberger, B., Santilli, M., Ray, D., Schlesinger, P., … Rolla, A. (2006). Inhibition of Amazon deforestation and fire by parks and indigenous lands. *Conservation Biology*, *20*(1), 65–73. https://doi.org/10.1111/j.1523-1739.2006.00351.x

Nguy-Robertson, A., Gitelson, A., Peng, Y., Viña, A., Arkebauer, T., & Rundquist, D. (2012). Green leaf area index estimation in maize and soybean: Combining vegetation indices to achieve maximal sensitivity. *Agronomy Journal*, *104*(5), 1336–1347. https://doi.org/10.2134/agronj2012.0065

Nicholson, S. E., Tucker, C. J., & Ba, M. B. (1998). Surface Vegetation : An Example from the West African Sahel. *Bulletin of the American Meteorological Society*, *79*(5), 815–829. https://doi.org/https://doi.org/10.1175/1520-0477

Nicolai-Shaw, N., Zscheischler, J., Hirschi, M., Gudmundsson, L., & Seneviratne, S. I. (2017). A drought event composite analysis using satellite remote-sensing based soil moisture. *Remote Sensing of Environment*, *203*, 216–225. https://doi.org/10.1016/j.rse.2017.06.014

Nobre, C. A., Marengo, J. A., Seluchi, M. E., Cuartas, L. A., & Alves, L. M. (2016). Some Characteristics and Impacts of the Drought and Water Crisis in Southeastern Brazil during 2014 and 2015. *Journal of Water Resource and Protection*, *08*(02), 252–262. https://doi.org/10.4236/jwarp.2016.82022

Noojipady, P., Morton, C. D., Macedo, N. M., Victoria, C. D., Huang, C., Gibbs, K. H., & Bolfe, L. E. (2017). Forest carbon emissions from cropland expansion in the Brazilian Cerrado biome. *Environmental Research Letters*, *12*(2). https://doi.org/10.1088/1748-9326/aa5986

Numata, I., Silva, S. S., Cochrane, M. A., & d'Oliveira, M. V. (2017). Fire and edge effects in a fragmented tropical forest landscape in the southwestern Amazon. *Forest Ecology and Management*, *401*, 135–146. https://doi.org/10.1016/j.foreco.2017.07.010

Oliveira, U., Silveira, B., -Filho, S., Paglia, A. P., Brescovit, A. D., De Carvalho, C. J. B., … Santos, A. J. (2017). Biodiversity conservation gaps in the Brazilian protected areas, (May), 1–9. https://doi.org/10.1038/s41598-017-08707-2

Otkin, J. A., Svoboda, M., Hunt, E. D., Ford, T. W., Anderson, M. C., Hain, C., & Basara, J. B. (2017). Flash Droughts: a Review and Assessment of the Challenges Imposed By Rapid Onset Droughts in the United States. *Bulletin of the American Meteorological Society*, (MAY), BAMS-D-17-0149.1. https://doi.org/10.1175/BAMS-D-17-0149.1

Oya, T., Nepomuceno, A. L., Neumaier, N., Renato, J., Tobita, S., & Ito, O. (2004). Drought Tolerance Characteristics of Brazilian Soybean Cultivars - Evaluation and characterization of drought tolerance of various Brazilian soybean cultivars in the fi eld. *Plant Production Science*, *7*(October 2003), 129–137.

Oyama, M. D., & Nobre, C. A. (2004). Climatic consequences of a large-scale desertification in northeast Brazil: A GCM simulation study. *Journal of Climate*, *17*(16), 3203–3213. https://doi.org/10.1175/1520-0442(2004)017<3203:CCOALD>2.0.CO;2

Pan, J., & Li, T. (2013). Extracting desertification from Landsat TM imagery based on spectral mixture analysis and Albedo-Vegetation feature space. *Natural Hazards*, *68*(2), 915–927. https://doi.org/10.1007/s11069-013-0665-3

Paredes-Trejo, F. J., Barbosa, H. A., & Lakshmi Kumar, T. V. (2017). Validating CHIRPS-based satellite precipitation estimates in Northeast Brazil. *Journal of Arid Environments*, *139*, 26–40. https://doi.org/10.1016/j.jaridenv.2016.12.009

Parente, L., Ferreira, L., Faria, A., Nogueira, S., Ara?jo, F., Teixeira, L., & Hagen, S. (2017). Monitoring the brazilian pasturelands: A new mapping approach based on the landsat 8 spectral and temporal domains. *International Journal of Applied Earth Observation and Geoinformation*, *62*(January), 135–143. https://doi.org/10.1016/j.jag.2017.06.003

PBMC, P. B. de M. C. (2016). *Mudanças Climáticas e Cidades*. Rio de Janeiro, RJ, Brazil. Retrieved from www.pbmc.coppe.ufrj.br/documentos/Relatorio_UM_v10-2017-1.pdf

Pereira, V. R., Blain, G. C., de Avila, A. M. H., Pires, R. C. de M., & Pinto, H. S. (2018). Impacts of climate change on drought: Changes to drier conditions at the beginning of the crop growing season in southern Brazil. *Bragantia*, *77*(1), 201–211. https://doi.org/10.1590/1678-4499.2017007

Perez-marin, A. M., Cavalcante, A. de M. B., Medeiros, S. S. de, Tinôco, L. B. de M., & Salcedo, I. H. (2012). Núcleos de desertificação no semiárido brasileiro : ocorrência natural ou antrópica ? *Parcerias Estratégicas*, *17*(34), 87–106.

Petta, R. A., Carvalho, L. V. De, Erasmi, S., & Jones, C. (2013). Evaluation of Desertification Processes in Seridó Region (NE Brazil). *International Journal of Geosciences*, *04*(05), 12–17. https://doi.org/10.4236/ijg.2013.45B003

Pezzi, L. P., & Cavalcanti, I. F. a. (2001). The relative importance of ENSO and tropical Atlantic sea surface temperature anomalies for seasonal precipitation over South America: a numerical study. *Climate Dynamics*, *17*, 205–212. https://doi.org/10.1007/s003820000104

Phillips, O. L., Aragao, L. E. O. C., Lewis, S. L., Fisher, J. B., Lloyd, J., Lopez-Gonzalez, G., … Torres-Lezama, A. (2009). Drought Sensitivity of the Amazon Rainforest. *Science*, *323*(5919), 1344–1347. https://doi.org/10.1126/science.1164033

Piles, M., Camps, A., Vall-llossera, M., Corbella, I., Panciera, R., Rudiger, C., … Walker, J. (2011). Downscaling SMOS-Derived Soil Moisture Using MODIS Visible/Infrared Data. *IEEE Transactions on Geoscience and Remote Sensing*, *49*(9), 3156–3166.

https://doi.org/10.1109/TGRS.2011.2120615

Povitkina, M. (2018). The limits of democracy in tackling climate change. *Environmental Politics*, *27*(3), 411–432. https://doi.org/10.1080/09644016.2018.1444723

Prince, S. D., Wessels, K. J., Tucker, C. J., & Nicholson, S. E. (2007). Desertification in the Sahel: a reinterpretation of a reinterpretation. *Global Change Biology*, *13*(7), 1308–1313. https://doi.org/10.1111/j.1365-2486.2007.01356.x

Privette, J. L., Myneni, R. B., Knyazikhin, Y., Mukelabai, M., Roberts, G., Tian, Y., … Leblanc, S. G. (2002). Early spatial and temporal validation of MODIS LAI product in the southern Africa Kalahari. *Remote Sensing of Environment*, *83*(1–2), 232–243. https://doi.org/10.1016/S0034-4257(02)00075-5

Rada, N. (2013). Assessing Brazil's Cerrado agricultural miracle. *Food Policy*, *38*(1), 146–155. https://doi.org/10.1016/j.foodpol.2012.11.002

Rajan, N., Maas, S. J., & Cui, S. (2015). Extreme drought effects on summer evapotranspiration and energy balance of a grassland in the Southern Great Plains. *Ecohydrology*, *8*(7), 1194–1204. https://doi.org/10.1002/eco.1574

Rao, V. B., Franchito, S. H., Santo, C. M. E., & Gan, M. A. (2016). An update on the rainfall characteristics of Brazil: Seasonal variations and trends in 1979-2011. *International Journal of Climatology*, *36*(1), 291–302. https://doi.org/10.1002/joc.4345

Rappaport, D. I., Morton, D. C., Longo, M., Keller, M., Dubayah, R., & Dos-Santos, M. N. (2018). Quantifying long-term changes in carbon stocks and forest structure from Amazon forest degradation. *Environmental Research Letters*, *13*(6). https://doi.org/10.1088/1748-9326/aac331

Redo, D., Aide, T. M., & Clark, M. L. (2013). Vegetation change in Brazil's dryland ecoregions and the relationship to crop production and environmental factors: Cerrado, Caatinga, and Mato Grosso, 2001-2009. *Journal of Land Use Science*, *8*(2), 123–153. https://doi.org/10.1080/1747423X.2012.667448

Resende, N. C., Miranda, J. H., Cooke, R., Chu, M. L., & Chou, S. C. (2019). Impacts of regional climate change on the runoff and root water uptake in corn crops in Parana, Brazil. *Agricultural Water Management*, *221*(May), 556–565. https://doi.org/10.1016/j.agwat.2019.05.018

Reynolds, J. F., Grainger, A., Stafford Smith, D. M., Bastin, G., Garcia-Barrios, L., Fernández, R. J., … Zdruli, P. (2011). Scientific concepts for an integrated analysis of desertification. *Land Degradation and Development*, *22*(2), 166–183. https://doi.org/10.1002/ldr.1104

Reynolds, J. F., Smith, D. M. S., Lambin, E. F., Turner, B. L., Mortimore, M., Batterbury, S. P. J., … Walker, B. (2007). Global Desertification: Building a Science for Dryland

Development. *Science*, *316*(5826), 847–851. https://doi.org/10.1126/science.1131634

Ribeiro Neto, A., da Paz, A. R., Marengo, J. A., & Chou, S. C. (2016). Hydrological Processes and Climate Change in Hydrographic Regions of Brazil. *Journal of Water Resource and Protection*, *08*(12), 1103–1127. https://doi.org/10.4236/jwarp.2016.812087

Richards, P. D., Myers, R. J., Swinton, S. M., & Walker, R. T. (2012). Exchange rates, soybean supply response, and deforestation in South America. *Global Environmental Change*, *22*(2), 454–462. https://doi.org/10.1016/j.gloenvcha.2012.01.004

Rodrigues, J. A., Libonati, R., Pereira, A. A., Nogueira, J. M. P., Santos, F. L. M., Peres, L. F., … Setzer, A. W. (2019). How well do global burned area products represent fire patterns in the Brazilian Savannas biome? An accuracy assessment of the MCD64 collections. *International Journal of Applied Earth Observation and Geoinformation*, *78*(February), 318–331. https://doi.org/10.1016/J.JAG.2019.02.010

Rodrigues, R., & McPhaden, M. (2014). Why did the 2011-2012 La Nina cause a severe drought in the Brazilian Northeast. *Geophysical Research Letters*, 1–7. https://doi.org/10.1002/2013GL058703.Received

Rouault, M., & Richard, Y. (2004). Intensity and spatial extension of drought in South Africa at different time scales. *Water SA*, *29*(4), 489–500. https://doi.org/10.4314/wsa.v29i4.5057

Ruhoff, A. L., Paz, A. R., Aragao, L. E. O. C., Mu, Q., Malhi, Y., Collischonn, W., … Running, S. W. (2013). Assessment of the MODIS global evapotranspiration algorithm using eddy covariance measurements and hydrological modelling in the Rio Grande basin. *Hydrological Sciences Journal*, *58*(October), 1658–1676. https://doi.org/10.1080/02626667.2013.837578

Running, S. W., Nemani, R. R., Heinsch, F. A., Zhao, M., Reeves, M., & Hashimoto, H. (2006). A Continuous Satellite-Derived Measure of Global Terrestrial Primary Production. *BioScience*, *54*(6), 547. https://doi.org/https://doi.org/10.1641/0006-3568

Ruviaro, C. F., Barcellos, J. O. J., & Dewes, H. (2014). Market-oriented cattle traceability in the Brazilian Legal Amazon. *Land Use Policy*, *38*, 104–110. https://doi.org/10.1016/j.landusepol.2013.08.019

Sakamoto, T., Wardlow, B. D., Gitelson, A. A., Verma, S. B., Suyker, A. E., & Arkebauer, T. J. (2010). A Two-Step Filtering approach for detecting maize and soybean phenology with time-series MODIS data. *Remote Sensing of Environment*, *114*(10), 2146–2159. https://doi.org/10.1016/j.rse.2010.04.019

Salazar, A., Baldi, G., Hirota, M., Syktus, J., & McAlpine, C. (2015). Land use and land cover change impacts on the regional climate of non-Amazonian South America: A review. *Global and Planetary Change*, *128*, 103–119. https://doi.org/10.1016/j.gloplacha.2015.02.009

Samain, O., Kergoat, L., Hiernaux, P., Guichard, F., Mougin, E., Timouk, F., & Lavenu, F. (2008). Analysis of the in situ and MODIS albedo variability at multiple timescales in the sahel. *Journal of Geophysical Research Atmospheres*, *113*(14), 1–16. https://doi.org/10.1029/2007JD009174

Samanta, A., Ganguly, S., Hashimoto, H., Devadiga, S., Vermote, E., Knyazikhin, Y., … Myneni, R. B. (2010). Amazon forests did not green-up during the 2005 drought. *Geophysical Research Letters*, *37*(5), 1–5. https://doi.org/10.1029/2009GL042154

Sampaio, G., Nobre, C., Costa, M. H., Satyamurty, P., Soares-Filho, B. S., & Cardoso, M. (2007). Regional climate change over eastern Amazonia caused by pasture and soybean cropland expansion. *Geophysical Research Letters*, *34*(17), 1–7. https://doi.org/10.1029/2007GL030612

Santos, M. G., Oliveira, M. T., Figueiredo, K. V., Falcão, H. M., Arruda, E. C. P., Almeida-Cortez, J., … Antonino, A. C. D. (2014). Caatinga, the Brazilian dry tropical forest: Can it tolerate climate changes? *Theoretical and Experimental Plant Physiology*, *26*(1), 83–99. https://doi.org/10.1007/s40626-014-0008-0

Sasana, H., & Ghozali, I. (2017). The Impact of Fossil and Renewable Energy Consumption on the Economic Growth in Brazil, Russia, India, China and South Africa. *International Journal of Energy Economics and Policy* |, *7*(3), 194–200. Retrieved from http:www.econjournals.com

Schaaf, C. B., Gao, F., Strahler, A. H., Lucht, W., Li, X., Tsang, T., … Roy, D. (2002). First operational BRDF, albedo nadir reflectance products from MODIS. *Remote Sensing of Environment*, *83*(1–2), 135–148. https://doi.org/10.1016/S0034-4257(02)00091-3

Schwartzman, S., Boas, A. V., Ono, K. Y., Fonseca, M. G., Doblas, J., Zimmerman, B., … Torres, M. (2013). The natural and social history of the indigenous lands and protected areas corridor of the Xingu River basin. *Philosophical Transactions of the Royal Society B: Biological Sciences*, *368*(1624), 20130308–20130308. https://doi.org/10.1098/rstb.2013.0308

Sellers, P. J., Bounoua, L., Collatz, G. J., Randall, D. A., Dazlich, D. A., Los, S. O., … Jensen, T. G. (1996). Comparison of Radiative and Physiological Effects of Doubled Atmospheric CO2 on Climate. *Science*, *271*(5254), 1402–1406. https://doi.org/10.1126/science.271.5254.1402

Semmens, K. A., Anderson, M. C., Kustas, W. P., Gao, F., Alfieri, J. G., McKee, L., … Vélez, M. (2016). Monitoring daily evapotranspiration over two California vineyards using Landsat 8 in a multi-sensor data fusion approach. *Remote Sensing of Environment*, *185*, 155–170. https://doi.org/10.1016/j.rse.2015.10.025

Senay, G. B., Friedrichs, M., Singh, R. K., & Velpuri, N. M. (2016). Evaluating Landsat 8 evapotranspiration for water use mapping in the Colorado River Basin. *Remote Sensing of Environment*, *185*, 171–185. https://doi.org/10.1016/j.rse.2015.12.043

Seneviratne, S. I., Corti, T., Davin, E. L., Hirschi, M., Jaeger, E. B., Lehner, I., … Teuling, A. J. (2010). Investigating soil moisture-climate interactions in a changing climate: A review. *Earth-Science Reviews*, *99*(3–4), 125–161. https://doi.org/10.1016/j.earscirev.2010.02.004

Sentelhas, P. C., Battisti, R., S., C. G. M., B., F. J. R., Hampf, A. C., Nendel, C., … Nendel, C. (2015). The soybean yield gap in Brazil – magnitude, causes and possible solutions for sustainable production. *The Journal of Agricultural Science*, *153*(08), 1394–1411. https://doi.org/10.1017/S0021859615000313

Serrão, E. A. S., Nepstad, D., & Walker, R. (1996). Upland agricultural and forestry development in the Amazon: Sustainability, criticality and resilience. *Ecological Economics*, *18*(1), 3–13. https://doi.org/10.1016/0921-8009(95)00092-5

Setzer, A. W., Pereira, M. C., & Pereira, A. C. (1994). Satellite studies of biomass burning in Amazonia - some practical aspects. *Remote Sensing Reviews*, *10*(1–3), 91–103. https://doi.org/10.1080/02757259409532238

Shao, Y., Lunetta, R. S., Wheeler, B., Iiames, J. S., & Campbell, J. B. (2016). An evaluation of time-series smoothing algorithms for land-cover classifications using MODIS-NDVI multi-temporal data. *Remote Sensing of Environment*, *174*, 258–265. https://doi.org/10.1016/j.rse.2015.12.023

Shieh, G. S. (1998). A weighted Kendall's tau statistic. *Statistics & Probability Letters*, *39*(1), 17–24. https://doi.org/10.1016/S0167-7152(98)00006-6

Shimizu, M. H., Ambrizzi, T., & Liebmann, B. (2017). Extreme precipitation events and their relationship with ENSO and MJO phases over northern South America. *International Journal of Climatology*, *37*(6), 2977–2989. https://doi.org/10.1002/joc.4893

Shukla, J., Nobre, C., & Sellers, P. (1990). Amazon Deforestation and Climate Change. *Science*, *247*(4948), 1322–1325. https://doi.org/10.1126/science.247.4948.1322

Sietz, D., Untied, B., Walkenhorst, O., Lüdeke, M. K. B., Mertins, G., Petschel-Held, G., & Schellnhuber, H. J. (2006). Smallholder agriculture in Northeast Brazil: Assessing heterogeneous human-environmental dynamics. *Regional Environmental Change*, *6*(3), 132–146. https://doi.org/10.1007/s10113-005-0010-9

Silva, C. V. J., Barlow, J., Young, P. J., Berenguer, E., França, F., Aragão, L. E. O. C., … Xaud, H. A. M. (2018). Drought-induced Amazonian wildfires instigate a decadal-scale disruption of forest carbon dynamics. *Philosophical Transactions of the Royal Society B: Biological Sciences*, *373*(1760). https://doi.org/10.1098/rstb.2018.0043

Silva, P. F. da, Lima, J. R. de S., Antonino, A. C. D., Souza, R., de Souza, E. S., Silva, J. R. I., & Alves, E. M. (2017). Seasonal patterns of carbon dioxide, water and energy fluxes over the Caatinga and grassland in the semi-arid region of Brazil. *Journal of Arid Environments*, *147*, 71–82. https://doi.org/10.1016/j.jaridenv.2017.09.003

Silvério, D. V, Brando, P. M., Macedo, M. N., Beck, P. S. A., Bustamante, M., & Coe, M. T. (2015). Agricultural expansion dominates climate changes in southeastern Amazonia: the overlooked non-GHG forcing. *Environmental Research Letters*, *10*(10), 104015. https://doi.org/10.1088/1748-9326/10/10/104015

Soares-Filho, B., Silvestrini, R., Nepstad, D., Brando, P., Rodrigues, H., Alencar, A., … Stickler, C. (2012). Forest fragmentation, climate change and understory fire regimes on the Amazonian landscapes of the Xingu headwaters. *Landscape Ecology*, *27*(4), 585–598. https://doi.org/10.1007/s10980-012-9723-6

Tagliapietra, E. L., Streck, N. A., Da Rocha, T. S. M., Richter, G. L., Da Silva, M. R., Cera, J. C., … Junior Zanon, A. (2018). Optimum leaf area index to reach soybean yield potential in subtropical environment. *Agronomy Journal*, *110*(3), 932–938. https://doi.org/10.2134/agronj2017.09.0523

Teixeira, M. A., Murray, M. L., & Carvalho, M. (2006). Assessment of land use and land use change and forestry (LULUCF) as CDM projects in Brazil. *Ecological Economics*, *60*(1), 260–270. https://doi.org/10.1016/j.ecolecon.2005.12.003

Thompson, I., Mackey, B., McNulty, S., & Mosseler, A. (2009). *Forest Resilience, Biodiversity, and Climate Change: a synthesis of the biodiversity/resilience/stability relationship in forest ecosystems. Secretariat of the Convention on Biological Diversity, Montreal. Technical Series no. 43. Secretariat of the Convention on Biological Diversity.* (Vol. 43). Montreal, Canada: Secretariat of the Convention on Biological Diversity.

Tomasella, J., Silva Pinto Vieira, R. M., Barbosa, A. A., Rodriguez, D. A., Oliveira Santana, M. de, & Sestini, M. F. (2018). Desertification trends in the Northeast of Brazil over the period 2000–2016. *International Journal of Applied Earth Observation and Geoinformation*, *73*(August 2017), 197–206. https://doi.org/10.1016/j.jag.2018.06.012

Tong, X., Brandt, M., Hiernaux, P., Herrmann, S. M., Tian, F., Prishchepov, A. V., & Fensholt, R. (2017). Revisiting the coupling between NDVI trends and cropland changes in the Sahel drylands: A case study in western Niger. *Remote Sensing of Environment*, *191*, 286–296. https://doi.org/10.1016/j.rse.2017.01.030

Toutin, T. (2004). Geometric processing of remote sensing images: Models, algorithms and methods. *International Journal of Remote Sensing*, *25*(10), 1893–1924. https://doi.org/10.1080/0143116031000101611

Tyukavina, A., Hansen, M. C., Potapov, P. V., Stehman, S. V., Smith-Rodriguez, K., Okpa, C., & Aguilar, R. (2017). Types and rates of forest disturbance in Brazilian Legal Amazon, 2000–2013. *Science Advances*, *3*(4), e1601047. https://doi.org/10.1126/sciadv.1601047

Uhl, C. (1990). Deforestation, fire susceptibility, and potential tree responses to fire in the eastern Amazon. *Ecology1*, *71*(2), 437–449.

Uhl, C., Kauffman, J. B., & Cummings, D. L. (1988). Fire in the Venezuelan Amazon 2: Environmental Conditions Necessary for Forest Fires in the Evergreen Rainforest of Venezuela. *Oikos*, *53*(2), 176. https://doi.org/10.2307/3566060

UN. (1994). *United Nations Convention to Combat Desertification in Countries Experiencing Serious Drought and/or Desertification, Particularly in Africa*. New York, NY.

Uvo, C. B., Repelli, C. A., Zebiak, S. E., & Kushnir, Y. (1998). The relationships between tropical Pacific and Atlantic SST and northeast Brazil monthly precipitation. *Journal of Climate*, *11*(4), 551–562. https://doi.org/10.1175/1520-0442(1998)011<0551:trbtpa>2.0.co;2

Van Hoek, M., Jia, L., Zhou, J., Zheng, C., & Menenti, M. (2016). Early drought detection by spectral analysis of satellite time series of precipitation and Normalized Difference Vegetation Index (NDVI). *Remote Sensing*, *8*(5). https://doi.org/10.3390/rs8050422

Van Loon, A. F., Gleeson, T., Clark, J., Van Dijk, A. I. J. M., Stahl, K., Hannaford, J., … Van Lanen, H. A. J. (2016). Drought in the Anthropocene. *Nature Geoscience*, *9*(2), 89–91. https://doi.org/10.1038/ngeo2646

Vera-Diaz, M. del C., Kaufmann, R. K., Nepstad, D. C., & Schlesinger, P. (2008). An interdisciplinary model of soybean yield in the Amazon Basin: The climatic, edaphic, and economic determinants. *Ecological Economics*, *65*(2), 420–431. https://doi.org/10.1016/j.ecolecon.2007.07.015

Verger, A., Filella, I., Baret, F., & Peñuelas, J. (2016). Vegetation baseline phenology from kilometric global LAI satellite products. *Remote Sensing of Environment*, *178*, 1–14. https://doi.org/10.1016/j.rse.2016.02.057

Vicente-Serrano, S. M., Gouveia, C., Camarero, J. J., Begueria, S., Trigo, R., Lopez-Moreno, J. I., … Sanchez-Lorenzo, A. (2013). Response of vegetation to drought time-scales across global land biomes. *Proceedings of the National Academy of Sciences*, *110*(1), 52–57. https://doi.org/10.1073/pnas.1207068110

Vicente-Serrano, Sergio M. (2007). Evaluating the impact of drought using remote sensing in a Mediterranean, Semi-arid Region. *Natural Hazards*, *40*(1), 173–208. https://doi.org/10.1007/s11069-006-0009-7

Vicente-Serrano, Sergio M., Beguería, S., & López-Moreno, J. I. (2010). A multiscalar drought index sensitive to global warming: The standardized precipitation evapotranspiration index. *Journal of Climate*, *23*(7), 1696–1718. https://doi.org/10.1175/2009JCLI2909.1

Vieira, R. M. S. P., Tomasella, J., Alvalá, R. C. S., Sestini, M. F., Affonso, A. G., Rodriguez, D. A., … Santana, M. O. (2015). Identifying areas susceptible to desertification in the Brazilian northeast. *Solid Earth*, *6*(1), 347–360. https://doi.org/10.5194/se-6-347-2015

Villas-Bôas, A. (2012). *De Olho na Bacia do Xingu. Série Cartô Brasil Socioambiental*. São Paulo, Brazil: Instituto Socioambiental.

Wessels, K. J., van den Bergh, F., & Scholes, R. J. (2012). Limits to detectability of land degradation by trend analysis of vegetation index data. *Remote Sensing of Environment*, *125*, 10–22. https://doi.org/10.1016/j.rse.2012.06.022

Wilhelmi, O. V., & Wilhite, D. A. (2002). Assessing Vulnerability to Agricultural Drought: A Nebraska Case Study. *Natural Hazards*, *25*(1), 37–58. https://doi.org/10.1023/A:1013388814894

Wilhite, D. A. (2000). Drought as a natural hazard: Concepts and definitions. In *Drought: A Global Assessment* (pp. 3–18).

Wongchuig Correa, S., Paiva, R. C. D. de, Espinoza, J. C., & Collischonn, W. (2017). Multi-decadal Hydrological Retrospective: Case study of Amazon floods and droughts. *Journal of Hydrology*, *549*, 667–684. https://doi.org/10.1016/j.jhydrol.2017.04.019

WorldBank. (2012). *Turn down the heat*. Washington, DC.

Wright, J. S., Fu, R., Worden, J. R., Chakraborty, S., Clinton, N. E., Risi, C., … Yin, L. (2017). Rainforest-initiated wet season onset over the southern Amazon. *Proceedings of the National Academy of Sciences*, *114*(32), 8481–8486. https://doi.org/10.1073/pnas.1621516114

Yagci, A. L., Di, L., & Deng, M. (2015). The effect of corn-soybean rotation on the NDVI-based drought indicators: A case study in Iowa, USA, using vegetation condition index. *GIScience and Remote Sensing*, *52*(3), 290–314. https://doi.org/10.1080/15481603.2015.1038427

Yang, Y., Saatchi, S. S., Xu, L., Yu, Y., Choi, S., Phillips, N., … Myneni, R. B. (2018). Post-drought decline of the Amazon carbon sink. *Nature Communications*, *9*(1). https://doi.org/10.1038/s41467-018-05668-6

Yao, G., Hertel, T. W., & Taheripour, F. (2018). Economic drivers of telecoupling and terrestrial carbon fluxes in the global soybean complex. *Global Environmental Change*, *50*(November 2017), 190–200. https://doi.org/10.1016/j.gloenvcha.2018.04.005

Yuan, W., Liu, S., Yu, G., Bonnefond, J. M., Chen, J., Davis, K., … Verma, S. B. (2010). Global estimates of evapotranspiration and gross primary production based on MODIS and global meteorology data. *Remote Sensing of Environment*, *114*(7), 1416–1431. https://doi.org/10.1016/j.rse.2010.01.022

Yuan, X., Ma, Z., Pan, M., & Shi, C. (2015). Microwave remote sensing of short-term droughts during crop growing seasons. *Geophysical Research Letters*, *42*(11), 4394–4401. https://doi.org/10.1002/2015GL064125

Zemp, D. C., Schleussner, C. F., Barbosa, H. M. J., Hirota, M., Montade, V., Sampaio, G., … Rammig, A. (2017). Self-amplified Amazon forest loss due to vegetation-atmosphere feedbacks. *Nature Communications*, *8*, 1–10. https://doi.org/10.1038/ncomms14681

Zhang, X., Chen, N., Li, J., Chen, Z., & Niyogi, D. (2017). Multi-sensor integrated framework and index for agricultural drought monitoring. *Remote Sensing of Environment*, *188*, 141–163. https://doi.org/10.1016/j.rse.2016.10.045

Zika, M., & Erb, K. H. (2009). The global loss of net primary production resulting from human-induced soil degradation in drylands. *Ecological Economics*, *69*(2), 310–318. https://doi.org/10.1016/j.ecolecon.2009.06.014